IEC TS 62882

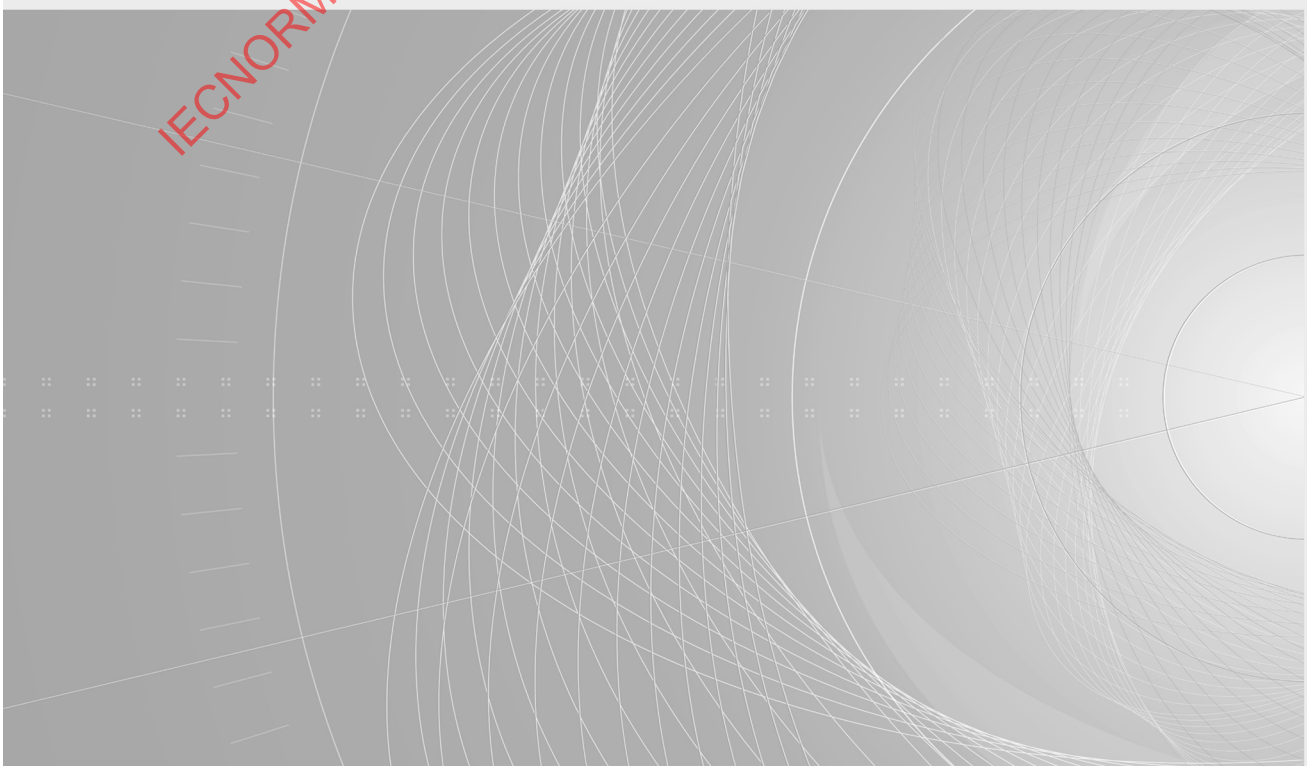
Edition 1.0 2020-09

TECHNICAL SPECIFICATION

IECNORM.COM : Click to view the full PDF of IEC TS 62882:2020

colour inside

Hydraulic machines – Francis turbine pressure fluctuation transposition



IEC TS 62882:2020-09(en)

THIS PUBLICATION IS COPYRIGHT PROTECTED
Copyright © 2020 IEC, Geneva, Switzerland

All rights reserved. Unless otherwise specified, no part of this publication may be reproduced or utilized in any form or by any means, electronic or mechanical, including photocopying and microfilm, without permission in writing from either IEC or IEC's member National Committee in the country of the requester. If you have any questions about IEC copyright or have an enquiry about obtaining additional rights to this publication, please contact the address below or your local IEC member National Committee for further information.

IEC Central Office
3, rue de Varembé
CH-1211 Geneva 20
Switzerland

Tel.: +41 22 919 02 11
info@iec.ch
www.iec.ch

About the IEC
The International Electrotechnical Commission (IEC) is the leading global organization that prepares and publishes International Standards for all electrical, electronic and related technologies.

About IEC publications
The technical content of IEC publications is kept under constant review by the IEC. Please make sure that you have the latest edition, a corrigendum or an amendment might have been published.

IEC publications search - webstore.iec.ch/advsearchform
The advanced search enables to find IEC publications by a variety of criteria (reference number, text, technical committee,…). It also gives information on projects, replaced and withdrawn publications.

IEC Just Published - webstore.iec.ch/justpublished
Stay up to date on all new IEC publications. Just Published details all new publications released. Available online and once a month by email.

IEC Customer Service Centre - webstore.iec.ch/csc
If you wish to give us your feedback on this publication or need further assistance, please contact the Customer Service Centre: sales@iec.ch.

Electropedia - www.electropedia.org
The world's leading online dictionary on electrotechnology, containing more than 22 000 terminological entries in English and French, with equivalent terms in 16 additional languages. Also known as the International Electrotechnical Vocabulary (IEV) online.

IEC Glossary - std.iec.ch/glossary
67 000 electrotechnical terminology entries in English and French extracted from the Terms and Definitions clause of IEC publications issued since 2002. Some entries have been collected from earlier publications of IEC TC 37, 77, 86 and CISPR.

IECNORM.COM : Click to view the full PDF of IEC TS 62882:2020

IEC TS 62882

Edition 1.0 2020-09

TECHNICAL SPECIFICATION

IECNORM.COM : Click to view the full PDF of IEC TS 62882:2020

colour inside

Hydraulic machines – Francis turbine pressure fluctuation transposition

INTERNATIONAL
ELECTROTECHNICAL
COMMISSION

ICS 27.140

ISBN 978-2-8322-8786-6

Warning! Make sure that you obtained this publication from an authorized distributor.

® Registered trademark of the International Electrotechnical Commission

CONTENTS

FOREWORD 9
INTRODUCTION 11
1 Scope 12
2 Normative references 13
3 Terms, definitions, symbols and units 13
3.1 General terms and definitions 13
3.2 Units 13
3.3 Overview of the terms, definitions, symbols and units used in this document 14
3.3.1 Subscripts and symbols 15
3.3.2 Geometric terms and definitions 16
3.3.3 Physical quantities and properties terms and definitions 17
3.3.4 Discharge, velocity and speed terms and definitions 17
3.3.5 Pressure terms and definitions 18
3.3.6 Specific energy terms and definitions 18
3.3.7 Height and head terms and definitions 19
3.3.8 Power and torque terms and definitions 20
3.3.9 Efficiency terms and definitions 21
3.3.10 General terms and definitions relating to fluctuating quantities 21
3.3.11 Fluid dynamic and scaling terms and definitions 24
3.3.12 Dimensionless terms and definitions 24
4 Description of pressure fluctuation phenomena 25
4.1 General 25
4.2 Pressure fluctuations overview 30
4.3 General description of draft tube flow in Francis turbines 32
4.4 Detailed description of pressure fluctuation phenomena 34
4.4.1 Mode 1: Pressure fluctuation in high load 34
4.4.2 Mode 2: Pressure fluctuation in best operation range 35
4.4.3 Mode 3: Pressure fluctuation in upper part load 35
4.4.4 Mode 4: Pressure fluctuation in part load 36
4.4.5 Mode 5: Pressure fluctuation in deep part load 38
4.4.6 Modes 6.a and 6.b: Rotor-stator interaction (RSI) pressure fluctuation 39
5 Specifications of pressure fluctuation measurement and analysis 41
5.1 General 41
5.1.1 Overview 41
5.1.2 Purpose of the measurements 41
5.1.3 Procedures and parameters to record 42
5.1.4 Locations of pressure fluctuation test transducers 43
5.1.5 Data acquisition for pressure fluctuation measurements 44
5.1.6 Transducers and calibration 45
5.2 Pressure fluctuation on a model turbine 45
5.2.1 General 45
5.2.2 Homology and limitations 46
5.2.3 Detailed procedures 46
5.3 Special requirements and information for a prototype turbine 48
5.3.1 General 48
5.3.2 Source of information 48

IECNORM.COM : Click to view the full PDF of IEC TS 62882:2020

5.3.3 Important aspects 48
5.4 Analysis, presentation and interpretation of results 49
5.4.1 General 49
5.4.2 Time-domain analysis 49
5.4.3 Frequency-domain analysis 50
5.4.4 Non-dimensional frequency and pressure 50
5.4.5 Presentation and interpretation of pressure fluctuations 50
6 Identification of potential resonances in test rig and prototype 51
6.1 General 51
6.2 Identify resonance in test rig 53
6.3 Possible resonance and self-excited pressure fluctuation in prototype 53
6.3.1 General 53
6.3.2 Draft tube vortex related resonances and self-excited pressure fluctuation in prototype 53
6.3.3 Rotor-stator interaction (RSI) related resonance 55
6.3.4 Resonance with fluctuation modes not treated in this document 55
7 Transposition method and procedure 56
7.1 General 56
7.2 Parameters influencing transposition 56
7.2.1 Model test head 56
7.2.2 Thoma number 56
7.2.3 Froude number 57
7.3 Relevant quantities for transposition 57
7.3.1 Fluctuation frequency 57
7.3.2 Fluctuation amplitude 57
7.4 Transposable types of fluctuations 57
7.5 Statistical analysis of model and prototype transposition accuracy 58
8 Mitigations 59
8.1 Draft tube vortex phenomena 59
8.1.1 General 59
8.1.2 Draft tube fins 59
8.1.3 Draft tube with a central column 60
8.1.4 Air admission 61
8.1.5 AVR or PSS parameter tuning 62
8.2 Runner inter-blade vortex 63
8.3 Blade interaction 63
8.4 Operation restriction 63
Annex A (informative) Example of pressure fluctuation records 64
Annex B (informative) Typical pressure fluctuation transducers parameters for model test 83
Annex C (informative) Pressure transducer dynamic calibration 84
C.1 Fast valve opening method 84
C.2 Rotating valve method 84
C.3 Electrical spark method 85
Annex D (informative) Proposed remote pressure measurement fluctuation correction 86
D.1 General 86
D.2 Correction method theory 86
D.3 Measuring and estimating tube frequency response 87

IECNORM.COM : Click to view the full PDF of IEC TS 62882:2020

D.4 Pressure fluctuation correction 89
D.5 Limitations 92
Annex E (informative) Forced response analysis for Francis turbines operating in part load conditions 93
E.1 General 93
E.2 Systematic methodology based on detailed modelling of hydroelectric power plant 93
E.2.1 Description of the test case 93
E.2.2 Modelling of the hydraulic power plant 94
E.2.3 Forced response analysis of the test case 97
E.3 Simplified approach based on the hydroacoustic properties of the hydraulic system 100
E.3.1 General 100
E.3.2 Cavitating draft tube first natural frequency 100
E.3.3 Hydraulic circuit natural frequencies 101
E.3.4 Example of applications 102
E.3.5 Limitations of the methodology 107
Annex F (informative) Influence of Thoma number on pressure fluctuation 108
Annex G (informative) Transposition of synchronous pressure fluctuations from model to prototype for Francis turbines operating at off-design conditions 110
G.1 General 110
G.1.1 Overview 110
G.1.2 Step 1: 1-D numerical modelling of both the test rig at the model scale and the corresponding hydropower unit operating in off-design conditions 110
G.1.3 Step 2: Experimental identification of the parameters of interest on the reduced scale model 112
G.1.4 Step 3: Transposition of the hydroacoustic parameters from model to prototype 115
G.1.5 Step 4: Prediction of the precession frequency and eigenfrequencies at the prototype scale 116
G.1.6 Step 5: Prediction of pressure fluctuations at the prototype scale 116
G.2 Concluding remark: use of the local cavitation coefficient for transposition from model to prototype 116
Annex H (informative) Statistical analysis of pressure fluctuation data 119
H.1 Normalizing step for the comparison of data 119
H.2 Collected data 121
H.3 Draft tube zone phenomena 121
H.4 Vaneless zone phenomena 126
H.5 Spiral case phenomena 130
Annex J (informative) Gathering worldwide pressure fluctuation data 134
J.1 Chinese test cases 134
J.2 France test case 135
J.3 Norway test case 137
Bibliography 138

Figure 1 – Reference diameter of Francis turbine 16
Figure 2 – Reference level of the Francis turbine 19
Figure 3 – Flux diagram for power and discharge 20
Figure 4 – Illustration of some definitions related to fluctuating quantities 23

IECNORM.COM : Click to view the full PDF of IEC TS 62882:2020

Figure 5 – Discharge range for the various fluctuation modes 30
Figure 6 – Efficiency hill chart with pictures of swirling flow 31
Figure 7 – Example of a waterfall diagram of pressure amplitudes measured in the draft tube cone 32
Figure 8 – Velocity triangles at inlet and outlet of the runner blade 33
Figure 9 – Influence of the discharge on the circumferential component of the absolute velocity 34
Figure 10 – Elliptical vortex rope precessing in the draft tube cone at upper part load 36
Figure 11 – Decomposition between the synchronous and asynchronous component of part load draft tube pressure fluctuations 37
Figure 12 – Example of inter-blade vortex 38
Figure 13 – Modulation process between runner blade flow field and guide vanes flow field 39
Figure 14 – Diametrical modes shapes representation according to k values 40
Figure 15 – Suggested locations of pressure transducers 43
Figure 16 – Turbine hill-chart with exploration paths 45
Figure 17 – Schematic of the axial aeration device 47
Figure 18 – Schematic arrangement for pressure fluctuation transducers 49
Figure 19 – Typical plot showing pressure fluctuation coefficient versus relative discharge 51
Figure 20 – Elementary hydroacoustic oscillator 52
Figure 21 – Part load vortex rope in the draft tube and its fluctuation frequency range and corresponding risk of resonance with the generator local mode of oscillation valid for both F_{grid} = 50 Hz and F_{grid} = 60 Hz 54
Figure 22 – Waterfall diagram of the pressure fluctuations as function of the frequency and Froude number for a given Thoma number 57
Figure 23 – Example of fins in the draft tube and influence on the pressure fluctuations 60
Figure 24 – Example of the draft tube with central column extension 61
Figure 25 – Typical runner cone extensions used for reducing draft tube pressure fluctuations 61
Figure 26 – Central and peripheral air admission locations for draft tube pressure fluctuations on a radial flow turbine 62
Figure 27 – Central air admission 62
Figure A.1 – Example 1: a case corresponding to mode 1 (a limited high load) 66
Figure A.2 – Example 2: a case corresponding to mode 1 (a large overload) 68
Figure A.3 – Example 3: a case corresponding to mode 2 70
Figure A.4 – Example 4 : a case corresponding to mode 3 72
Figure A.5 – Example 5 : a case corresponding to mode 4.a and 4.b 74
Figure A.6 – Example 6: a case corresponding to mode 4.a and 4.b 76
Figure A.7 – Example 7: a case corresponding to mode 4.c 78
Figure A.8 – Example 8: a case corresponding to mode 5.b 80
Figure A.9 – Example 9: a case corresponding to mode 6.a 82
Figure C.1 – Pressure transducer dynamic calibration schematic diagram with fast open valve method 84
Figure C.2 – Pressure transducer dynamic calibration with rotating valve method 85

IECNORM.COM : Click to view the full PDF of IEC TS 62882:2020

Figure C.3 – Spark plug used as to generate an impulse excitation in water for pressure transducer dynamic calibration 85
Figure D.1 – Typical results obtained by shutting off drainage valve 88
Figure D.2 – Signal and spectrum of four remote sensors and one local sensor 90
Figure D.3 – Signal and spectrum of four remote sensors (corrected) and one local sensor 91
Figure E.1 – SIMSEN model of the test case 94
Figure E.2 – Performance hill chart of the Francis turbine for different guide vane openings 94
Figure E.3 – Elementary hydraulic pipe of length dx and its equivalent circuit 96
Figure E.4 – Forced response for a = 50 m/s (left) and a = 60 m/s (right) 97
Figure E.5 – Forced response for a = 70 m/s (left) and a = 80 m/s (right) 98
Figure E.6 – Forced response for a = 90 m/s (left) and a = 100 m/s (right) 98
Figure E.7 – Damping and eigenfrequency for a = 50 m/s (left) and a = 60 m/s (right) 98
Figure E.8 – Damping and eigenfrequency for a = 70 m/s (left) and a = 80 m/s (right) 98
Figure E.9 – Damping and eigenfrequency for a = 90 m/s (left) and a = 100 m/s (right) 99
Figure E.10 – Eigenmode for a = 50 m/s and eigenfrequency f = 4,18 Hz 99
Figure E.11 – Eigenmode for a = 50 m/s and eigenfrequency f = 3,67 Hz 99
Figure E.12 – Eigenmode for a = 100 m/s and eigenfrequency f = 2,61 Hz 99
Figure E.13 – Draft tube modelled with cavitation compliance and draft tube inductance 100
Figure E.14 – Simplified model of a cavitation draft tube connected to a tailrace pipe composed by cavitation compliance of the draft tube and downstream inductance of the tailrace pipe 101
Figure E.15 – Hydraulic system modelled by an equivalent pipe and corresponding modes shapes for the first and second natural frequencies 102
Figure E.16 – Hydraulic systems 1, 2 and 3 103
Figure F.1 – Influence of Thoma number on pressure fluctuation 108
Figure F.2 – Example of waterfall diagram of the pressure fluctuations as function of the frequency and Thoma number 109
Figure G.1 – Peak-to-peak value of pressure fluctuations as a function of the discharge factor measured on the model and the corresponding prototype 110
Figure G.2 – Layout of EPFL test rig PF3 1-D hydroacoustic model 111
Figure G.3 – Electrical T-shaped representation of the cavitation vortex rope developing in Francis turbine draft tube in part load conditions 111
Figure G.4 – Excitation system and 3D cut-view of the rotating valve 113
Figure G.5 – Strouhal number of the precession frequency as a function of the swirl number computed with Formula (G.6) 114
Figure G.6 – Strouhal number of the first eigenfrequency of the test rig as a function of swirl number (a), the wave speed in the draft tube determined in the 1-D model (b) 115
Figure G.7 – Predicted values of precession frequency and first eigenfrequency at the prototype scale as a function of the output power of the generating unit 116
Figure G.8 – Comparison between observed and predicted values of the precession frequency f_{rope} and the first eigenfrequency f_0 of a 444 MW hydropower unit (HYPERBOLE project test case) 117
Figure G.9 – Hill chart comparing the measured and the predicted resonance conditions assuming a constant pressure value in the draft tube cone of the prototype 118
Figure H.1 – Pressure fluctuations versus discharge factor 120

IECNORM.COM : Click to view the full PDF of IEC TS 62882:2020

Figure H.2 – Normalized discharge of pressure fluctuations 120
Figure H.3 – Normalized pressure amplitude of pressure fluctuations 120
Figure H.4 – Comparison of pressure fluctuations of model and prototype 120
Figure H.5 – Set of pressure fluctuation of models and prototypes for draft tube analysis 121
Figure H.6 – Difference between pressure fluctuations between the model and the prototype 122
Figure H.7 – Standard deviation of difference of pressure fluctuation 122
Figure H.8 – Transposition accuracy for draft tube cone 123
Figure H.9 – Transposition of each power plant test case for the draft tube cone 126
Figure H.10 – Set of pressure fluctuation of models and prototypes for vaneless zone analysis 127
Figure H.11 – Difference between pressure fluctuations between the model and the prototype 127
Figure H.12 – Standard deviation of difference of pressure fluctuation 128
Figure H.13 – Transposition accuracy for vaneless zone 128
Figure H.14 – Transposition of each power plant test case for vaneless zone 129
Figure H.15 – Set of pressure fluctuation of models and prototypes for spiral case analysis 130
Figure H.16 – Difference between pressure fluctuations between the model and the prototype 131
Figure H.17 – Standard deviation of difference of pressure fluctuation 131
Figure H.18 – Transposition accuracy for spiral case 132
Figure H.19 – Transposition of each power plant test cases for spiral case 133
Figure J.1 – Comparison of pressure fluctuations on the draft tube for 10 Chinese model and prototype references 135
Figure J.2 – Comparison of pressure fluctuations on the draft tube for one France model and prototype reference 136
Figure J.3 – Comparison of pressure fluctuations on the spiral case for one France model and prototype reference 136
Figure J.4 – Comparison of pressure fluctuations on the draft tube for one Norway model and prototype reference 137

Table 1 – Pressure fluctuation overview matrix 27
Table 2 – Locations of pressure fluctuations transducers 44
Table 3 – Accuracy for transposition of fluctuation amplitude in draft tube cone 58
Table 4 – Accuracy for transposition of fluctuation amplitude in vaneless zone 58
Table 5 – Accuracy for transposition of fluctuation amplitude in spiral case 59
Table D.1 – $f_{1/4}$ and dec calculated for p_1 to p_4 88
Table D.2 – Estimated frequencies based on tubing mechanical characteristics 89
Table D.3 – Peak-to-peak value on the raw signals 90
Table D.4 – Wave speed and damping ratio 90
Table D.5 – Peak-to-peak value on the corrected signals 92
Table E.1 – Francis turbine parameters 94
Table E.2 – Parameters of the hydraulic systems 1, 2 and 3 103
Table E.3 – Parameters of the equivalent pipe of the hydraulic system 1 104

IECNORM.COM : Click to view the full PDF of IEC TS 62882:2020

Table E.4 – Estimation of the natural frequencies f_0 to f_6 of the hydraulic system 1 based on Formulae (E.9) and (E.11) and comparison with results obtained with eigenvalue calculation and corresponding errors 105
Table E.5 – Parameters of the equivalent pipe of the hydraulic system 2 105
Table E.6 – Estimation of the natural frequencies f_0 to f_6 of the hydraulic system 2 based on Formulae (E.10) and (E.11) and comparison with results obtained with eigenvalue calculation and corresponding errors 105
Table E.7 – Parameters of the equivalent pipe of the hydraulic system 3 106
Table E.8 – Estimation of the natural frequencies f_0 to f_6 of the hydraulic system 3 based on Formulae (E.10) and (E.11) and comparison with results obtained with eigenvalue calculation and corresponding errors 107
Table E.9 – Pressure mode shape obtained by eigenvalue and eigenvector calculation for the three first natural frequencies f_1, f_2 and f_3 of the hydraulic systems 1 and 2 107
Table H.1 – World hydropower plant references 121

IECNORM.COM : Click to view the full PDF of IEC TS 62882:2020

INTERNATIONAL ELECTROTECHNICAL COMMISSION

_____

HYDRAULIC MACHINES – FRANCIS TURBINE PRESSURE FLUCTUATION TRANSPOSITION

FOREWORD

1) The International Electrotechnical Commission (IEC) is a worldwide organization for standardization comprising all national electrotechnical committees (IEC National Committees). The object of IEC is to promote international co-operation on all questions concerning standardization in the electrical and electronic fields. To this end and in addition to other activities, IEC publishes International Standards, Technical Specifications, Technical Reports, Publicly Available Specifications (PAS) and Guides (hereafter referred to as "IEC Publication(s)"). Their preparation is entrusted to technical committees; any IEC National Committee interested in the subject dealt with may participate in this preparatory work. International, governmental and non-governmental organizations liaising with the IEC also participate in this preparation. IEC collaborates closely with the International Organization for Standardization (ISO) in accordance with conditions determined by agreement between the two organizations.
2) The formal decisions or agreements of IEC on technical matters express, as nearly as possible, an international consensus of opinion on the relevant subjects since each technical committee has representation from all interested IEC National Committees.
3) IEC Publications have the form of recommendations for international use and are accepted by IEC National Committees in that sense. While all reasonable efforts are made to ensure that the technical content of IEC Publications is accurate, IEC cannot be held responsible for the way in which they are used or for any misinterpretation by any end user.
4) In order to promote international uniformity, IEC National Committees undertake to apply IEC Publications transparently to the maximum extent possible in their national and regional publications. Any divergence between any IEC Publication and the corresponding national or regional publication shall be clearly indicated in the latter.
5) IEC itself does not provide any attestation of conformity. Independent certification bodies provide conformity assessment services and, in some areas, access to IEC marks of conformity. IEC is not responsible for any services carried out by independent certification bodies.
6) All users should ensure that they have the latest edition of this publication.
7) No liability shall attach to IEC or its directors, employees, servants or agents including individual experts and members of its technical committees and IEC National Committees for any personal injury, property damage or other damage of any nature whatsoever, whether direct or indirect, or for costs (including legal fees) and expenses arising out of the publication, use of, or reliance upon, this IEC Publication or any other IEC Publications.
8) Attention is drawn to the Normative references cited in this publication. Use of the referenced publications is indispensable for the correct application of this publication.
9) Attention is drawn to the possibility that some of the elements of this IEC Publication may be the subject of patent rights. IEC shall not be held responsible for identifying any or all such patent rights.

The main task of IEC technical committees is to prepare International Standards. In exceptional circumstances, a technical committee may propose the publication of a technical specification when

- the required support cannot be obtained for the publication of an International Standard, despite repeated efforts, or
- the subject is still under technical development or where, for any other reason, there is the future but no immediate possibility of an agreement on an International Standard.

Technical specifications are subject to review within three years of publication to decide whether they can be transformed into International Standards.

IEC TS 62882, which is a Technical Specification, has been prepared IEC technical committee 4: Hydraulic turbines.

IECNORM.COM : Click to view the full PDF of IEC TS 62882:2020

The text of this Technical Specification is based on the following documents:

Enquiry draft	Report on voting
4/375/DTS	4/398/RVDTS

Full information on the voting for the approval of this technical specification can be found in the report on voting indicated in the above table.

This document has been drafted in accordance with the ISO/IEC Directives, Part 2.

The committee has decided that the contents of this document will remain unchanged until the stability date indicated on the IEC website under "http://webstore.iec.ch" in the data related to the specific document. At this date, the document will be

- reconfirmed,
- withdrawn,
- replaced by a revised edition, or
- amended.

IMPORTANT – The 'colour inside' logo on the cover page of this publication indicates that it contains colours which are considered to be useful for the correct understanding of its contents. Users should therefore print this document using a colour printer.

IECNORM.COM : Click to view the full PDF of IEC TS 62882:2020

INTRODUCTION

With the increased amount of renewable energy that is being added to the electrical grid in the form of wind and solar, in addition to new energy in the form of nuclear, the grid needs to integrate more hydropower generation with flexible operation to balance loads. To meet this challenge, the hydraulic stability of the machine has become more and more important.

The current document provides a technical specification for Francis turbine pressure fluctuations. This document aims to describe pressure fluctuations, their phenomena and related problems, to define the relationship between model and prototype fluctuations, to identify methods to predict pressure fluctuations in prototypes through transposition of model measurements, and to suggest potential mitigations.

In this document, the term "turbine" refers to Francis turbines and pump-turbine operating as a turbine.

This document excludes all matters of purely commercial interest, except those inextricably bound within the conduct of the tests.

IECNORM.COM : Click to view the full PDF of IEC TS 62882:2020

HYDRAULIC MACHINES – FRANCIS TURBINE PRESSURE FLUCTUATION TRANSPOSITION

1 Scope

IEC 62882, which is a Technical Specification, provides pressure fluctuation transposition methods for Francis turbines and pump-turbines operating as turbines, including:

– description of pressure fluctuations, the phenomena causing them and the related problems;
– characterization of the phenomena covered by this document, including but not limited to inter-blade vortices, draft tube vortices rope and rotor-stator interaction;
– demonstration that both operating conditions and Thoma numbers (cavitation conditions) are primary parameters influencing pressure fluctuations;
– recommendation of ways to measure and analyse pressure fluctuations;
– identification of potential resonances in test rigs and prototypes;
– identification of methods, to transpose the measurement results from model to prototype or provide ways to predict pressure fluctuations in prototypes based on statistics or experience;
– recommendation of a data acquisition system, including the type and mounting position of model and prototype transducers and to define the similitude condition between model and prototype;
– presentation of pressure fluctuation measurements comparing the model turbine and the corresponding prototype;
– discussion of parameters used for the transposition from model to prototype, for example, the peak to peak value at 97 % confidence interval, the RMS value or the standard deviation in the time domain and the relation of main frequency and the rotational frequency in the frequency domain obtained by FFT;
– discussion of the uncertainty of the pressure fluctuation transposition from model to prototype;
– discussion of factors which influence the transposition, including those which cannot be simulated on the model test rig such as waterway system and mechanical system;
– establishment of the transposition methods for different types of pressure fluctuations;
– suggestion of possible methods for mitigating pressure fluctuation;
– definition of the limitations of the specification.

This document is limited to normal operation conditions. Hydraulic stability phenomena related to von Kármán vortices, transients, runaway speed and speed no load are excluded from this document.

This document provides means to identify potential resonances in model test rigs and prototype turbines. Scaling-up resonance conditions are not treated in this document. When resonance exists, the transposition methods identified in this document do not apply. Under these conditions, the relationship between model and prototype pressure fluctuations cannot be determined.

This document is concerned neither with the structural details of the machines nor the mechanical properties of their components, so long as these characteristics do not affect model pressure fluctuations or the relationship between model and prototype pressure fluctuations.

IECNORM.COM : Click to view the full PDF of IEC TS 62882:2020

2 Normative references

The following documents are referred to in the text in such a way that some or all of their content constitutes requirements of this document. For dated references, only the edition cited applies. For undated references, the latest edition of the referenced document (including any amendments) applies.

IEC 60193:2019, *Hydraulic turbines, storage pumps and pump-turbines – Model acceptance tests*

3 Terms, definitions, symbols and units

For the purposes of this document, the following terms and definitions apply.

ISO and IEC maintain terminological databases for use in standardization at the following addresses:

- IEC Electropedia: available at http://www.electropedia.org/
- ISO Online browsing platform: available at http://www.iso.org/obp

The contracting parties shall, in advance of the test, agree to clarification in writing of any term, definition or unit of measure in question.

IECNORM.COM : Click to view the full PDF of IEC TS 62882:2020

3.1 General terms and definitions

Entry number	Term	Definition
3.1.1	Point	item established by one or more consecutive sets of readings and/or recordings at unchanged operating condition and settings, sufficient to calculate the performance of the machine at this operating condition and these settings
3.1.2	Test	collection of points that is adequate to establish the performance of the machine over a specified range of operating conditions
3.1.3	Hydraulic performance	performance parameters attributable to the machine due to hydrodynamic effects
3.1.4	Main hydraulic performance data	subset of the hydraulic performance parameters, i.e. power, discharge and/or specific hydraulic energy, efficiency, pressure fluctuation, steady-state runaway speed and/or discharge[a]
3.1.5	Additional data	subset of hydraulic performance data, which can be determined for information on the model[b]
3.1.6	Guarantees	specified performance data contractually agreed to

[a] The influence of cavitation shall be considered.

[b] The prediction of the corresponding prototype data is less accurate than that achievable for the main hydraulic performance data, due to application of approximate similarity rules.

3.2 Units

The International System of Units (SI, see ISO 80000-4 [193][1]) has been used throughout this document.

All terms are given in SI base units or derived coherent units[2]. The basic equations are valid using these units. If other units are used for certain data which are not coherent SI units, proper consideration shall be provided. Examples of non-coherent units include kilowatt instead of watt

[1] Numbers in square brackets refer to the Bibliography.

[2] $N = kg \cdot m \cdot s^{-2}$ $Pa = kg \cdot m^{-1} \cdot s^{-2}$ $J = kg \cdot m^2 \cdot s^{-2}$ $W = kg \cdot m^2 \cdot s^{-3}$

for power, kilopascal or bar instead of pascal for pressure, min^{-1} instead of s^{-1} for rotational speed. Temperatures may be given in degrees Celsius since absolute temperatures (in kelvins) are rarely required.

Any other system of units may be used, but only if agreed in writing by the contracting parties.

3.3 Overview of the terms, definitions, symbols and units used in this document

Subclause	Title
3.3.1	Subscripts and symbols
3.3.2	Geometric terms
3.3.3	Physical quantities and properties
3.3.4	Discharge, velocity and speed terms
3.3.5	Pressure terms
3.3.6	Specific energy terms
3.3.7	Height and head terms
3.3.8	Power and torque terms
3.3.9	Efficiency terms
3.3.10	General terms relating to fluctuating quantities
3.3.11	Fluid dynamic and scaling terms
3.3.12	Dimensionless terms

IECNORM.COM : Click to view the full PDF of IEC TS 62882:2020

3.3.1 Subscripts and symbols

Entry number	Subscript or symbol	Definition
3.3.1.1	1	high pressure[a] section of the machine to which the performance guarantees refer
3.3.1.2	2	low pressure[a] section of the machine to which the performance guarantees refer
3.3.1.3	1', 1''.	high pressure measuring sections[b]
3.3.1.4	2', 2''.	low pressure measuring sections[c]
3.3.1.5	H	subscript denoting values related to a given head
3.3.1.6	sp	subscript denoting values of quantities such as rotational speed, discharge, etc., for which other quantities are guaranteed
3.3.1.7	max or min	subscript denoting maximum or minimum values of any term
3.3.1.8	P	subscript denoting values related to the full size machine
3.3.1.9	M	subscript denoting values related to the model
3.3.1.10	ref	subscript denoting values related to a specified reference condition
3.3.1.11	opt	subscript denoting the best efficiency point
3.3.1.12	amb	subscript referring to surrounding atmospheric conditions
3.3.1.13	pl	subscript denoting values related to the operating conditions of the prototype in the plant
3.3.1.14	R	subscript referring to runaway conditions
3.3.1.15	B	subscript referring to the runner blade of a machine
3.3.1.16	G	subscript referring to the guide vane of a machine
3.3.1.17	a	subscript referring to an axial component of force or torque
3.3.1.18	r	subscript referring to a radial component of force or torque
3.3.1.19	m	meridional direction in a rotating system
3.3.1.20	u	rotational direction in a rotating system
3.3.1.21	x, y, z	subscript referring to machine coordinates
3.3.1.22	th	subscript referring to theoretical value
3.3.1.23	h	subscript referring to hydraulic value

[a] The terms "high pressure" and "low pressure" define the two sides of the machine irrespective of the flow direction and therefore are independent of the mode of operation of the machine.

[b] Whenever possible, these sections should coincide with section 1; otherwise the measured values shall be adjusted to section 1.

[c] Whenever possible, these sections should coincide with section 2; otherwise, the measured values shall be adjusted to section 2 (see IEC 60193).

IECNORM.COM : Click to view the full PDF of IEC TS 62882:2020

3.3.2 Geometric terms and definitions

Entry number	Term	Definition	Symbol	Unit
3.3.2.1	Area	net cross-sectional area normal to nominal flow direction	A	m^2
3.3.2.2	Surface area	total area of a surface (of the runner, flow passages, etc.)	S	m^2
3.3.2.3	Guide vane opening	average shortest distance between adjacent guide vanes (at a specified section if necessary)	a	m
3.3.2.4	Guide vane angle	average vane angle measured from the closed position	α	°
3.3.2.5	Reference diameter	reference diameter of the hydraulic machine (see Figure 1)	D	m
3.3.2.6	Number of runner blades	number of runner blades	Z_B	-
3.3.2.7	Number of guide vanes	number of guide vanes	Z_G	-
3.3.2.8	Length scale ratio	ratio of representative prototype to model lengths[a]	λ_L	-
3.3.2.9	Level	elevation of a point in the system above the specified reference datum[b]	z	m
3.3.2.10	Dimension	corresponding model and prototype dimension	L	m

[a] In normal cases, this is the reference diameter of the machine. In cases where it is difficult to verify this reference, then another significant length may be taken.

[b] Usually mean sea level.

IECNORM.COM : Click to view the full PDF of IEC TS 62882:2020

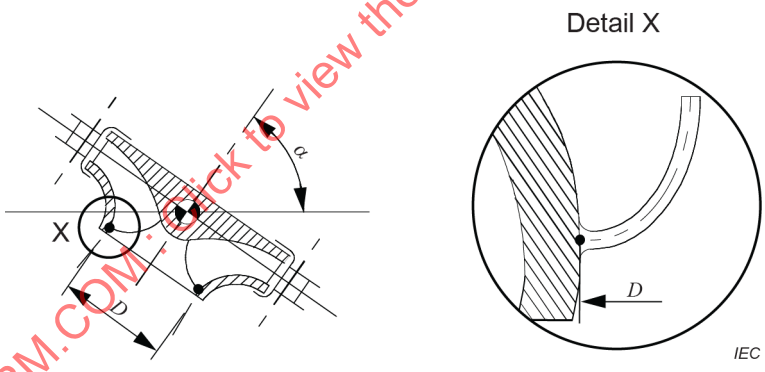


Figure 1 – Reference diameter of Francis turbine

3.3.3 Physical quantities and properties terms and definitions

Entry number	Term	Definition	Symbol	Unit
3.3.3.1	Acceleration due to gravity	local value of gravitational acceleration at the place of testing as a function of altitude and latitude (see IEC 60193)	g	$m \cdot s^{-2}$
3.3.3.2	Temperature	temperature of water in Celsius (see IEC 60193)	θ	°C
3.3.3.3	Density	mass per unit volume of water (see IEC 60193)	ρ, ρ_w [a]	$kg \cdot m^{-3}$
3.3.3.4	Vapour pressure (absolute)	absolute partial pressure of saturated vapour in a medium where liquid and gaseous phases of a body are in thermodynamic balance[b]	p_{va}	Pa
3.3.3.5	Dynamic viscosity	quantity characterizing the mechanical behaviour of a fluid (see ISO 80000-4)	μ	Pa·s
3.3.3.6	Kinematic viscosity	ratio of the dynamic viscosity to the density of a fluid (see IEC 60193)	ν	$m^2 \cdot s^{-1}$

[a] ρ is commonly used instead of ρ_w.

[b] The vapour pressure depends only on the temperature.

3.3.4 Discharge, velocity and speed terms and definitions

Entry number	Term	Definition	Symbol	Unit
3.3.4.1	Discharge (volume flow rate)	volume of water per unit time passing through any section in the system	Q	$m^3 \cdot s^{-1}$
3.3.4.2	Mass flow rate	mass of water flowing through any section of the system per unit time[a]	(ρQ)	$kg \cdot s^{-1}$
3.3.4.3	Measured discharge	volume of water per unit time flowing through any measuring section	Q_1, or Q_2,	$m^3 \cdot s^{-1}$
3.3.4.4	Discharge at reference section	volume of water per unit time flowing through the reference section 1 or 2	Q_1 or Q_2	$m^3 \cdot s^{-1}$
3.3.4.5	Leakage flow	volumetric loss as illustrated in Figure 3	q	$m^3 \cdot s^{-1}$
3.3.4.6	Mean velocity	discharge Q divided by area A of the cross-section	v	$m \cdot s^{-1}$
3.3.4.7	Angular speed	radians per second	ω	$rad \cdot s^{-1}$
3.3.4.8	Absolute velocity	velocity measured in stationary reference frame	c	$m \cdot s^{-1}$
3.3.4.9	Peripheral velocity	peripheral velocity at the reference diameter: $u = \pi D n$	u	$m \cdot s^{-1}$
3.3.4.10	Relative velocity	velocity measured in moving (including rotating) reference frame	w	$m \cdot s^{-1}$
3.3.4.11	Rotational speed	number of revolutions per unit time	n	s^{-1}
3.3.4.12	Discharge at the best efficiency	best efficiency discharge at a given head	$Q_{opt,H}$	$m^3 \cdot s^{-1}$

[a] Both ρ and Q shall be determined at the same section and at the conditions existing in that section. The mass flow rate is constant between two sections if no water is added or removed.

IECNORM.COM : Click to view the full PDF of IEC TS 62882:2020

3.3.5 Pressure terms and definitions

Entry number	Term	Definition	Symbol	Unit
3.3.5.1	Absolute pressure	static pressure of a fluid measured with reference to a perfect vacuum	p_{abs}	Pa
3.3.5.2	Ambient pressure	absolute pressure ambient air[a]	p_{amb}	Pa
3.3.5.3	Gauge pressure	difference between the absolute static pressure of a fluid at the reference level of the pressure measuring instrument and the ambient pressure at the place and time of measurement: $p = p_{abs} - p_{amb}$	p	Pa
3.3.5.4	Peak-to-peak value of pressure fluctuation with a 97% confidence interval	difference between the maximum and minimum values of a pressure fluctuation signal which is determined with the aid of probability distribution applying counting methods and assuming a probability (e.g. 97 %). Note 1 to entry: Values occurring outside of this probability are ignored.	$\tilde{p}$	Pa

[a] Values for standard atmosphere are given as a function of elevation in IEC 60193.

3.3.6 Specific energy terms and definitions

In the International System of Units, mass (kg) is one of the base quantities. The energy per unit mass, known as specific energy, is used in this document as a primary term.

The term "head", which is energy per local unit weight, has the disadvantage that weight is a force which depends on the local value of acceleration due to gravity g, which changes mainly with latitude but also with altitude. Nevertheless, it will remain in use because it is very common. Therefore, both related energy terms are listed, the specific energy terms in 3.3.6 and head terms in 3.3.7. They differ only by the factor g.

Entry number	Term	Definition	Symbol	Unit
3.3.6.1	Specific hydraulic energy of machine	specific energy of water available between the high and low pressure reference sections 1 and 2 of the machine, taking into account the influence of compressibility (see IEC 60193)	E	$J \cdot kg^{-1}$
3.3.6.2	Suction specific potential energy of the machine	specific potential energy at section 2 corresponding to the difference between the reference level of the machine and the piezometric level at section 2 (see IEC 60193)	E_s	$J \cdot kg^{-1}$
3.3.6.3	Net positive suction specific energy	absolute specific energy at section 2 minus the specific energy due to the vapour pressure p_{va} referred to the reference level of the machine	$NPSE$	$J \cdot kg^{-1}$
3.3.6.4	Thoma number	dimensionless term indicating the conditions of cavitation under which the machine operates[a]	σ	-
3.3.6.5	Plant Thoma number	value of the Thoma number at the operating conditions of the prototype (see IEC 60193)	σ_{pl}	-

[a] It is expressed as the ratio of net positive suction specific energy NPSE to a specific hydraulic energy E (see IEC 60193).

IECNORM.COM : Click to view the full PDF of IEC TS 62882:2020

3.3.7 Height and head terms and definitions

Entry number	Term	Definition	Symbol	Unit
3.3.7.1	Net head	$H = E / g$ For the definition of E, see 3.3.6.1.	H	m
3.3.7.2	Suction height	$Z_s = E_s / g$ For the definition of E_s, see 3.3.6.2.	Z_s	m
3.3.7.3	Net positive suction head	$NPSH = NPSE / g$ For the definition of NPSE, see 3.3.6.3.	$NPSH$	m
3.3.7.4	Reference level of the machine	elevation of a point of the machine taken as reference for the setting of the machine (see Figure 2)	z_r	m
3.3.7.5	Cavitation reference level	elevation of a point of the machine taken as reference for cavitation evaluation during model tests	z_c	m
3.3.7.6	Reference level of the pressure measuring instrument	elevation of a pressure measuring device (see IEC 60193)	z_M	m
3.3.7.7	Distance between the reference level of the machine and the reference level of the instrument	$z_{rM} = z_r - z_M$	z_{rM}	m
3.3.7.8	Velocity head based on runner speed	$H_{dyn,u} = u^2/2g$	$H_{dyn,u}$	m
3.3.7.9	Velocity head based on runner speed at inlet diameter	$H_{dyn,u1} = u_1^2/2g$	$H_{dyn,u1}$	m

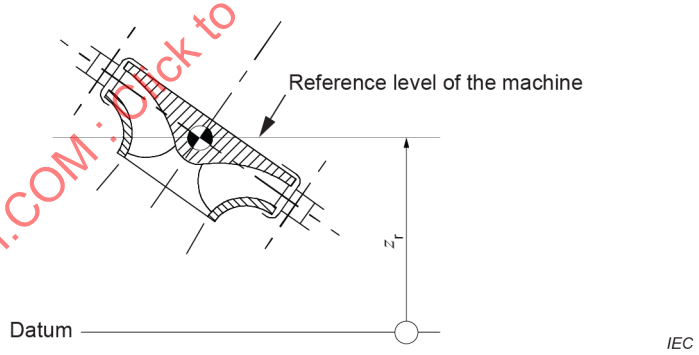
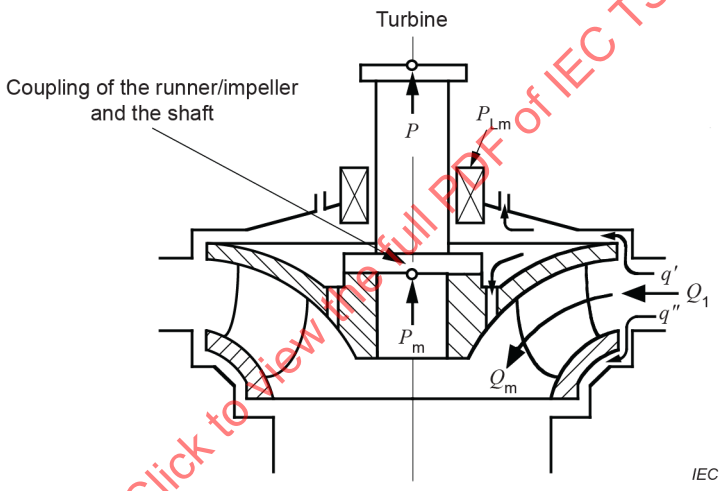


Figure 2 – Reference level of the Francis turbine

IECNORM.COM : Click to view the full PDF of IEC TS 62882:2020

3.3.8 Power and torque terms and definitions

Entry number	Term	Definition	Symbol	Unit
3.3.8.1	Hydraulic power	hydraulic power available for producing power: $P_h = E(\rho Q)_1$	P_h	W
3.3.8.2	Mechanical power of the machine (power)	mechanical power delivered by the turbine shaft, assigning to the hydraulic machine the mechanical losses of the relevant bearings and shaft seals (see Figure 3)	P	W
3.3.8.3	Mechanical power losses	mechanical power dissipated in guide bearings, thrust bearings and shaft seals of the hydraulic machine	P_{Lm}	W
3.3.8.4	Shaft torque	torque applied to the shaft of the hydraulic machine and corresponding to the mechanical power of the machine	T	N · m
3.3.8.5	Mechanical power of runner	mechanical power transmitted through the coupling of the runner and the shaft	P_m	W



NOTE 1

$q = q' + q''$

$Q_1 = Q_m + q$

$P_h = E(\rho Q)_1$

$P = P_m - P_{Lm}$

NOTE 2 The formulae ignore the compressibility of the water.

NOTE 3 For detailed analysis of internal losses, refer to IEC 60193.

NOTE 4 The disk friction losses and leakage losses (volumetric losses) are considered as hydraulic losses in 3.3.9.1. These "disk friction losses" are the friction losses of the outer surfaces of the runner/impeller not in contact with the flow Q_m passing the runner/impeller blades.

Figure 3 – Flux diagram for power and discharge

IECNORM.COM : Click to view the full PDF of IEC TS 62882:2020

3.3.9 Efficiency terms and definitions

Entry number	Term	Definition	Symbol	Unit
3.3.9.1	Hydraulic efficiency	ratio of mechanical power of the runner to the hydraulic power: $\eta_h = P_m / P_h$	η_h	-
3.3.9.2	Mechanical efficiency	$\eta_m = P / P_m$	η_m	-
3.3.9.3	Efficiency	$\eta = P / P_h = \eta_h \cdot \eta_m$	η	-

3.3.10 General terms and definitions relating to fluctuating quantities

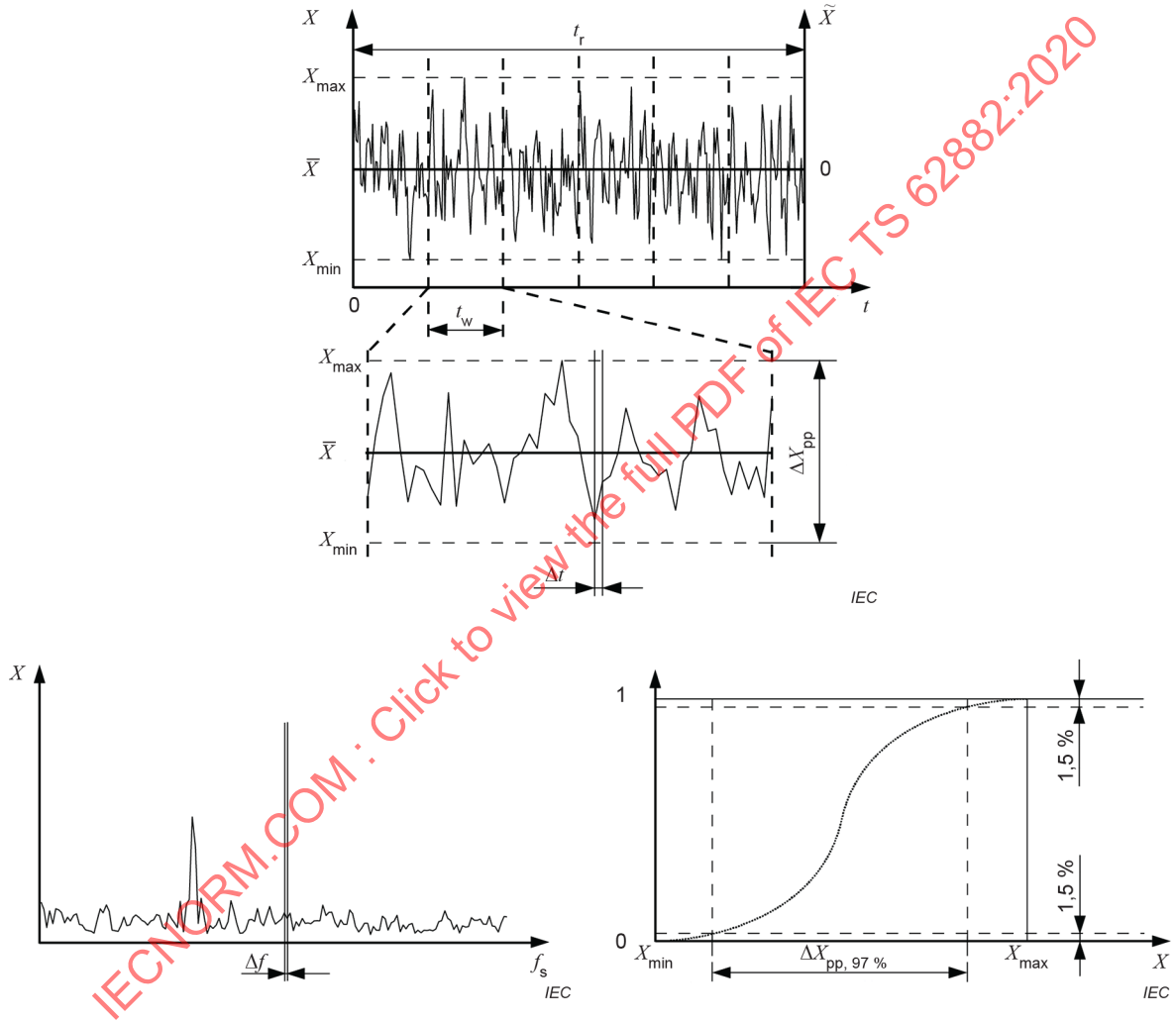
IEC 60994 and IEC 60193 provide a reference for terms relating to these quantities. The following table lists the terms relevant to this document, some of which are illustrated in Figure 4.

IECNORM.COM : Click to view the full PDF of IEC TS 62882:2020

Entry number	Term	Definition	Symbol
3.3.10.1	Discrete quantity	quantity represented by a sequence of its momentary values	X
3.3.10.2	Discrete quantity n	value of the quantity n	X_n
3.3.10.3	Number of samples	total number of discrete quantities	N
3.3.10.4	Number of samples in a time window	total number of discrete quantities used in the time window duration	N_w
3.3.10.5	Mean value	algebraic sum of the discrete quantities divided by the number of samples $\bar{X} = \frac{\sum_1^N X_n}{N}$	$\bar{X}$
3.3.10.6	Fluctuation of quantity	oscillatory variation of a quantity X referred to its mean value during a time interval Δt previously selected	$\tilde{X}(t)$
3.3.10.7	Maximum value	maximum value in a chosen time interval	X_{max}
3.3.10.8	Minimum value	minimum value in a chosen time interval	X_{min}
3.3.10.9	Standard deviation (effective value referred to the mean)	root-mean-square value of the deviation of a set of numbers from the mean value $\tilde{X}_{eff} = \sqrt{\frac{\sum_1^N (X_n - \bar{X})^2}{N}}$	$\tilde{X}_{eff}$
3.3.10.10	Root-mean-square value	square root of the mean value squared $X_{rms} = \sqrt{\frac{\sum_1^N X_n^2}{N}}$	X_{rms}
3.3.10.11	Peak-to-peak value	$\Delta X_{pp} = X_{max} - X_{min}$	ΔX_{pp}
3.3.10.12	Peak-to-peak value with a 97% confidence interval	difference between the maximum and minimum values of a signal which is determined using a probability distribution function for a given probability value (e.g. 97 %) Note 1 to entry: This function is estimated by applying statistical counting. The signal values outside of the corresponding confidence interval are excluded.	$\Delta X_{pp,97\%}$
3.3.10.13	Amplitude	maximum value of a sinusoidal quantity $X(t)$: $A = \frac{1}{2}\Delta X_{pp}$	A
3.3.10.14	Time	time interval	t
3.3.10.15	Sampling time interval	time interval between two consecutive samples	Δt
3.3.10.16	Frequency	inverse of period s^{-1} (Hz)	f
3.3.10.17	Sampling frequency (sampling rate)	inverse of the sampling time interval $f_s = 1 / \Delta t$	f_s
3.3.10.18	Time window duration	selected time window for frequency analyses by Fourier transform methods: $t_w = N_w \cdot \Delta t$	t_w
3.3.10.19	Frequency resolution	frequency interval between two consecutive values in the discrete Fourier transform $\Delta f = 1 / t_w = f_s / N_w$	Δf

IECNORM.COM : Click to view the full PDF of IEC TS 62882:2020

Entry number	Term	Definition	Symbol
3.3.10.20	Signal record time duration (acquisition time)	period of time during which a signal from a transducer is recorded (in seconds)	t_r
3.3.10.21	Synchronous pressure fluctuation	pressure fluctuation in the same phase over a cross section perpendicular to the nominal flow direction	$\tilde{p}_{syn}$
3.3.10.22	Asynchronous pressure fluctuation	pressure fluctuation phase which varies over a cross section perpendicular to the nominal flow direction	$\tilde{p}_{asyn}$



IECNORM.COM : Click to view the full PDF of IEC TS 62882:2020

a) A pressure fluctuation signal over a defined signal recording time (t_r). A minimum of five window time lengths (t_w) shall be included in each signal record time duration.

b) The signal transformed into the frequency domain using Fourier analysis. The frequency resolution (Δf) required for each analysis is determined by the speed of rotation of the machine.

c) Using probability distribution, each measure point from Figure 4a) is cumulated, and extreme deviations from the mean fluctuation are removed. A 97 % interval of confidence is illustrated in this figure.

Figure 4 – Illustration of some definitions related to fluctuating quantities

3.3.11 Fluid dynamic and scaling terms and definitions

Entry number	Term	Definition	Symbol	Unit
3.3.11.1	Reynolds number	ratio of inertia forces to viscous forces: $Re = D \cdot u \,/\, \nu$	Re	-
3.3.11.2	Froude number [a]	square root of the ratio of inertia forces to gravity forces: $Fr = \left[\frac{E}{gD}\right]^{1/2}$	Fr	-
3.3.11.3	Weber number [b]	ratio of inertia forces to surface tension forces: $We = \left[\frac{\rho \cdot L \cdot v^2}{\sigma^*}\right]^{1/2}$ where v is the velocity σ^* is the surface tension ρ is the density L is a linear dimension	We	-
3.3.11.4	Euler number	ratio of pressure forces to inertia forces: $Eu = \frac{\Delta p}{\rho v^2}$ where Δp is the differential pressure	Eu	-
3.3.11.5	Mach number	ratio of flow velocity to local speed of sound: $Ma = v/a$ where v is the fluid velocity a is the pressure wave propagation velocity	Ma	
3.3.11.6	Strouhal number	dimensionless number describing oscillating flow mechanism: $St = fL/v$ where $f$is the frequency of fluctuation L is the characteristic length v is the fluid velocity	St	

[a] See ISO 80000-11 [194].

[b] Other definitions of these numbers can be found in relevant scientific works.

IECNORM.COM : Click to view the full PDF of IEC TS 62882:2020

3.3.12 Dimensionless terms and definitions

Machine performance may be characterized by dimensionless terms based on $E = 1$, $D = 1$ and $\rho = 1$ or on $n = 1$, $D = 1$ and $\rho = 1$.

The units are: H (m); D (m); E (J·kg^{-1}); n (s^{-1}); ρ (kg·m^{-3}); T (N·m); P (W); Q (m^3·s^{-1}).

The relations of these dimensionless terms to other existing definitions are given below.

Entry number	Term	Definition	Symbol	Relations
3.3.12.1	Speed factor	$\frac{nD}{E^{0,5}}$	n_{ED}	$= \frac{1}{E_{nD}^{0,5}}$
3.3.12.2	Discharge factor	$\frac{Q_1}{D^2 E^{0,5}}$	Q_{ED}	$= \frac{Q_{nD}}{E_{nD}^{0,5}}$
3.3.12.3	Torque factor	$\frac{T_m}{\rho_1 D^3 E}$	T_{ED}	$= \frac{T_{nD}}{E_{nD}} = \frac{P_{ED}}{2\pi n_{ED}}$
3.3.12.4	Power factor[a]	$\frac{P_m}{\rho_1 D^2 E^{1,5}}$	P_{ED}	$= Q_{ED}\eta_{hT}$ (turbine) $= \frac{Q_{ED}}{\eta_{hP}}$ (pump) $= \frac{P_{nD}}{E_{nD}^{1,5}} = P_{nD} n_{ED}^3$ $= 2\pi n_{ED} T_{ED}$
3.3.12.5	Thoma number	$\frac{NPSE}{E}$	σ	$= \frac{\sigma_{nD}}{E_{nD}} = \sigma_{nD} n_{ED}^2$
3.3.12.6	Cavitation coefficient	$\frac{NPSE}{n^2 D^2}$	σ_{nD}	$= \sigma E_{nD} = \frac{\sigma}{n_{ED}^2}$
3.3.12.7	Specific speed	$\frac{nQ^{0,5}}{E^{0,75}}$	N_{QE}	$= n_{ED} Q_{ED}^{0,5} = \frac{Q_{nD}^{0,5}}{E_{nD}^{0,75}}$
3.3.12.8	Factor of pressure fluctuation	$\frac{\tilde{p}}{\rho E}$	$\tilde{P}_E$	
3.3.12.9	Coefficient of pressure fluctuation	$\frac{\tilde{p}}{\rho n^2 D^2}$	$\tilde{P}_{nD}$	
3.3.12.10	Relative discharge	$\frac{Q_H}{Q_{opt,H}}$	$Q_{H,rel}$	
3.3.12.11	Frequency coefficient	f/n	f_n	

[a] Reference is made to the mechanical power of the runner/impeller, usually measured on the model.

IECNORM.COM : Click to view the full PDF of IEC TS 62882:2020

4 Description of pressure fluctuation phenomena

4.1 General

Pressure fluctuations are a natural occurrence in hydraulic machinery and can be of both periodic and stochastic nature. They are influenced by machine design, operating conditions and by the dynamic response of the water conduits and rotating components. Pressure fluctuations are actually a part of hydroacoustic phenomena involving unsteady pressure and flow velocity distributions. They can result in fluctuations of shaft torque, rotational speed, hydraulic loads, etc., as well as vibrations of the machine.

Low frequency disturbances are of special interest because they can propagate to the whole water conduit and the rotating parts of the electric machine.

The draft tube surge of Francis turbines and reversible pump-turbines is perhaps the most commonly identified phenomenon among low frequency pressure fluctuations. In these

machines, an outlet swirl motion can develop at the runner low pressure side, inducing pressure fluctuations. In addition, cavitation can change the natural frequencies of the hydraulic system.

Turbine runners give an excitation at the rotational frequency multiplied by the number of runner blades, usually defined as the blade passing frequency. Due to the interaction of the runner blades with the guide vanes, stay vanes or spiral case, higher frequencies may be generated as multiples of the blade passing frequency.

Stochastic pressure fluctuations due to turbulent flow separation or intermittent pressure pulses due to vortex breakdown can take place in the extended operating range.

In order to deal effectively with a fluctuation issue, it is fundamental to understand the mode of fluctuation in each specific case. Table 1 shows a simplified fluctuation classification of the most common modes that will be explained in more detail through 4.2 to 4.4. Examples of typical time and frequency domain evaluations have also been added in Annex A to assist with the identification.

NOTE1 Table 1 is not a complete catalogue of all possible fluctuation modes. Some modes have been reported or proposed in various publications but are not included in the table, because they are either not very common or because they are not currently well understood.

NOTE2 m,n and k are local integers of arbitrary values in Clause 4.

IECNORM.COM : Click to view the full PDF of IEC TS 62882:2020

Table 1 – Pressure fluctuation overview matrix

Mode	Name	Description	Characteristics	Reference	Main concern problems	Typical mitigation
1	High load	Axisymmetric cavitating vortex rope, possibly self-excited pressure fluctuation	f_n = 0,15 to 0,5 $Q_{H,ref}$ = 1,1 to 1,5	Annex A, examples 1, 2 (Figure A.1 and Figure A.2)	Power swings Noise Fatigue in DT cone, spiral case, head cover and thrust bearing	Air admission Draft tube fins Runner cone
2	Best operation range	No rope	f_n undefined $Q_{H,ref}$ = 0,8 to 1,25	Annex A, example 3 (Figure A.3)	None, smooth operation	N/A
3	Upper part load	Draft tube cork screw cavitating vortex rope	f_n = 1 to 5 modulated by precessing rope $Q_{H,ref}$ = 0,7 to 0,95	Annex A, example 4 (Figure A.4)	Shock phenomena on draft tube wall Noise Fatigue in DT cone, spiral case and head cover Axial vibrations	Air admission Draft tube fins Runner cone
4.a	Part load	Part load stable vortex, one thread, asynchronous part	f_n = 0,2 to 0,4 $Q_{H,ref}$ = 0,4 to 0,95	Annex A, example 5 (Figure A.5)	Noise Fatigue in DT cone and head cover DT cone leakage Shaft line radial vibration	Air admission Draft tube fins Runner cone
4.b	Part load	Part load stable vortex, one thread, synchronous part	f_n = 0,2 to 0,4 $Q_{H,ref}$ = 0,4 to 0,95	Annex A, example 6 (Figure A.6)	Noise Fatigue in DT cone, runner, spiral case and penstock Axial vibrations Power swings	Air admission Draft tube fins Runner cone Power system stabilizer tuning
4.c	Part load	Part load stable vortex, several threads	f_n = (0,2 to 0,4) × (number of threads) $Q_{H,ref}$ = 0,4 to 0,6	Annex A, example 7 (Figure A.7)	Same as mode 4.a and 4.b	Air admission Draft tube fins Runner cone
5.a	Deep part load	Runner inter-blade vortices	f_n = 10 to 30 $Q_{H,ref}$ = 0,1 to 0,5	Annex A, example 8 (Figure A.8)	Runner fatigue Cavitation inside runner waterway	Air injection upstream or downstream of the runner

IECNORM.COM : Click to view the full PDF of IEC TS 62882:2020

Mode	Name	Description	Characteristics	Reference	Main concern problems	Typical mitigation
5.b	Deep part load	Random behaviour	Broadband excitation $Q_{H,ref}$ = 0,1 to 0,5	Annex A, example 8 (Figure A.8)	Noise Runner fatigue Shaft line torsional vibration Power swings	Air injection upstream or downstream of the runner
6.a	Rotor-stator interaction	Observed in stationary frame	$f_n = m \times Z_B$ $Q_{H,ref}$ = 0 to 1,5	Annex A, example 9 (Figure A.9)	Noise Fatigue in guide vanes, stay ring, spiral case, head cover and penstock Hydroacoustic or hydro mechanical resonance with spiral case, penstock, head cover, guide vanes and power house or parts of it	Modification of Z_B Runner blade inlet edge and guide vane shape modification Modification of vaneless zone Modification of natural frequency of structure Air injection
6.b	Rotor-stator interaction	Observed in rotating frame	$f_n = n \times Z_G$ $Q_{H,ref}$ = 0 to 1,5		Fatigue in runner Hydroacoustic resonance with runner	Modification of runner eigenfrequency Modification of vaneless zone Modification of natural frequency of structure Air injection
7.a	Speed no load	Hydro-mechanical mode, runaway operation of pump-turbines or high head turbines	f = 0,05 Hz to 0,12 Hz $Q_{H,ref}$ = ~0	Not addressed in this document	Difficult (sometimes impossible) synchronization with power network	Runner blade inlet edge modification Misaligned guide vanes Inlet valve partial closure
7.b	Speed no load	Flow separation in runner, guide vanes and stay vanes	f_n undefined Broad band excitation, random behavior	Not addressed in this document	Noise Vibration Pressure fluctuations Runner lifetime reduction	
8	Rotating stall	Pump-turbines and high head Francis turbines Interaction between runner, guide vanes and stay vanes: turbine brake operation	f_n = 0,5 to 0,7 $Q_{speed\ no\ load}$	Not addressed in this document	Stay vanes, guide vanes, runner blades and penstock pressure Radial thrust Torque oscillation	Runner blade inlet edge modification

IECNORM.COM : Click to view the full PDF of IEC TS 62882:2020

Mode	Name	Description	Characteristics	Reference	Main concern problems	Typical mitigation
9	von Karman vortices	Stay vanes, guide vanes or runner blades trailing edge von Karman vortices	St = 0,1 to 0,3	Not addressed in this document	Noise Fluid structure interaction and resonance Stay vanes, guide vanes or runner blade cracks Resonance with structures	Profile trailing edge modification Structural modification (detuning)

IECNORM.COM : Click to view the full PDF of IEC TS 62882:2020

4.2 Pressure fluctuations overview

Figure 5 shows a graphical representation of the pressure fluctuation modes that are treated in this document with corresponding discharge ranges. For a specific turbine, each fluctuation mode usually covers a smaller range than indicated in this diagram.

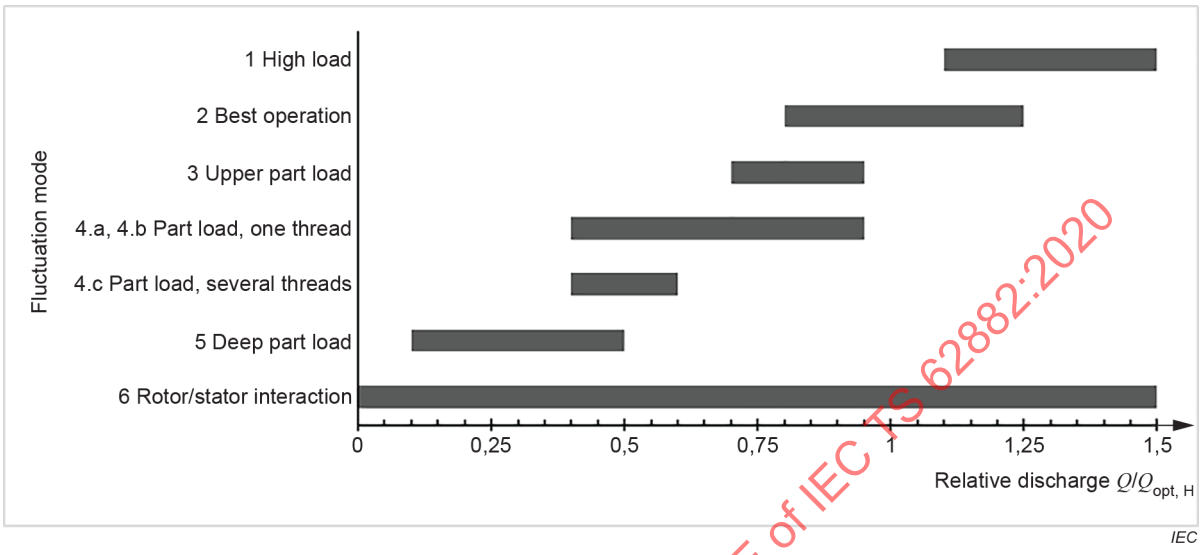
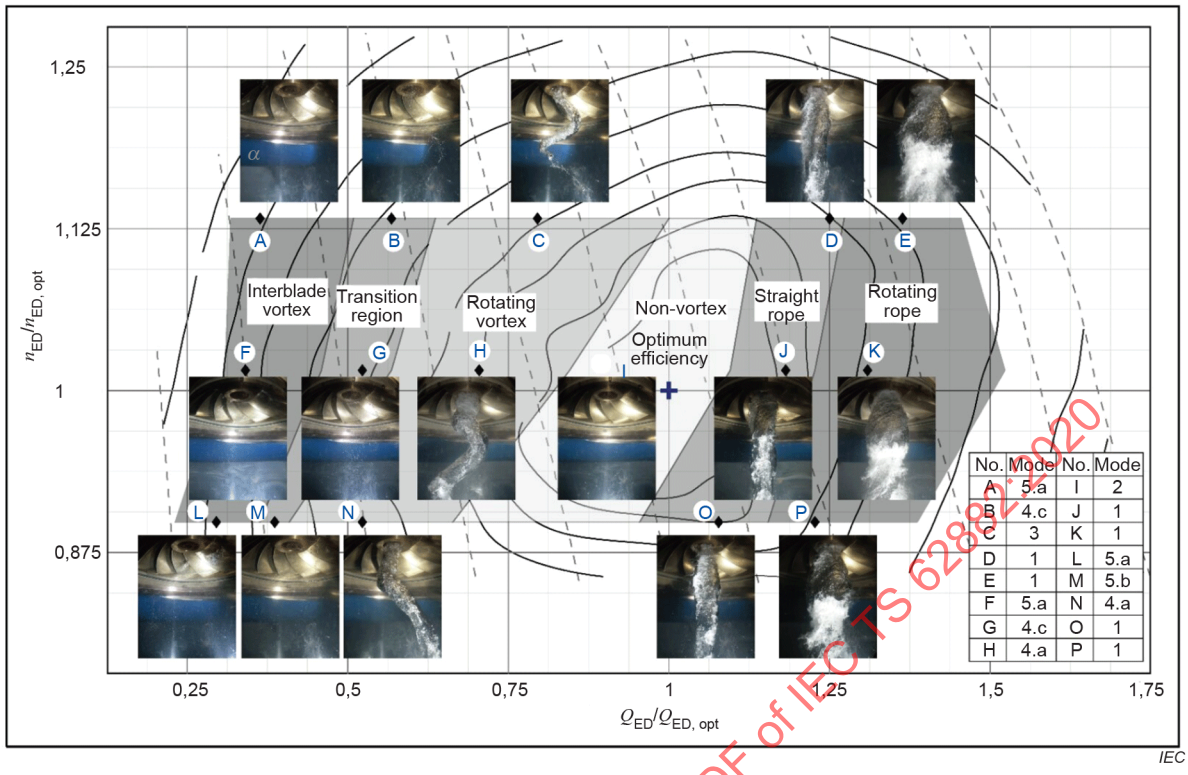


Figure 5 – Discharge range for the various fluctuation modes

Table 1 contains more detailed information for each mode. Figure 6 illustrates typical operation associated within a given mode and the corresponding location on a hill chart. Figure 7 shows a waterfall diagram of the fluctuations, which is a common way to present the data.

IECNORM.COM : Click to view the full PDF of IEC TS 62882:2020



No.	Mode	No.	Mode
A	5.a	I	2
B	4.c	J	1
C	3	K	1
D	1	L	5.a
E	1	M	5.b
F	5.a	N	4.a
G	4.c	O	1
H	4.a	P	1

More detailed descriptions of each fluctuation mode are provided in 4.3.

Key

— constant efficiency line

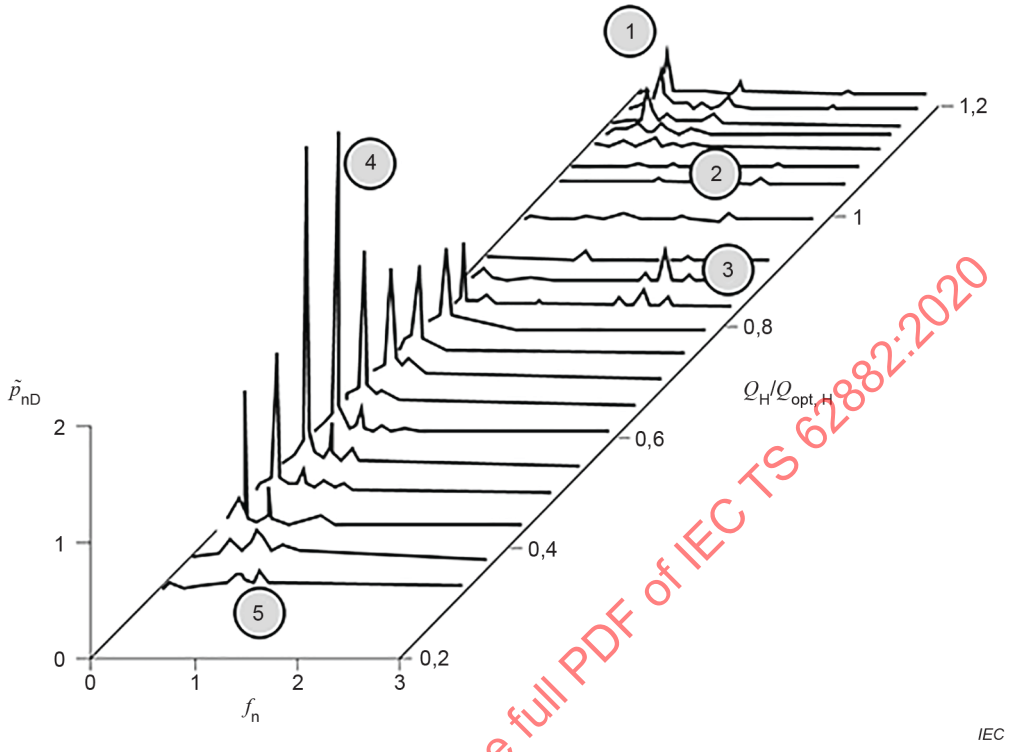
--- constant guide vane angle

\+ optimum efficiency point

NOTE A to P is operation point and draft tube phenomena; "mode" is the corresponding fluctuation mode in Table 1.

Figure 6 – Efficiency hill chart with pictures of swirling flow

IECNORM.COM : Click to view the full PDF of IEC TS 62882:2020



NOTE The numbers 1 to 5 correspond to the modes in Table 1.

Figure 7 – Example of a waterfall diagram of pressure amplitudes measured in the draft tube cone

IECNORM.COM : Click to view the full PDF of IEC TS 62882:2020

4.3 General description of draft tube flow in Francis turbines

Francis turbines operating at off design conditions may present instabilities in terms of pressure, discharge, rotational speed and torque. These phenomena are strongly linked to cavitating vortex cores in the draft tube that are induced by swirling flow at the runner outlet. The absolute velocity $\vec{c}$ of the flow within the turbine can be decomposed as the sum of the peripheral velocity of the turbine $\vec{u}$ and of the relative velocity $\vec{w}$ and is given by:

$$\vec{c} = \vec{u} + \vec{w}$$

NOTE In 4.3, subscript 1 refers to the high pressure side of the runner, subscript 2 refers to the low pressure side of the runner.

Velocity triangles at the inlet and outlet of a Francis turbine runner corresponding to operation at optimum operating conditions are illustrated in

Figure 8. The absolute velocity at the outlet $\vec{c_2}$ is usually designed to be nearly axial at the best efficiency point. The influence of the discharge on the velocity triangle at the runner outlet is illustrated in Figure 9. For discharges lower than the optimum discharge, the flow at the runner outlet contains a positive (i.e. in the runner rotation direction) absolute circumferential

velocity $\overrightarrow{c_{u2}}$, while for discharges larger than the optimum discharge, the circumferential velocity $\overrightarrow{c_{u2}}$ is negative.

As illustrated in Figure 9, the swirl below the turbine features either a precessing helical vortex rope for part load conditions or an axisymmetric vortex rope, with one or more elongated cells for full load conditions. The cavitation developing in the draft tube modifies the hydrodynamic characteristics of the draft tube flow, thereby modifying the natural frequencies of the entire hydraulic system. The volume of the gaseous vortex rope increases when the Thoma number σ is reduced. As a result, the natural frequencies of the hydraulic system decrease with the Thoma number. During part load operation, the interaction between the synchronous part of the excitation and the system natural frequencies may result in forced response hydroacoustic resonance and induce a so called draft tube surge and electrical power swing. During full load operation, the resulting axisymmetric vortex rope developing in the draft tube may, under certain conditions, start breathing as a result of the hydroacoustic system self-excitation. This phenomenon occurs when the hydraulic system damping becomes positive, resulting in a system instability. Possible resonances or system self-excitations are directly linked to the hydraulic system hydroacoustic characteristics. Their risk of occurrence therefore cannot be directly transposed from the model test to the prototype and requires specific methodologies for detailed analysis and prediction (see Annex E).

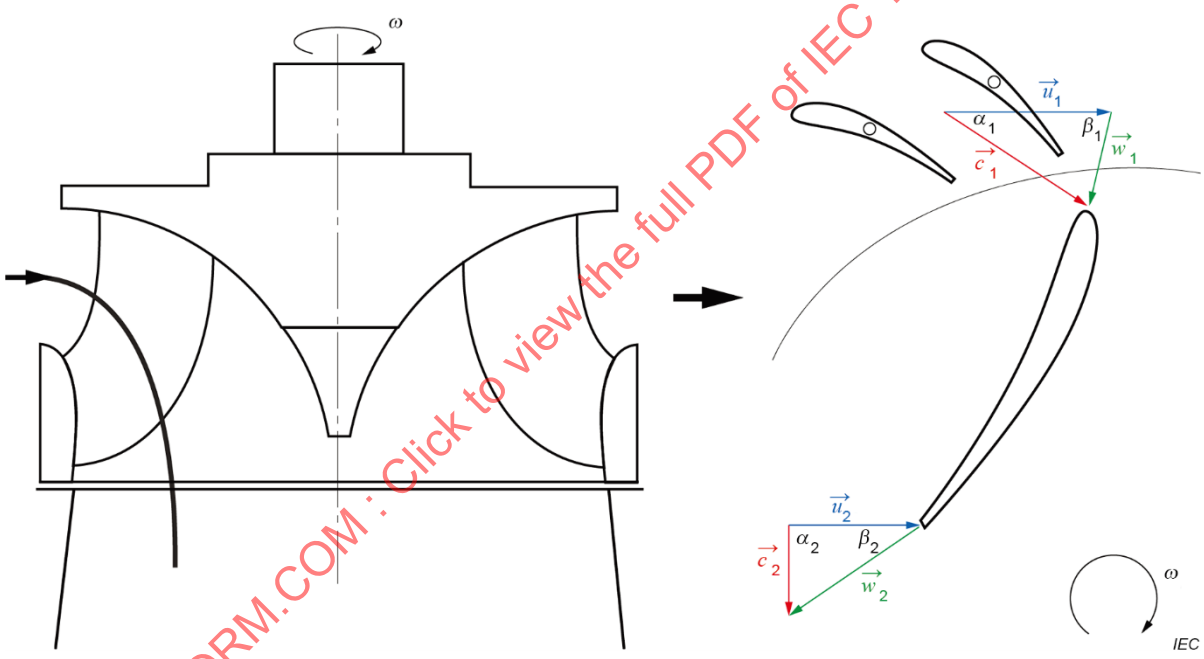


Figure 8 – Velocity triangles at inlet and outlet of the runner blade

IECNORM.COM : Click to view the full PDF of IEC TS 62882:2020

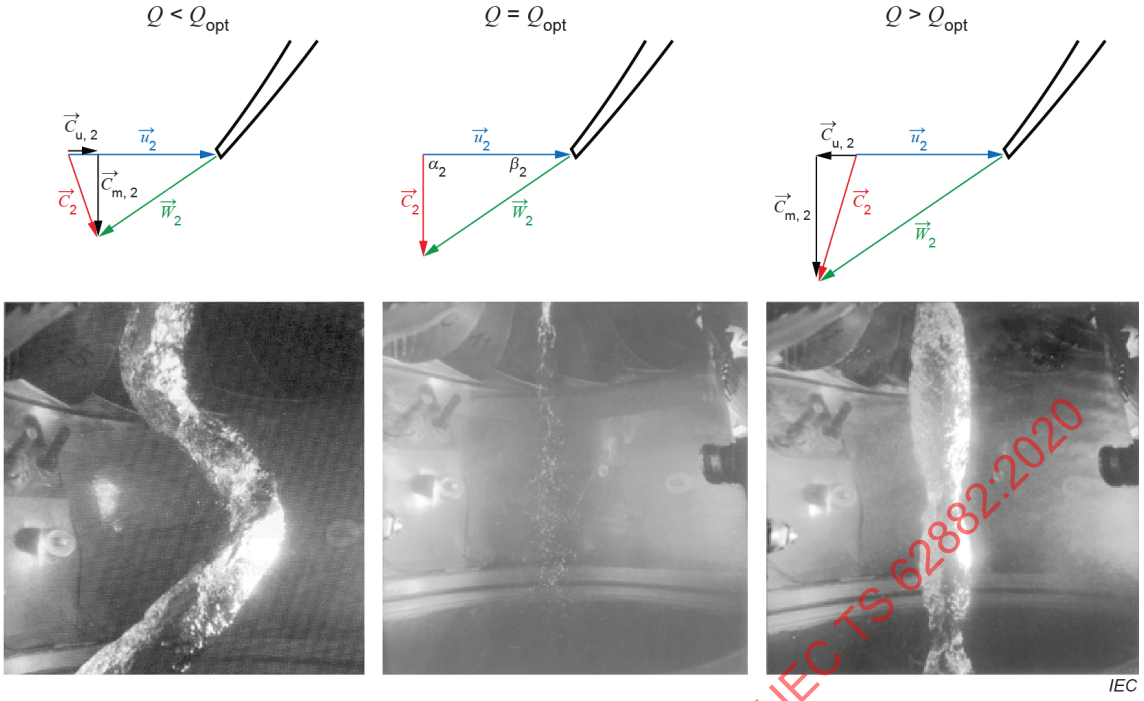


Figure 9 – Influence of the discharge on the circumferential component of the absolute velocity

IECNORM.COM : Click to view the full PDF of IEC TS 62882:2020

4.4 Detailed description of pressure fluctuation phenomena

4.4.1 Mode 1: Pressure fluctuation in high load

4.4.1.1 General characteristics

During full or overload operation, the cavitation rope may act as an energy source under certain conditions. This leads to self-excited pressure oscillations in the whole hydraulic system. These pressure fluctuations can be harmful to the mechanical and hydraulic system. Depending on the turbine relative location in the hydraulic circuit, the turbine discharge may oscillate and generate power swings. The frequency of the pressure fluctuation is usually lower than the rotational speed and corresponds to one of the hydro acoustic system natural frequencies.

4.4.1.2 Model test examples

See Figure A.1 and Figure A.2. The positions of pressure fluctuations transducers are shown on Figure 15. This mode occurs when the turbine is operating with discharges that are larger than the best efficiency point. In this mode, the draft tube cavity has an axisymmetric shape with one or several elongated cells. There is no precession of the rope in the draft tube and therefore no asynchronous component is present, leaving only the synchronous component.

Figure A.1 shows a case corresponding to limited high load, with $Q_{H,ref}$ = 1,26. This is often close to the maximum output design limit of a prototype turbine.

Review of the frequency domain shows the 14,7 Hz (f_n = 0,85) fluctuation. There are also some overtones and undertones present, indicating that the curve shape deviates from a perfect sine wave. The fluctuation originates in the draft tube (p_1 and p_2) and travels through the guide vanes up to the spiral case with only slight reduction in amplitude, as you would expect from a synchronous fluctuation. In the vaneless zone ($p_5(1)$ and $p_5(2)$), we can also see 225 Hz, which is the runner vane passing frequency. The 225 Hz fluctuation stays only in the vaneless zone and does not travel into the draft tube or spiral case.

Looking at the time domain, we see that the fluctuations in the draft tube (p_1 and p_2) are synchronous. The shapes of the time signals are very similar in the draft tube, vaneless zone and spiral case which is typical for synchronous fluctuations. The difference is that the vaneless zone fluctuations have the 225 Hz runner passing fluctuations superimposed.

In Figure A.2, we see an example of a large overload, $Q_{H,ref}$ = 1,44. This is normally far beyond the maximum output of the prototype turbine. It is nevertheless instructive to see that for this case the fluctuation amplitude in the draft tube is just as high as in high partial load.

In the frequency plane, we see the frequency 2,7 Hz (f_n = 0,15). This is a very distinct frequency, with no overtones. The amplitudes in the draft tube, vaneless zone and spiral case are the same. The vaneless zone also has the runner blade passing frequency (228 Hz) present with small amplitude.

Looking at the time domain, we see that the fluctuations in the draft tube (p_1 and p_2) are synchronous. The shapes of the time signals are very similar in the draft tube, vaneless zone and spiral case, which is also typical for synchronous fluctuations. The vaneless zone fluctuations have the 228 Hz runner passing fluctuations superimposed. It is also interesting to see the phase difference from the draft tube (p_1 and p_2) to the spiral case (p_3). The spiral case is approximately 0,03 s behind the draft tube, indicating that it takes 0,03 s for the pressure to travel from the draft tube to the spiral case. Considering that the speed of sound in a vapour/water mixture can be as low as 30 m/s, this time lag seems reasonable.

4.4.2 Mode 2: Pressure fluctuation in best operation range

4.4.2.1 General

This is an operation around the point of best efficiency at each head. During this operation, the flow in the draft tube cone is roughly axial. With little flow rotation, the centrifugal forces are small and a vapour cavity will not develop in the centre of the draft tube. Thus, the fluctuation amplitudes in the draft tube cone are generally small.

4.4.2.2 Model test examples

See Figure A.3. For this example, $Q_{H,ref}$ = 1,0. We see that the fluctuations in the draft tube, p_1 and p_2, have small amplitudes, approximately 10 % of the highest fluctuation amplitude. There is also no clear dominant frequency.

It is worth noting that the amplitude of fluctuations in the vaneless zone, p_5, is at its normal level in this mode.

4.4.3 Mode 3: Pressure fluctuation in upper part load

4.4.3.1 General characteristics

For the upper part load range pressure fluctuations may appear in the frequency range of 1 time to 5 times the runner rotational speed and feature modulations with vortex rope precession. It has been pointed out that for this particular operating point, the vortex rope features an elliptical cross section which is self-rotating.

Moreover, a "shock phenomenon" may occur in the same operating range and induce structural vibrations due to vortex rope impacts on the draft tube wall, usually in the inner part of the draft tube bend. Upper part load pressure fluctuations may also lead to resonance with the hydraulic system. In addition, the physical modulation process was identified to be related to the elliptical shape of the vortex rope cross section observed at upper part load. The motion of the elliptical vortex rope at upper part load can be decomposed into precession movement with fluctuation

IECNORM.COM : Click to view the full PDF of IEC TS 62882:2020

frequency ω_{rope} and self-rotation of the vortex rope with fluctuation frequency ω* as illustrated in Figure 10. From this follows the modulation process of the pressure fluctuations.

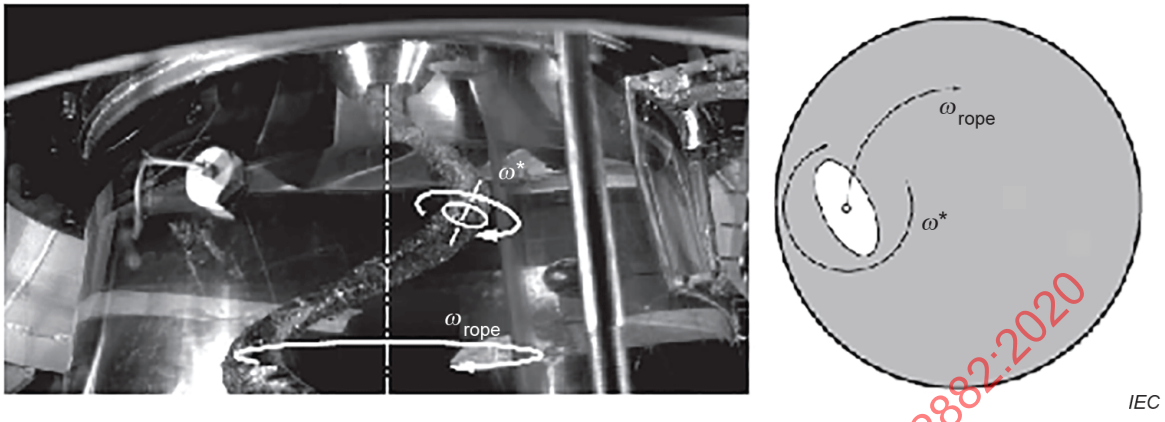


Figure 10 – Elliptical vortex rope precessing in the draft tube cone at upper part load

4.4.3.2 Model test examples

See Figure A.4. This mode is a special high frequency (f_n = 1 to 5) fluctuation produced typically at $Q_{H,ref}$ = 0,7~0,95. Other fluctuation modes, in particular mode 4, are often present together with this fluctuation.

Visually, we see a draft tube cavity, shaped like a "rope", which is rotating in the draft tube.

In Figure A.4, $Q_{H,ref}$ = 0,82. In the frequency domain, we see two dominant frequencies for p_1 and p_2. The frequency f_n = 0,3 is connected to fluctuation mode 4, while f_n = 2,0 is connected to this mode 3. As we see in the time domain, the mode 3 fluctuation is synchronous. In the frequency domain, we can thus see it at all transducer locations with the same amplitude. In comparison, we note that the mode 4 fluctuation is mainly asynchronous. Consequently, it has very low amplitude upstream of the draft tube, in p_3 and p_5.

4.4.4 Mode 4: Pressure fluctuation in part load

4.4.4.1 General

This mode is one of the most common fluctuation phenomena in hydro turbines. It can be further subdivided as indicated in 4.4.4.2 and 4.4.4.3.

4.4.4.2 Modes 4.a and 4.b – Part load

4.4.4.2.1 General characteristics

Swirling flow is defined to result from both axial and vortex motion. Increasing the swirl momentum at the inlet of the Francis turbine draft tube by reducing discharge, the draft tube flow starts from purely steady axial flow and suddenly becomes unsteady and features a precessing vortex. This phenomenon is known as the vortex breakdown and is expected when reverse flow occurs along the axis. The precessing motion of the vortex induced by the swirling flow depends on the ratio between the axial and swirl momentum and leads to pressure fluctuations with a frequency in the range between 0,2 times and 0,4 times the runner rotational frequency.

Furthermore, the pressure fluctuations in the draft tube can be decomposed into two components (see Figure 11):

a) an asynchronous component;

IECNORM.COM : Click to view the full PDF of IEC TS 62882:2020

b) a synchronous component.

The asynchronous part of the pressure fluctuations leads to unsteady pressure forces acting on the draft tube wall as well as on the runner itself and thus induces radial forces on the unit shaft line. The pressure waves induced by the synchronous part may result in hydroacoustic resonance with possible pressure fluctuations in the penstock and unit power swing. Using three pressure transducers located in a cross section of the draft tube, it is possible to determine both the asynchronous and the synchronous parts of the pressure fluctuations.

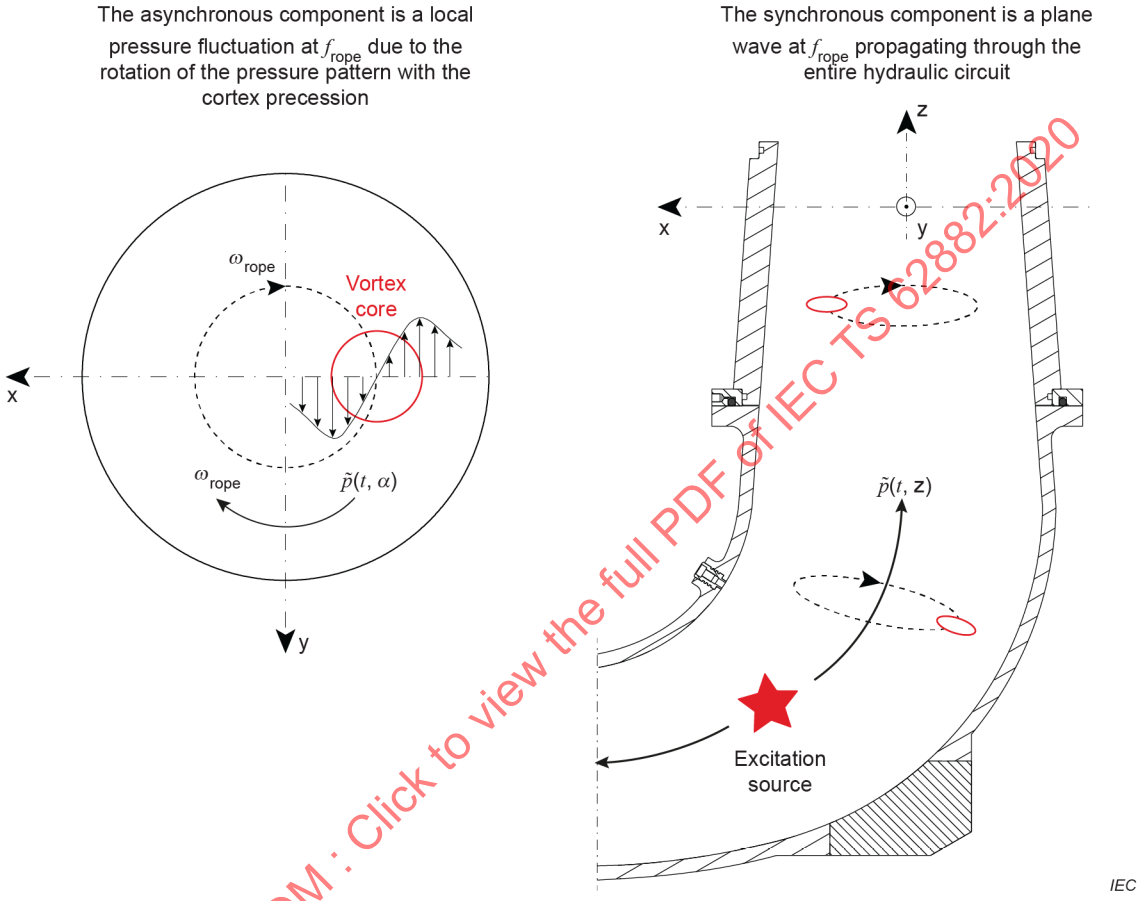


Figure 11 – Decomposition between the synchronous and asynchronous component of part load draft tube pressure fluctuations

IECNORM.COM : Click to view the full PDF of IEC TS 62882:2020

4.4.4.2.2 Model test examples

See Figure A.5 and Figure A.6. This mode occurs when the turbine is operating with discharges below the best efficiency point, in the range $Q_{H,ref}$ = 0,4~0,95. In this mode, the draft tube cavity has a shape like a spiral shaped rope that rotates around the draft tube cone. The rotation results in an asynchronous component of the pressure fluctuation.

Figure A.5 is for $Q_{H,ref}$ = 0,63. We see a fluctuation with f_n = 0,25 and close to 180° phase difference between p_1 and p_2, which indicates asynchronous fluctuation. Even so, a smaller synchronous component can be detected and is also present as a fluctuation with the same frequency at $p_5(1)$, $p_5(2)$ and p_3. In this case, the amplitude for blade passing frequency is very small, although clearly detectable in the frequency domain for $p_5(1)$ and $p_5(2)$.

Figure A.6 is for $Q_{H,ref}$ = 0,84. For both p_1 and p_2, f_n = 0,31, but in this case the synchronous component is bigger. This explains the difference in amplitude between p_1 and p_2, as seen most clearly in the frequency domain. The amplitude for each pressure transducer depends on the

phase relationship between the synchronous and asynchronous fluctuations for each particular transducer location. We also see that the blade passing frequency has high amplitude in $p_5(1)$.

4.4.4.3 Mode 4.c – Part load

4.4.4.3.1 General characteristics

This mode occurs at the low end of the part load range, typically $Q_{H,ref}$ = 0,4~0,6, where the rope in the draft tube is not stable and can disintegrate into several separate threads. Each thread will then give rise to its own fluctuation, resulting in a frequency two times to seven times higher than the frequency during operation at mode 4.a or mode 4.b.

4.4.4.3.2 Model test examples

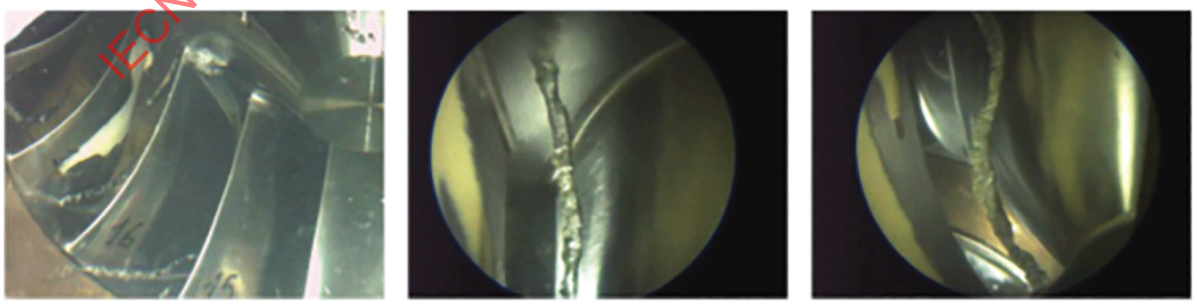
See Figure A.7, which is for $Q_{H,ref}$ = 0,50. The dominant frequency for p_1 is f_n = 1,00, while for p_2 f_n = 0,77. We also see that the frequency spectrum is much broader than for the examples with higher flow, indicating larger stochastic component. It is also difficult to identify a clear phase relationship between p_1 and p_2. Nevertheless, a small component with f_n = 0,21 can be found in p_3, indicating that a small synchronous component is present that is not connected to the formation of several threads. As expected, the blade passing frequency is clearly seen in $p_5(1)$ and $p_5(2)$.

4.4.5 Mode 5: Pressure fluctuation in deep part load

4.4.5.1 General characteristics

Decreasing the discharge of a Francis turbine by closing the guide vanes leads to an inappropriate angle of attack of the blade at the runner inlet with flow separation occurring on the blade suction side with possible recirculation in the inter-blade channel. This recirculation induces a vortex attached at the hub and extending along the blade suction side to the runner outlet close to the band. Depending on the cavitation Thoma number, cavitation appears in the vortex center (see Figure 12). Pressure fluctuations induced by the inter-blade vortex are characterized by a frequency corresponding to 10 times to 30 times the runner rotation frequency and result in force variations on the runner blades.

At deep part load, the draft tube flow features random behaviour with possible vortex rope which may appear and disappear without periodic characteristics leading to pressure fluctuations with broad frequency band. Cases are reported where the wide frequency range excited prototype shaft line torsional fluctuations that themselves induced resonance with the penstock due to rotational speed and head oscillations.



IEC

SOURCE: Yamamoto, 2016 [105]

Figure 12 – Example of inter-blade vortex

IECNORM.COM : Click to view the full PDF of IEC TS 62882:2020

4.4.5.2 Model test examples

See Figure A.8. The discharge for this mode is normally below the turbine continuous operating range, $Q_{H,ref}$ < 0,5. The flow in the draft tube is highly irregular and no clear frequency component is identifiable.

Figure A.8 is for $Q_{H,ref}$ = 0,25. In the frequency domain for p_1 and p_2, we see the presence of many frequencies over a large frequency range. Much of this "noise" is also present at p_3, $p_5(1)$ and $p_5(2)$. In $p_5(1)$ and $p_5(2)$, the runner blade passing frequency is present as usual.

4.4.6 Modes 6.a and 6.b: Rotor-stator interaction (RSI) pressure fluctuation

4.4.6.1 General characteristics

Francis turbines are subject to pressure fluctuations resulting from the interaction of the rotating parts and the stationary parts of the machine. This rotor-stator interaction (RSI) is the consequence of the interaction between the rotating flow perturbations caused by the runner blades and the flow perturbations caused by the guide vanes wakes (see Figure 13). This interaction induces pressure waves propagating in the entire hydraulic machine. As a result, the RSI phenomena may cause two different kinds of pressure fluctuations in the machine:

– diametrical pressure mode rotating in the vaneless zone between the guide vane and the runner blades;
– standing or travelling waves in the spiral case, also known as "phase resonance".

The first phenomenon may cause hydromechanics resonance between the rotating diametrical pressure mode and the structure of the runner or of the head cover and may induce strong vibrations, noise, crack or premature guide vanes bearing wear. The second phenomenon may cause resonance with the power house structure that generates unacceptable vibrations and noise. The standing wave phenomenon may also affect the penstock, and the interaction between the hydraulic machine and the hydraulic circuit.

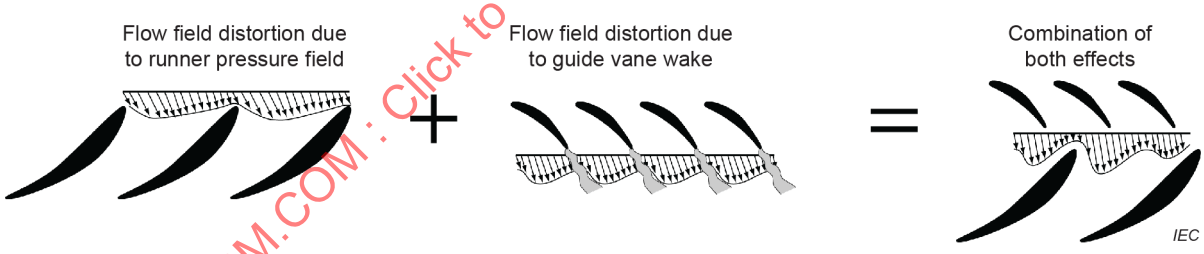


Figure 13 – Modulation process between runner blade flow field and guide vanes flow field

IECNORM.COM : Click to view the full PDF of IEC TS 62882:2020

The diametrical mode pressure field taking place in the vaneless zone can be characterized by two modes numbers k_1 and k_2 indicating the number pressure maximum and minimum of the diametrical modes. The diametrical mode number can be computed according to the number of runner blades Z_B and the number of guide vanes Z_G defined as follows:

$$k_1 = m \cdot Z_B - n \cdot Z_G \text{ and } k_2 = m \cdot Z_B + n \cdot Z_G$$

where

m and n are integers of arbitrary values.

The diametrical mode is rotating with the respective spinning speed in the stationary frame of reference given by:

$$\omega_1 = m \cdot Z_B \cdot \omega_B / k_1 \text{ and } \omega_2 = m \cdot Z_B \cdot \omega_B / k_2$$

Furthermore, the sign of the diametrical mode numbers k_1 and k_2 indicates that the diametrical mode is rotating in the same direction as the runner when positive, and counter-rotating when negative. It is also important to notice that lower amplitudes are expected for higher k values, because of the high harmonic number. As a result, k_2 is usually not relevant. Figure 14 presents an illustration of the meaning of the k values. It could be mentioned that a value of k = 0 leads to synchronous pressure fluctuations in the vaneless gap inducing periodic axial pressure force on the shaft line, while a value of k = ±1 leads to unbalanced rotating pressure force inducing radial force on the shaft line.

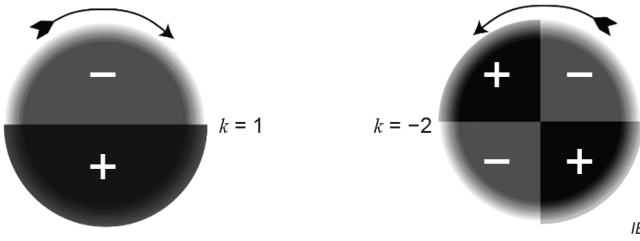


Figure 14 – Diametrical modes shapes representation according to k values

In a stationary frame of reference, the measured frequency is the runner speed times the number of blades, while in a frame of reference that rotates with the runner, the measured frequency is the runner speed times the number of guide vanes and/or stay vanes. Overtones of these frequencies may also be present.

While rotor-stator interaction is normal in all turbines, the consequences may be serious when they are in resonance with hydroacoustic and/or mechanical eigenfrequencies of turbine parts. Issues include structural failure of runner, spiral case and penstock, unacceptable noise phenomena and possible fatigue.

The RSI phenomenon is of most concern in high head Francis and pump turbines. In these types of turbines, the distance from the guide vane exit to the runner blade inlet is roughly constant over the guide vane height. As a result, the wake from the guide vane will reach the complete edge of the runner at approximately the same time. In low head turbines, the distance between guide vane and runner blade is larger and varies over the guide vane height. This means that the wake from one system will benefit from dissipation and reach the other system at different times and different tangential position at different elevations and the pressure variation will be smoothed out.

It can be noted that, since the hydroacoustic and mechanical eigenfrequencies are not directly scalable between model and prototype, the consequences of RSI phenomena cannot be directly predicted based on model tests. Nevertheless, model tests enable the measurement of the amplitude of the asynchronous pressure field in the vaneless zone, which can be used to validate or calibrate computational models for the prediction of dynamic blade loading. Moreover, measurements in the vaneless zone make it possible to determine the excitation source amplitude for both hydromechanical and hydroacoustic resonance evaluation.

It is also noted that the amplitude of this fluctuation mode is not related to runner outlet rotating speed ($\tilde{p}_{\mathrm{nD}}$) as for draft tube related phenomena, but rather to the runner inlet rotating speed ($\tilde{p}_{\mathrm{nD_1}}$). It is therefore recommended to plot this fluctuation amplitude divided by $\tilde{p}_{\mathrm{nD_1}}$ vs. the relative discharge for analysis of RSI phenomena.

4.4.6.2 Model test example

See Figure A.9, where the first diagram depicts the pressure fluctuation amplitude in the vaneless zone. The example shows the RSI fluctuation most commonly measured in model tests. It is measured in the static frame of reference and occurs for all discharges in various degrees. It comes from the pressure difference over the runner blade as it passes in front of a

IECNORM.COM : Click to view the full PDF of IEC TS 62882:2020

pressure transducer located in the head cover. Therefore, the runner blade passing frequency can be clearly identified in this fluctuation mode.

In the time domain of Figure A.9, we can note the typical "saw tooth" shape, meaning that the pressure increase is faster than the pressure decrease. This shape may also explain the overtones we can see in the frequency domain for $p_5(1)$ and $p_5(2)$. We also note that this fluctuation is localized to the vaneless zone and we do not see these frequencies in the other pressure transducers (except the 450 Hz overtone on p_3) in the frequency domain. This indicates that there is no significant hydroacoustic or mechanical eigenfrequencies in the system close to the blade passing frequency.

The RSI pressure fluctuation can also be measured in the rotating frame of reference and is then characterised by the guide vane passing frequency and its overtones. In some cases, the stay vane passing frequency may also be relevant, although this is not common.

Pressure measurements in the rotating frame of reference are uncommon. However, several instances of mechanical stress measurements on runners have identified the guide vane passing frequency.

For the guide vane passing frequency it is very important to ensure that vibrations and dynamic stresses do not exceed acceptable limits. Often this can only be achieved by avoiding hydroacoustic and mechanical resonance with the runner. Examples are known where runners have failed a very short time after commissioning due to such resonances.

5 Specifications of pressure fluctuation measurement and analysis

5.1 General

5.1.1 Overview

The purpose of Clause 5 is to detail how to measure and analyse pressure fluctuation. It is important to note that IEC 60193, IEC 60041 and IEC 60994, respectively deal with model testing, prototype testing and vibration and fluctuation measurements. Especially, in IEC 60193:2019, 7.2 is dedicated to fluctuating quantities and 7.2.2 to pressure fluctuations.

For pressure fluctuation amplitude analysis, the general use of a 97 % confidence interval is recommended to ensure mutually comparable results. The standard deviation may also be accepted if relevant parties agree.

Consequently, Clause 5 will underline the important points to take from these standards and complement them.

5.1.2 Purpose of the measurements

Generally, pressure fluctuation measurements are realized with the ultimate objective to have a prototype operating in stable conditions, free of harmful vibrations and with dynamic stress levels compatible with the expected useful life of the machine. Model testing is mainly done to document the design status with the objective of predicting the prototype behaviour and its stability by comparison with similar models.

According to IEC 60193, the main measurements that shall be carried out on the model are the following:

– relative magnitude of the pressure fluctuations within a specified operating range;
– nature of the pressure fluctuations, periodic or stochastic;
– dominant frequency of the pressure fluctuations, if any;

IECNORM.COM : Click to view the full PDF of IEC TS 62882:2020

– effect of corrective methods such as air admission (effectiveness and suitable location);
– intensity of the pressure fluctuations of the model compared with other models of similar specific speed.

Even though transposition of model test results is seen to have a good predictability for some phenomena, it is likely to encounter differences on prototype. It is therefore a good practice to measure these values on the prototype even if the prototype is operating with acceptable levels of vibration or if the model was operating smoothly. This could help underline problematic operating conditions which seemed normal at first.

In cases of a rough operating machine or wide operating range, for example with pressure fluctuation values above the guaranteed values, a detailed analysis shall be done. Dynamic measurements and pressure fluctuations measurements should be considered.

The prototype detailed analysis test covers the same type of measurements, except that there is usually no comparisons with models other than the homologous one.

In cases with bad accessibility, other dynamic measurement methods can be performed to supply root cause analysis.

5.1.3 Procedures and parameters to record

5.1.3.1 Model test

On the model, the test points should cover at least the specified discharge operating range under constant test specific hydraulic energy values and at least the minimum Thoma number for a given head or operating condition. The test head values often relate to prototype specific maximum and minimum operational heads and one or several rated operational heads in plants with large variations of specific hydraulic energy. A sufficient number of guide vane openings should be explored, particularly at part and full-discharge, to characterize in detail the fluctuation phenomena that occur with changes in the operating conditions. Knowing that upper part load happens in a narrow range of guide vane opening, the number of test points shall be higher where this phenomenon is expected.

5.1.3.2 Prototype measurement

On the prototype, the overall view of the pressure fluctuations is obtained by recording a sufficient number of test points between speed no load and full guide vane opening (at least every 5 % of rated power). Another way to obtain the big picture is by ramping up or down the guide vane opening sufficiently slowly (0,1 %/s on the servo-motor stroke) over the domain of operation. The latter is faster but known to give pressure fluctuation amplitudes different than those obtained by maintaining a constant guide vane opening. Moreover, depending on the chosen servo-motor slope, the apparition of the phenomenon can switch in flow (lag) or not happen at all. Thereafter, an additional number of test points at a constant guide vane opening can be performed near the limits of the normal operating range or contractual limits, and where amplitude of pressure fluctuation changes rapidly with flow. For each test point, the guide vane opening shall be constant to avoid flow or head variation due to load-frequency control. If possible, the head should be modified by starting/stopping adjacent units to measure its impact on important pressure fluctuation test points.

For standard checks of pressure fluctuations, in case of locally high vibrations, the unit shall be operated in this critical zone. The phenomenon shall be caught when it clearly occurs. The turbine should be measured in small steps of guide vane openings in and around this region, also by varying the surrounding conditions. Surrounding conditions may be including operation of other parallel machines, varying the tail water level and so on. Measurement transducer location shall be taken, as far and as available on the prototype.

In a less complex version to check the guarantees in sensitive operating points of a strong vibrating unit, the site measuring range should depend on the problem, the size and the accessibility of the prototype.

IECNORM.COM : Click to view the full PDF of IEC TS 62882:2020

Besides the pressure fluctuation signals, the following parameters should be recorded at the same time:

– the head/specific hydraulic energy;
– the rotational speed;
– the trigger signal (for phase angel calculation)
– the absolute discharge or relative discharge by Winter-Kennedy method;
– the unit power;
– the upstream water level and downstream water level, the latter being used to determine the Thoma number;
– the water temperature;
– the air discharge measurement for air admission;
– the guide vane opening and/or angle, servomotor stroke;
– the axial loads (optional);
– the shaft line radial displacement

5.1.4 Locations of pressure fluctuation test transducers

The location of pressure transducers should consider the need to capture all phenomena mentioned in Clause 4. Figure 15 shown below is based on IEC 60193:2019, Figure 90, which proposes a location for these transducers.

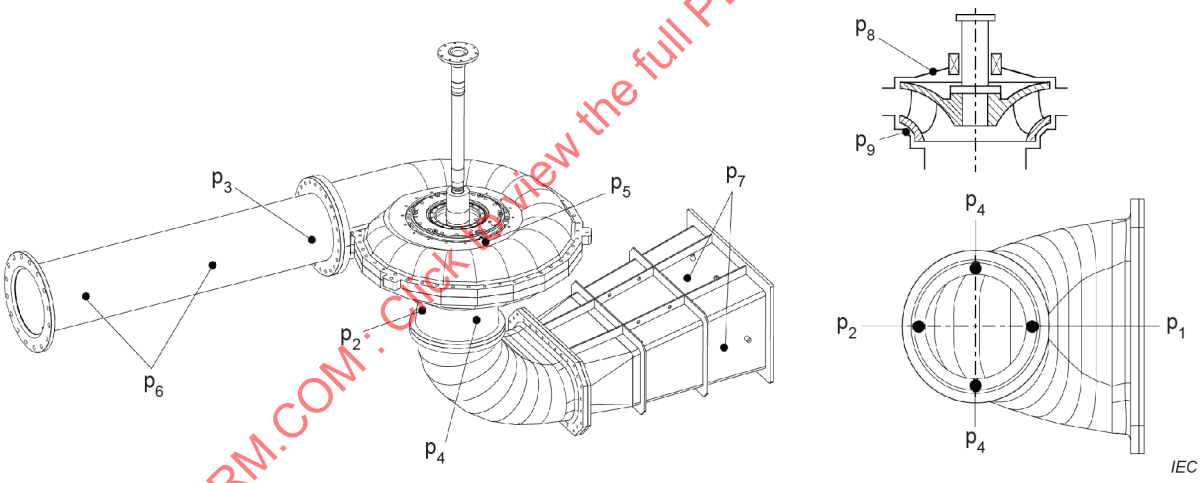


Figure 15 – Suggested locations of pressure transducers

Table 2 describes each transducers location shown in Figure 15 and links those locations to the phenomena listed in Table 1 they are intended to measure.

IECNORM.COM : Click to view the full PDF of IEC TS 62882:2020

Table 2 – Locations of pressure fluctuations transducers

Locations	Locations description	Mode in Table 1	Important content
p_1	Draft tube cone downstream 0,3∼1,0 D2 from the runner exit	1~5	Key
p_2	Draft tube cone upstream 0,3∼1,0 D2 from the runner exit	1~5	Key
p_3	Spiral case	1, 2 ,3, 4.b	Key
p_4	Draft tube cone 90° apart from p1 or p2, preferably two locations, the same section with p1 and p2	1~5	Optional
p_5	Vaneless zone, preferably two locations, upstream and downstream at the same diameter	6.a	Key
p_6	Penstock	1, 3, 4.b	Optional
p_7	Draft tube outlet	1~5	Optional
p_8	Head cover	6.a	Optional
p_9	Discharge ring	1 ,4, 6.a	Optional

For the purposes of this document, the measurement of p_1, p_2, p_3 and p_5 is necessary to determine the hydraulic excitation and is identified as key locations in Table 2. These locations also cover the main phenomena for which transposition is foreseen.

P_4 is important to confirm the rope rotation direction. It also adds precision to the amplitude and phase measurement. However, the rope rotation direction is predictable from the runner rotation direction. Also, p_1 and p_2 are sufficient to compute the phase difference. Therefore, it is not considered as necessary.

Other locations can be considered as optional. They can be used to add data and study the wave propagation in the waterway (p_6 and p_7) and around the runner (p_8 and p_9). Therefore, these locations could help doing more complex analysis such as resonance prediction.

IEC 60193 suggests that p_1 and p_2 are placed 0,3 diameter length to 1,0 diameter length from the low pressure side of the runner. There is a great margin between both values and pressure fluctuation measurement could vary noticeably from one elevation to the other. In order to compare adequately the model and prototype values, it is important to have the sensors at the same relative level, for example both at 0,3 times the runner diameter.

A typical location for p_5 is at mid-distance between the diameter of the guide vane outlet at full opening and the outer runner diameter at the crown.

5.1.5 Data acquisition for pressure fluctuation measurements

The fact that pressure fluctuation is a dynamic phenomenon brings additional complexity in term of data acquisition requirements. The system shall take into account the range of frequency that shall be measured and should prevent potential noise to distort the signal. The range measured frequency should allow cover of all the phenomena mentioned in Table 1.

Most of the information about signal conditioning, analog to digital conversion, sampling rate, duration of signal record, frequency resolution and phase information is important and discussed thoroughly in IEC 60193:2019, 7.2.1.2. The principles mentioned in this document apply to both model and prototype.

IECNORM.COM : Click to view the full PDF of IEC TS 62882:2020

It is recommended to use a system that allows having synchronous measurement in all channels or show a negligible delay (less than ±10° for the phase) between channels with respect to the phase difference at the frequency of interest. An example of such a system can be found in IEC 60193.

The maximum permissible error of the measuring chain shall be smaller than ±5 % of the maximum measured value.

5.1.6 Transducers and calibration

As for the data acquisition system, pressure transducers and calibration methods shall be chosen considering the dynamic nature of pressure fluctuations. Frequency response and sensitivity are amongst the most important parameters to look at. Pressure transducers type, calibration and installation are discussed in IEC 60193:2019, 7.2.2.3 and 7.2.2.4. The principles mentioned in this document apply to both model and prototype.

An important parameter to consider in the installation is the need to have a mounting allowing the sensor membrane to be flush with the hydraulic profile. Any chamber created between the sensor and the point of measurement can trigger resonances phenomena that will pollute the signal. This requirement can sometimes be hard to meet, especially on the prototype. Subclause 5.3 gives some information and references about these cases.

Typical parameters about pressure fluctuation transducers are shown in Annex B.

In addition, three typical calibration methods for dynamic pressure transducers are shown in Annex C.

5.2 Pressure fluctuation on a model turbine

5.2.1 General

As previously mentioned, IEC 60193 adequately covers model pressure fluctuation testing. Any test should comply with IEC 60193:2019 and more specifically with 5.1 and 7.2.2.

Requirements such as those mentioned in IEC 60193:2019, 5.1, and the operating ranges to be tested are treated adequately in IEC 60193.

Figure 16 shown below is based on IEC 60193:2019, Figure 92, and provides a good example on how to explore the operating range of a machine.

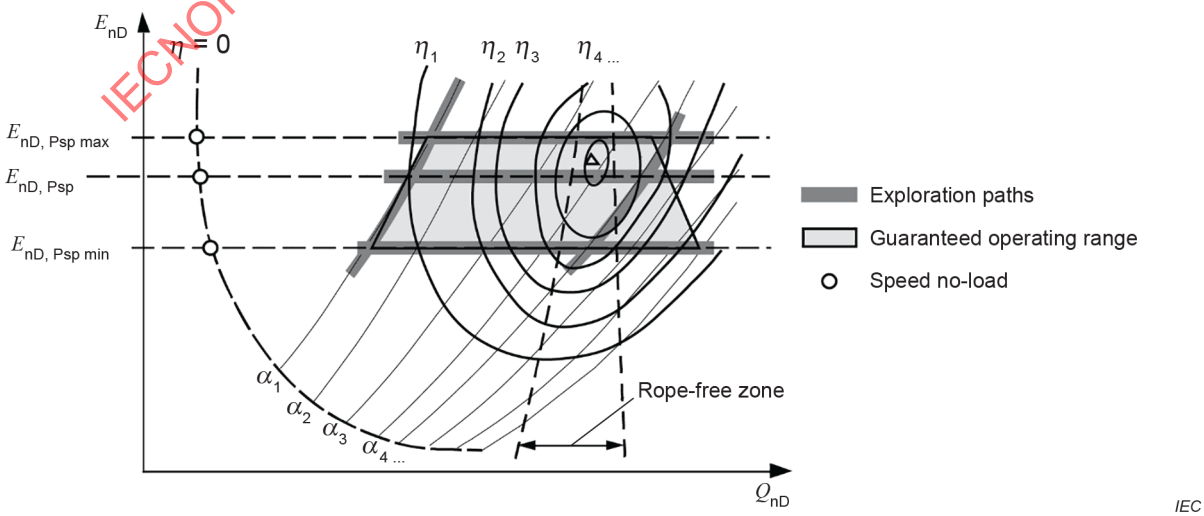


Figure 16 – Turbine hill-chart with exploration paths

IECNORM.COM : Click to view the full PDF of IEC TS 62882:2020

5.2.2 Homology and limitations

Pressure fluctuation scalability depends on homology between model and prototype. Therefore, model sensor location should be installed based on the position of the prototype sensor, accounting for the model-to-prototype scale factor. At the minimum, the homology requirement should comply with IEC 60193 requirements. However, as stated in 7.2.2.1.2 of IEC 60193:2019, and Clause 6 and Clause 7, numerous factors affect similitude between model and prototype that can influence results transposition.

5.2.3 Detailed procedures

5.2.3.1 General

IEC 60193:2019, 7.2.2.5, is dedicated to test procedures that are specific for pressure fluctuation model testing.

5.2.3.2 Test specific hydraulic energy

Selection of the test specific hydraulic energy shall depend on the test conditions and the limits of instrumentation; the importance of Froude similitude shall also be considered. Sometimes it can identify the possible resonance between the model and the test rig by changing the test specific hydraulic energy. For this topic, the recommendations of IEC 60193:2019, 7.2.2.5.1, can be followed.

5.2.3.3 The influence of Thoma number on pressure fluctuation

Concerning the reference level to be used, IEC 60193:2019, 7.2.2.5.2, gives some suggestions:

"*The reference level used for defining the Thoma number can influence the pressure fluctuation measurements if the Froude similitude is not fulfilled. In case the Froude similitude cannot be fulfilled, this reference level shall be agreed upon (see 5.3.5.2). For vertical units, the reference level can be at or below the low pressure side of the runner/impeller depending on the extent of the cavitation vortex rope in the draft tube.*"

For a normal case, the reference level to use for pressure fluctuation testing shall be the reference level as defined in Figure 2.

If draft tube cavitation compliance is studied to determine whether prototype resonance may occur, the pressure fluctuation should be measured in a range of Thoma numbers that allows similitude of the local Thoma number in the draft tube at the elevation of the largest cavitation development.

A pressure fluctuation test with variation of the Thoma number should be performed on the model to cover for all possible power plant tailwater level range.

5.2.3.4 Air admission

Air admission can be tested on the model to verify its effectiveness to reduce pressure fluctuations as well as provide qualitative insight into how the air flow impacts hydraulic efficiency. Such tests give only an approximate estimation of the air admission effect to be expected on the prototype, because the required similitude rules cannot be all respected. Nevertheless, some basic rules are given in 5.2.3.4 to perform such tests. Air admission tests are also useful to verify where atmospheric air admission is possible on the prototype (when such system is planned to be used on the prototype) and to estimate roughly the maximum possible air admission.

In addition to the typical parameters measured during pressure fluctuations tests, an air admission test requires the following measurements, all made at the same location in the aeration circuit.

IECNORM.COM : Click to view the full PDF of IEC TS 62882:2020

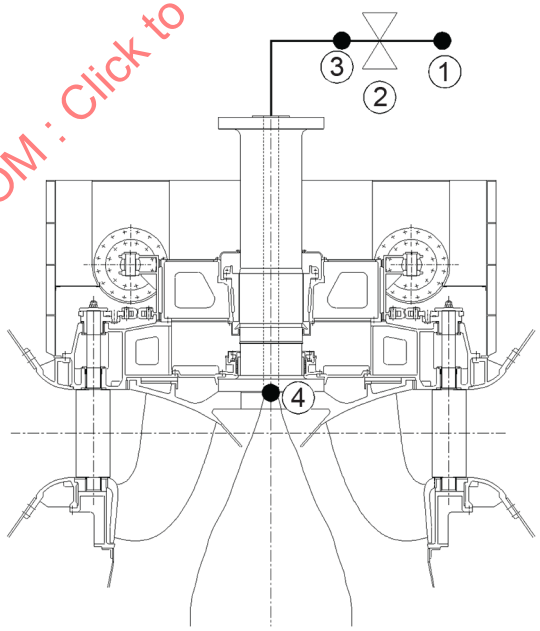
1) Air flow rate: This can be measured using an anemometer, a Pitot-tube or a mass flow meter. The preferred method is the mass flowmeter.
2) Air temperature: It should be measured as close as possible to the air admission location.
3) Air static pressure: it should be measured as close as possible to the air admission location. This measurement will be used to estimate the static pressure at the air injection location. To ensure an easy estimation of the static pressure at the air injection location, air velocity between the pressure measurement location and the injection location should be limited to a sufficiently low Mach number (typically lower than 0,4) in order to facilitate estimation of friction losses and avoid choking of the air flow. Loss characteristic of the piping between the pressure measurement location and the air injection location should be measured before the test when the model runner is open to the atmosphere.

When testing air admission on pressure fluctuation, the effect of a different air flow rate on each operating point of interest shall be tested. A sufficiently large air flow range, including no air, shall be tested, as air flow transposition from model to prototype is not precise.

On the model, testing air admission of pressure fluctuations is usually done using compressed air or atmospheric air. By doing so, in Thoma similitude, air will generally enter in the model at every operating point. This is generally not the case for atmospheric air admission on the prototype. To have the same limit of occurrence of the aerated vortex core on model and prototype, it is very important to determine the pressure at the air injection as it is sufficient to estimate where there will be atmospheric air admission on the prototype. And a low pressure air admission reservoir is needed on the model but this approach is usually not necessary. Using a low pressure reservoir also limits the air flow range that can be tested at the laboratory.

During the test of air admission on pressure fluctuations, Thoma and Froude similitude are the most important parameters. Reynolds and Weber similitude are neglected, though they have an effect. As it is also often not possible to respect Froude similitude, Thoma number will be defined at the air injection elevation or at an average elevation of the aerated volume. A simplified schematic of a device that allows air to be passed under the runner cone of a Francis turbine is illustrated in Figure 17.

IECNORM.COM : Click to view the full PDF of IEC TS 62882:2020



NOTE:

○,1 refers to the air pressure at the entrance of the aeration conduit

○,2 refers to controlling valve for air admission

○,3 refers to the air pressure after the valve

○,4 refers to the air pressure under the runner

Figure 17 – Schematic of the axial aeration device

During model testing, the impact of air flow rate, or air/water ratio, on pressure fluctuation can be documented. General aeration transposition can then be approximated from the following relationship:

$$\frac{\varphi_{\mathrm{p}}}{\varphi_{\mathrm{m}}} = \left(\frac{E_{\mathrm{p}}}{E_{\mathrm{m}}} \right)^{\frac{\gamma+1}{2}}$$

where

φ is the air/water ratio;

γ is an exponent that is used to account for the complex relationship between air absorption and relative velocity of the gaseous and liquid phases. Experiments show this value ranges from 1 to 3.

5.3 Special requirements and information for a prototype turbine

5.3.1 General

Generally, model pressure fluctuation measurements are performed for guarantee checks. The transposition of pressure fluctuations from model to prototype shall be analysed with rigor in order to compute comparable values.

For this document, the aim of prototype pressure fluctuation measurements is to verify the model test results, determine operating zone limits and verify pressure fluctuation guarantees. It can also be taken as a method to assess prototype pressure fluctuation.

5.3.2 Source of information

Field testing is particularity described in IEC 60041 and IEC 60994.

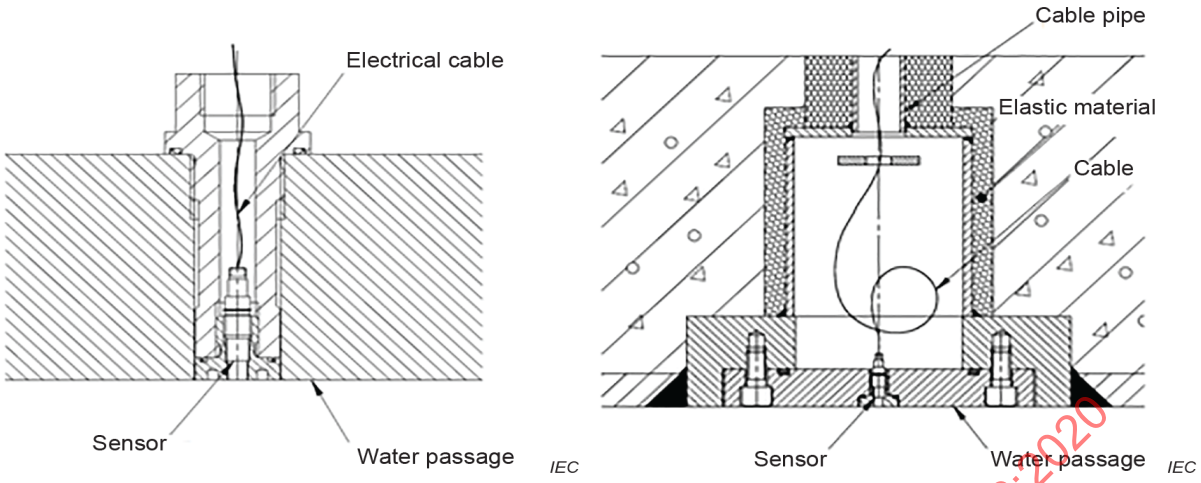
In IEC 60041:1991, 11.4.6.4 provides information about the pressure transducers in site.

In IEC 60994:1991, 5.1.1 describes the specific test procedure; Clause 6 deals with methods of measurement specific to prototypes; Clause 9 addresses data acquisition and processing issues; and Appendix D suggests a way to estimate the critical frequency of a connecting pipe.

5.3.3 Important aspects

Other than what is listed in 5.3.2, the most important aspect of prototype measurement is pressure transducer connection. Ideally, pressure transducer would be flush with the wetted internal surface since piping length and rigidity affect fluctuation measurement. Figure 18 shows two examples for draft tube and vaneless zone. If it is not possible on site, it is imperative to minimize the length of the channel connecting the sensor to the flow and maximize tubing rigidity.

IECNORM.COM : Click to view the full PDF of IEC TS 62882:2020



a) Head cover **b) Draft tube**

Figure 18 – Schematic arrangement for pressure fluctuation transducers

Also, the position of sensors on the model and on the prototype shall be identical, which otherwise would add a level of uncertainty. This is why pressure taps location shall be considered from the very beginning of the design stage and during construction.

If tubing is to be be used, theoretical estimate of the resonance frequency can be calculated (IEC 60994:1991, Appendix D) and looked for on the spectrum. However, to compute a statistical value on the time signal, the distorted part of the signal shall be removed using a low-pass filter (high frequencies, short tube length) or by post-processing methods such as an example presented in Annex D.

Pressure taps averaged mechanically using a manifold shall be measured individually for the test purposes. This may be the case for pressure location p_3 (spiral case inlet). If that is the case, a specific resonance frequency of each individual tap can be distinguished on the spectrum apart from the connecting pipe length.

Air admission is a good way of mitigation. For good comparison between model and prototype, a temporary way to block air admission, or even better control air flow, shall be considered at the design stage.

Ideally for pressure measurement, each connecting tube shall be inclined toward the duct without bends, so that air does not stay trapped. A flushing valve shall be installed to ensure there is no air or bubble in the connecting tubes. Automatic vents using a floating ball add damping so there shall be a valve to isolate them during the test. It is a good practice to look at the spectrum of a recording made during the opening of the flushing valve and shutting it fast to see which frequency shows up.

IECNORM.COM : Click to view the full PDF of IEC TS 62882:2020

5.4 Analysis, presentation and interpretation of results

5.4.1 General

Analysis of pressure fluctuation results shall be carried both in the time and frequency domain.

IEC 60193:2019, 7.2.2.7, deals with pressure fluctuation analysis in this matter.

5.4.2 Time-domain analysis

As described in IEC 60193:2019, 7.2.2.7.1.2,the time-domain analysis is necessary due to a certain amount of randomness in the pressure fluctuations. Therefore, it is useful to determine the total amount of fluctuation using a time-domain analysis.

The results presented in this document were computed using the probability distribution method based on a 97 % confidence interval as described in 3.3.10.11 and as illustrated in Figure 4.

Other analysis methods such as the standard deviation value can be used to characterize the amount of pressure fluctuation.

5.4.3 Frequency-domain analysis

Frequency-domain analysis is useful to determine the ratio between noise and periodic fluctuation. It allows the identification of dominant and important frequencies, and helps to associate the measurement with the phenomena described in Table 1. It also allows the identification of potential resonances. It is useful to compare the spectrum of the model and prototype for the same relative discharge to ensure the measured relative frequencies are the same.

Spectrum analysis using fast Fourier transform (FFT) is recommended. Typical FFT parameters, such as time window size and overlap weight, are discussed in IEC 60193:2019, 7.2.1. The quality of the analysis will depend on the data sampling time.

5.4.4 Non-dimensional frequency and pressure

All measured parameters mentioned in 5.1.3 can be useful in carrying on analysis necessary to achieve the goals of the measurements mentioned in 5.1.2, in particular, the prediction of prototype behaviour from model data.

The following dimensionless parameters, which are defined in Clause 3, should be analysed as proposed in 7.3, 7.4 and 7.5 of this document to represent adequately pressure fluctuation amplitudes and frequency with respect to discharge or rotational speed:

$$f_n,\ p_{nD}\ ,\ Q_{H,rel}$$

These dimensionless parameters are useful for pressure fluctuation comparisons and scale-up.

5.4.5 Presentation and interpretation of pressure fluctuations

IEC 60193 covers in detail the presentation and interpretation of pressure fluctuation results.

However, some emphasis should be made on certain elements, such as the dimensionless parameters mentioned in 5.4.4.

Figure 19 shows a typical plot showing the pressure fluctuation coefficient versus relative discharge.

IECNORM.COM : Click to view the full PDF of IEC TS 62882:2020

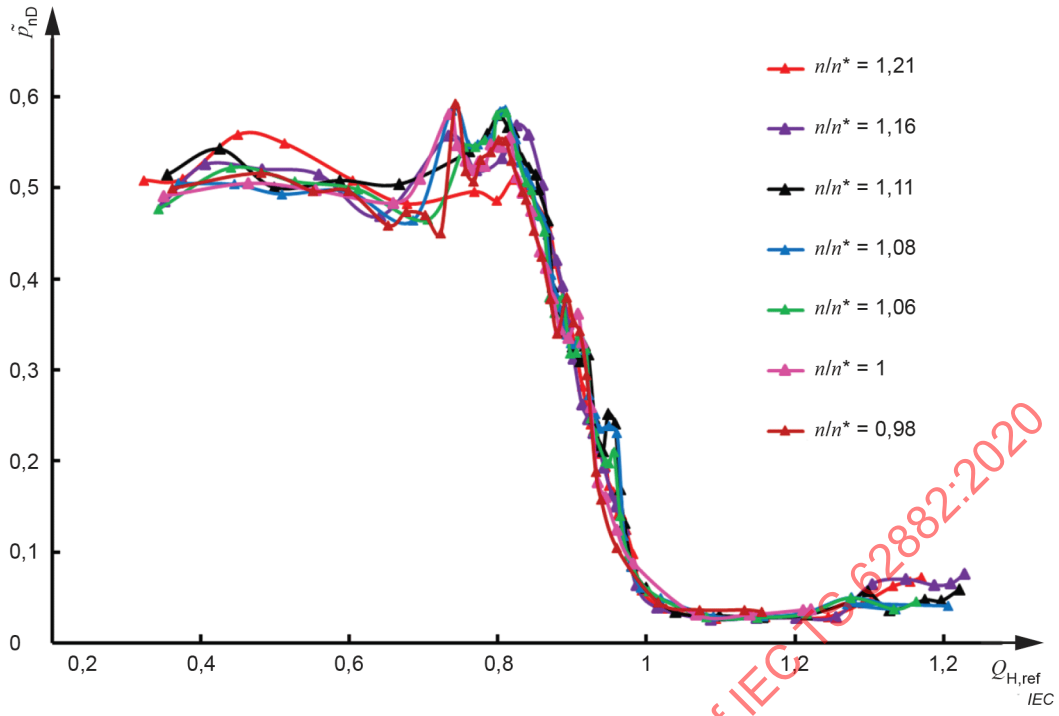


Figure 19 – Typical plot showing pressure fluctuation coefficient versus relative discharge

Amongst other things, these parameters are useful for analysing pressure fluctuation amplitudes in the context of:

– scaling;
– comparing operation at different heads;
– compare different machine.

Waterfall diagrams are useful when working in both the frequency and time domain. They can be useful to help:

– visualizing main frequencies;
– identifying resonance;
– identifying pressure fluctuation phenomena.

Also, analysing the pressure fluctuation signal in the time domain can be used to provide a first interpretation of results, which is useful for:

– comparing measurement in multiple channels;
– identifying phase shifts;
– identifying dominant frequencies.

Typical examples of these analyses are included in Annex A.

6 Identification of potential resonances in test rig and prototype

6.1 General

Hydroacoustic or hydromechanical resonance may occur at both the reduced scale model and on prototype scale. Hydroacoustic resonance may occur if a flow induced excitation frequency matches one of the hydroacoustic system natural frequencies, while hydromechanical resonance may occur when a flow induced excitation frequency matches a mechanical structure

IECNORM.COM : Click to view the full PDF of IEC TS 62882:2020

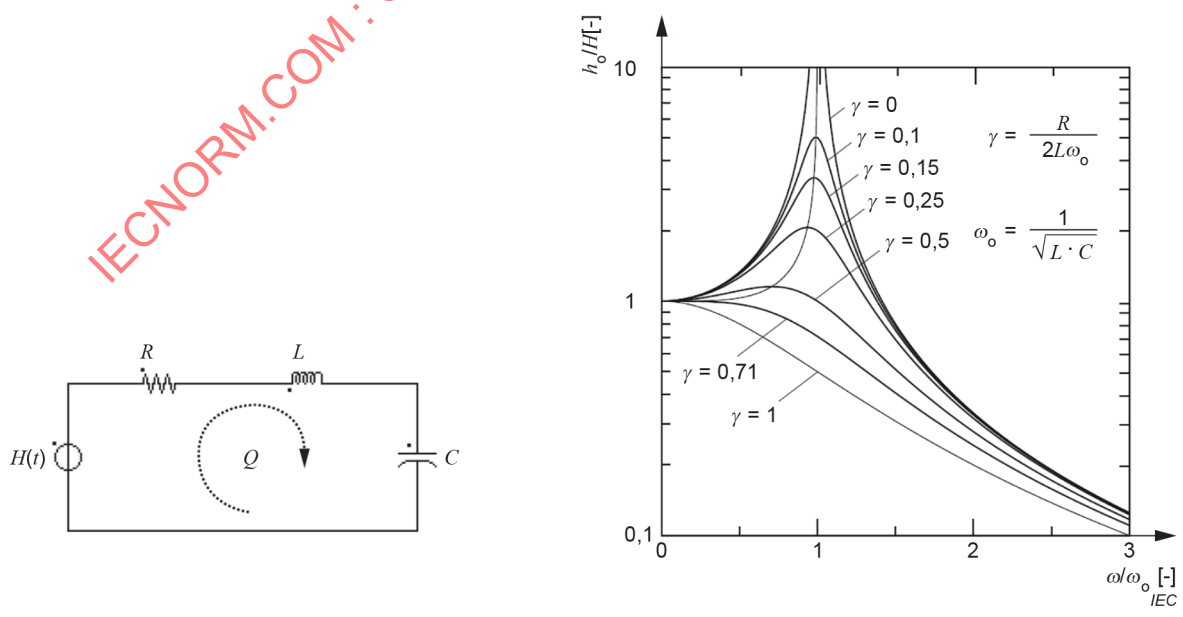
natural frequency. Moreover, at prototype scale, hydroelectrical resonance may occur if a flow induced excitation frequency matches an electrical system natural frequency. At the prototype scale, any of the aforementioned resonances may lead to extreme levels of pressure fluctuations, mechanical vibration or power fluctuations which may prevent safe and reliable operation and put the hydroelectric power plant at risk. At reduced model scale, possible resonances are usually not harmful for the installation as the exposition duration to such resonance remains short or can be avoided by operating parameter modification. However, possible resonance may lead to large pressure fluctuations amplitudes raising the question of its possible risk of occurrence at the prototype scale, while the direct transposition is normally not possible. Therefore, it is important to be able to identify when such a resonance occurs at reduced scale to discard the corresponding high pressure fluctuations amplitudes and avoid any misinterpretation. At the prototype scale, it is important to find ways to predict and anticipate possible resonance, and provide ways to identify it when it occurs and for troubleshooting purposes. It is important to mention that, as the test rig and prototype waterways and mechanical structure are not homologous, a direct transposition of resonance phenomena is not possible, and therefore they require appropriate tools and methodology to analyse them and predict them both in model and prototype.

In case resonance occurs, the system response amplitudes are strongly affected by the system characteristics parameters and damping, and by the excitation source frequency, amplitude and pattern. As far as hydroacoustic resonance is concerned, it could be illustrated considering an elementary hydroacoustic oscillator; nevertheless, the following conclusions apply to any kind of resonance. The hydroacoustic system of Figure 20 comprises a hydraulic resistance R, inductance L and capacitance C, modelling respectively hydraulic losses, inertia and compliance effects. The harmonic response of this system subject to pressure excitation source $H(t)$ evidences high pressure amplitudes when the excitation frequency matches the system's natural frequency, while the pressure amplitude reduces when the relative damping increases.

Consequently, as far as resonance phenomena are concerned, to avoid high system response amplitude, it is recommended to:

– avoid a match between the system natural frequency and excitation source frequency to avoid resonance;
– reduce the amplitude of the excitation source;
– increase the system damping.

IECNORM.COM : Click to view the full PDF of IEC TS 62882:2020



a) With undamped natural frequency ω_0

b) With corresponding harmonic response for different relative damping γ

Figure 20 – Elementary hydroacoustic oscillator

6.2 Identify resonance in test rig

If, due to the development of cavitation vortex rope in the draft tube, a resonance between the model and the test rig is suspected, it is recommended to conduct the measurements under different agreed test specific hydraulic energies, thus changing the hydraulic excitation frequency. By varying the value of the test specific hydraulic energy, the Froude number value also changes and modifies the pressure field in the draft tube. This influences the volume of the cavitation vortex rope if the Thoma number value is kept constant. In that case, a decrease or increase of the test specific hydraulic energy yields a decrease or increase of the Froude number value and consequently an increase or decrease of the cavitation vortex rope volume, respectively. The influence of the cavitation vortex rope volume on suspected resonance can also be investigated by varying the value of the Thoma number, the test specific hydraulic energy value being kept constant.

Modifying the test specific hydraulic energy requires a different model rotational speed and thus it modifies the excitation source frequency, while the modification of the cavitation conditions modifies the system hydroacoustic natural frequency. Both modifications result in a mismatch between the excitation frequency and the system natural frequency with the aim to bring the system out of resonance and demonstrate the origin of large pressure fluctuation amplitudes.

6.3 Possible resonance and self-excited pressure fluctuation in prototype

6.3.1 General

All pressure fluctuations phenomena which may develop within Francis turbines or pump-turbines, which are described in Table 1, may lead to possible resonance. Typical resonance that can be encountered at the prototype scale and ways to predict and analyse them are described in 6.3.

The first step of identifying possible resonance at prototype is to compare some prototype data with reduced scale model data. If significant differences are found on a specific operating range, resonance might be expected and requires more detailed analysis. The second step consists in using experimental methods and data as well as numerical tools to provide a clear explanation of the resonance root cause. Once the root cause is identified, one may refer to suggested means of mitigations provided in Clause 8.

6.3.2 Draft tube vortex related resonances and self-excited pressure fluctuation in prototype

At high load operation, the axisymmetric cavitating vortex rope may lead to hydraulic system self-excitation. Depending on the turbine relative location in the system, mechanical torque fluctuations may also arise and induce active power fluctuations. This phenomenon, which is not of forced response resonance type, arises when the damping of one or more system natural frequencies becomes positive. Thus, the characteristic frequency of the pressure oscillations corresponds to one of the hydroacoustic system's eigenfrequencies which are strongly affected by the cavitation compliance developing in the draft tube.

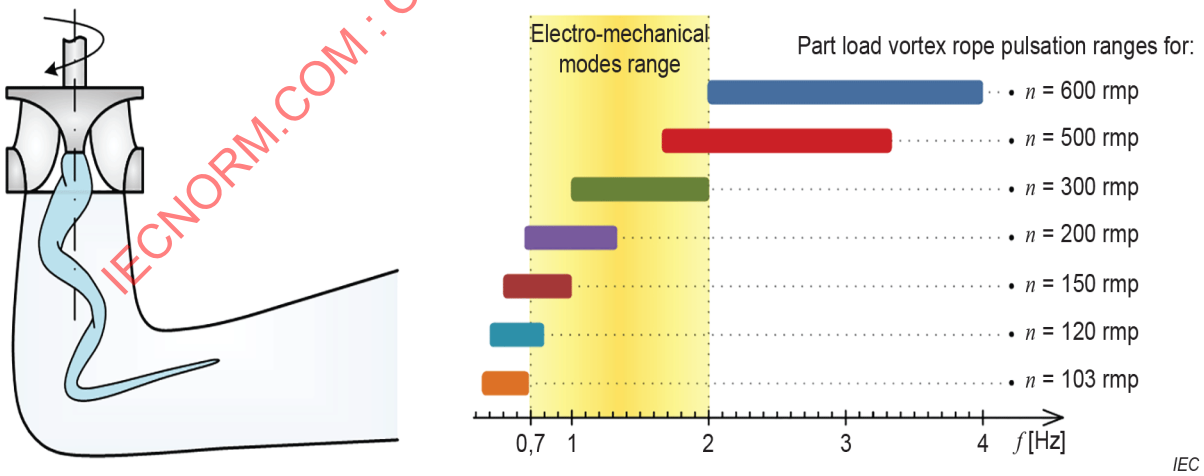
The prediction of the system full load self-excitation remains challenging, and available numerical models and experimental methods are mostly used for troubleshooting purposes. For this purpose, identification of the key hydroacoustic cavitating draft tube parameters, such as the vortex rope compliance and bulk viscosity using either CFD computation with cavitation models or test rig experimental identification methods, are possible ways to address full load stability assessment at the prototype scale. Moreover, coupling 1D hydroacoustic models with 3D unsteady CFD with cavitation models has made it possible to reproduce satisfactorily the full load self-excitation phenomenon. However, such kind of simulation is rather complex and requires significant computational effort. In cases where full load surge is found on both model and prototype, the related operating conditions may differ and the frequencies are usually different because of the different hydraulic waterways.

IECNORM.COM : Click to view the full PDF of IEC TS 62882:2020

At part load operation, hydroacoustic resonance between the synchronous part of the pressure fluctuations induced by the cavitation vortex rope and the hydraulic system may occur at a frequency corresponding to the vortex rope precession frequency of 0,2 times to 0,4 times the runner rotation frequencies. At upper part load, excitation frequencies between 1 time to 5 times the runner rotation frequencies can also be expected. In case of hydroacoustic resonance, standing wave will develop in the entire waterways and will be characterised by a phase shift between two pressure fluctuations recorded at two different locations. These two transducers should be located either close to zero or to 180° depending the transducer location along the waterway and the order of the mode excited by the standing wave. The pressure transducer should not be located at a pressure node. In addition, it has to be remembered that the hydroacoustic eigenfrequencies are affected by the number of units in operation which represent different boundary conditions depending on whether they operate or not and by the unit Thoma number, i.e. the net head and tail water conditions. Moreover, the possible resulting mechanical torque fluctuations may also induce active power fluctuations if hydroelectric resonance with the generator and related electrical system takes place. Indeed, synchronous generators are featuring a local mode of oscillation also known as "generator natural frequency" comprised in the range of 0,7 Hz to 2 Hz. Then, considering part load excitation frequency between 0,2 times to 0,4 times the runner rotation frequencies, a wide range of hydro unit may potentially be subject to hydroelectric resonance (see Figure 21). Generally, the active power fluctuations are affected by the electrical configuration, the voltage regulator and possible power system stabiliser. In practice, the operation below 50 % of the unit nominal power is often prohibited.

The prediction of possible hydroacoustic resonance under part load operation can be addressed by identifying the key hydroacoustic parameters either experimentally during model testing, or by CFD computation and then by computing the prototype hydroacoustic natural frequencies and checking possible resonances in case of match with the draft tube synchronous pressure fluctuations frequency. A forced response analysis of the hydroacoustic system would also help to assess the influence of the excitation source location on the risk of resonance. However, the prediction of the corresponding pressure fluctuation amplitudes remain a challenging task as the excitation source amplitude and the system damping remains difficult to quantify properly. Hydroelectric resonance assessment would require forced response analysis including the generator and electrical system modelling, in order to evaluate the resulting amplitude of active power fluctuations. Annex E is an example about forced response analysis for Francis turbines operating in part load conditions.

IECNORM.COM : Click to view the full PDF of IEC TS 62882:2020



Source: Silva, 2016 [164]

Figure 21 – Part load vortex rope in the draft tube and its fluctuation frequency range and corresponding risk of resonance with the generator local mode of oscillation valid for both F_{grid} = 50 Hz and F_{grid} = 60 Hz

At deep part load operation, the stochastic nature of the flow developing in the draft tube leads to broad band excitation. Then possible inter-blade vortices can take place in the runner

channels. The broad band excitation may lead to hydromechanical resonance with several different mechanical structures while inter-blade vortices with frequency range typically between 10 times to 30 times the runner rotations may lead to runner blades hydromechanical resonances. FEM structural analysis accounting for water added mass effect as well as for water compressibility enables to predict the structural eigenfrequencies of the turbine components; however, possible resonance with broad excitation remains difficult to predict as it depends on the excitation amplitudes and on the system damping. Nevertheless, these methods can be very effective in case of troubleshooting. Inter-blade vortex resonance can be addressed by identifying the excitation source amplitude and parameters either using CFD computation or on-board pressure measurement on the runner blades, or computing the structure's eigenfrequencies including the water effects.

6.3.3 Rotor-stator interaction (RSI) related resonance

Rotor-stator interaction may lead to hydromechanical resonance between the RSI pressure fluctuations generated in the vaneless zone with several different turbine mechanical or civil structures on the stationary frame or the rotating frame. Hydroacoustic resonance with the spiral case or with the penstock is also possible.

If the dominant excitation frequencies can be easily predicted with analytical methods based on the number of guide vanes and runner blades, the prediction of hydromechanical resonance is more challenging as it requires both the structural and excitation pattern and frequencies to coincide with the same number of diametral nodes to lead to resonance conditions. Nevertheless, FEM structural analysis accounting for water effect combined with CFD computation enables to fairly address pressure fluctuations amplitudes and structure forced response.

The prediction of hydroacoustic resonance with the spiral case also known as the phase resonance can be fairly addressed with hydroacoustic models. However, it requires a good estimation of the spiral case pressure wave propagation speed which is usually lower than in penstocks. Moreover, the possible resonance with the penstock remains difficult to predict and to quantify as it corresponds to very high order hydroacoustic mode due to the high RSI excitation frequency range. Also, a minor difference in penstock wave speed significantly affects the results. Nevertheless, it could be an efficient tool for troubleshooting when some parameters can be calibrated with on-site measurements.

6.3.4 Resonance with fluctuation modes not treated in this document

Pump-turbines and high head Francis turbines operated at speed no load may be subjected to hydromechanical instabilities that result from the interaction of the waterways hydraulic inertia and the unit rotating inertia which are linked through the hydraulic machine torque and discharge S-shape characteristic. A negative slope of the torque characteristic at runaway condition (zero torque) leads to stable conditions while a positive torque slope leads to unstable behaviour of the unit characterised by a period of oscillation of the rotational speed and head typically ranging from 10 s to 20 s. Such system self-excitation may lead to difficulties for the unit synchronization with the power network. Under given circumstances, the pump-turbine may act as energy source and excite also some waterways natural frequencies. The system stability can fairly be addressed with 1D model including the waterways, the hydraulic machine four-quadrant characteristic and the unit rotating inertia.

During the speed no load operation, stochastic flow may develop in the vaneless zone and propagate in the stationary and rotating frame and may lead to possible resonance with turbine mechanical structures. Rotating stall may also take place in the pump-turbine at speed no load or pump at part load operation. The corresponding pressure fluctuation frequency is usually below the runner rotational speed and may lead to hydroacoustic resonance with the manifold and waterways, especially during emergency shutdown in both turbine and pump operation modes. These problematics can be addressed by combined CFD and FEM with water influence analysis, but it requires significant computational resources as the prediction of exact flow patterns in the S-shape regions remains challenging. Combined 1D and 3D CFD computations enable to address resonance with waterways.

IECNORM.COM : Click to view the full PDF of IEC TS 62882:2020

Hydromechanical resonance between von Karman vortices developing at the trailing edge of stay vanes, guide vanes or runner blades and the corresponding mechanical structure may occur. FEM computation of the concerned mechanical structure taking into account water effect enables to predict fairly the structural natural frequencies, while excitation frequencies can be estimated in a first approximation based on a Strouhal number and an effective trailing edge thickness (geometric trailing edge thickness corrected with the displacement thickness of the boundary layer). If such resonance is suspected, CFD enables to compute von Karman vortices frequency more accurately according to the specific geometry and enable to evaluate dynamic amplification factors. A 2D CFD approach is usually sufficient to compare different profile excitation characteristics. Usually, the modification of the trailing edge shape enables to reduce significantly excitation source amplitude and solve resonance problems. Efficient trailing edge modifications such as Donaldson or symmetrical 30° profile have been applied successfully.

7 Transposition method and procedure

7.1 General

Prototype pressure fluctuation values may be calculated by converting the model test data according to the general similarity laws and comparable installation conditions of sensors within the hydraulic flow passage. The appropriate conversion procedures are described in 7.2 to 7.5.

7.2 Parameters influencing transposition

7.2.1 Model test head

For the reduced scale model test, it mainly ensures hydrodynamic similarity and kinematic similarity between model and homologous prototype besides geometry similarity. For other similitude numbers, it is hard to satisfy simultaneously. Apart from the runner diameter, there is a significant difference between the model turbine test head and prototype operating head, which represents a difference in Reynolds number, Froude number and Weber number.

Investigations of pressure fluctuations were made in high, medium and low specific speed Francis turbines. The investigations covered six typical operation conditions, including overload, full load, best operation range, part load, deep part load and no load condition. It was found that the test head had little influence on the Francis turbine draft tube and vaneless zone pressure fluctuation (modes 1 to 6) when the Thoma number was kept constant.

7.2.2 Thoma number

The Thoma number can have a substantial influence on pressure fluctuation amplitude and even the pressure fluctuation frequency spectrum. In the prototype, the Thoma number may vary in different operating conditions. It is recommended that pressure fluctuation measurements in model tests are performed at representative Thoma number for actual operation.

There is currently no perfect agreement on which the Thoma number best serves the purpose of transposition from model to prototype. Two competing claims are:

– Thoma reference elevation taken at guide vane centreline;
– Thoma reference elevation taken in the middle of the draft tube cone. This elevation approximately corresponds to the centre of the draft tube vortex.

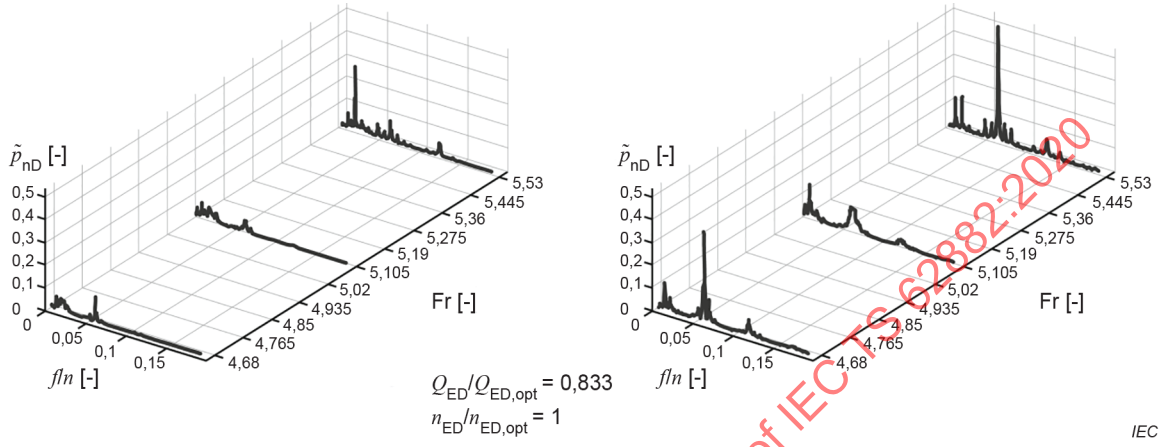
It is recommended that the involved parties agree on which reference elevation to use for each particular model test.

An example of the influence of Thoma number on pressure fluctuation is shown in Annex F.

IECNORM.COM : Click to view the full PDF of IEC TS 62882:2020

7.2.3 Froude number

The Froude number affects the distribution of cavitation in the flow as it determines the pressure gradient relatively to the size of the machine (see 5.2.3.2). The Froude number is usually smaller on the prototype than in the model. Due to the difference of Froude numbers, the vortex rope on the scale model is more narrow and longer than on the prototype. Figure 22 a) and Figure 22 b) are examples of the influence of the Froude number on the pressure fluctuation on a spiral case and upstream cone of model turbine, respectively, for a given Thoma number.



a) At the spiral case **b) At the upstream cone**

Figure 22 – Waterfall diagram of the pressure fluctuations as function of the frequency and Froude number for a given Thoma number

7.3 Relevant quantities for transposition

7.3.1 Fluctuation frequency

The frequency is transposed by the frequency coefficient:

$$f_{n,P} = f_{n,M}$$

7.3.2 Fluctuation amplitude

The pressure fluctuation amplitude in the draft tube, vaneless zone and spiral case is transposed as:

$$\left(\tilde{p}_{nD}\right)_P = \left(\tilde{p}_{nD}\right)_M$$

For comparison of different designs regarding pressure fluctuation in the vaneless zone, it is more appropriate to use D_1 instead of D for normalization:

$$\left(\tilde{p}_{nD_1}\right)_P = \left(\tilde{p}_{nD_1}\right)_M$$

7.4 Transposable types of fluctuations

The frequency of pressure fluctuations can normally be transposed from model to prototype with good accuracy.

IECNORM.COM : Click to view the full PDF of IEC TS 62882:2020

In favourable conditions for the model tests and in case that no significant interaction with the external system is present, pressure fluctuation amplitudes may be transposed from the model to the prototype.

Due to interaction with external systems, the detailed analysis of prototype pressure fluctuation amplitudes including risk of resonance would require a dynamic response analysis of the full-size machine layout, including water conduits, manifold, gate chambers, tailrace tunnels, etc. Due to the complexity of the prototype plant configuration, it is in practice very difficult to make such analysis on a comprehensive numerical model including all relevant system components. A proposed methodology for risk assessment is given in Annex E.

Pressure fluctuations representing purely local phenomena, such as the "asynchronous" draft tube pressure fluctuations attached to the vortex rope precession, do not interact with the rest of the hydraulic or electromechanical system, and thus may be transposed relatively well by just applying the appropriate scale factors. Other examples are pressure fluctuations due to interaction of runner/impeller blades and guide vanes.

Other components, such as the "synchronous" part of draft tube pressure fluctuation, always interact with the rest of the system and cannot normally be directly transposed. Items concerned are, for instance, the fluctuations of turbine intake pressure, discharge, and shaft torque. A method about synchronous pressure fluctuation transposition is shown as Annex G.

7.5 Statistical analysis of model and prototype transposition accuracy

In order to quantify the accuracy that may be expected for transposition of pressure fluctuation amplitude, a statistical analysis of model and prototype test results on several power plants has been done. Table 3 to Table 5 show the statistical accuracy of the transposition.

Table 3 – Accuracy for transposition of fluctuation amplitude in draft tube cone

Flow Q_H / Q_{optH}	Average value of $\Delta\tilde{p}_{nD,97\%}$	Standard deviation of $\Delta\tilde{p}_{nD,97\%}$	2 x standard deviation of $\Delta\tilde{p}_{nD,97\%}$
0,25~0,60	0,07	0,14	0,28
0,60~0,95	0,01	0,09	0,17
0,95~1,15	0,01	0,05	0,10
1,15~1,40	0,00	0,12	0,23

Table 4 – Accuracy for transposition of fluctuation amplitude in vaneless zone

Flow Q_H / Q_{optH}	Average value of $\Delta\tilde{p}_{nD,97\%}$	Standard deviation of $\Delta\tilde{p}_{nD,97\%}$	2 x standard deviation of $\Delta\tilde{p}_{nD,97\%}$
0,25~0,60	-0,10	0,11	0,21
0,60~0,95	-0,09	0,13	0,25
0,95~1,40	-0,09	0,06	0,11

IECNORM.COM : Click to view the full PDF of IEC TS 62882:2020

Table 5 – Accuracy for transposition of fluctuation amplitude in spiral case

Flow Q_H / Q_{optH}	Average value of $\Delta\tilde{p}_{nD,97\%}$	Standard deviation of $\Delta\tilde{p}_{nD,97\%}$	2 x standard deviation of $\Delta\tilde{p}_{nD,97\%}$
0,25~0,60	0,05	0,11	0,22
0,60~0,95	-0,03	0,08	0,16
0,95~1,15	-0,04	0,05	0,10
1,15~1,40	-0,06	0,06	0,11

The statistical definition of accuracy is that 95 % of observed prototype pressure fluctuation amplitudes are expected to fall within the measured value of corresponding model pressure fluctuation amplitude plus or minus the accuracy.

Further details of the statistical analysis can be found in Annex H.

8 Mitigations

8.1 Draft tube vortex phenomena

8.1.1 General

The characteristics of the vortex rope give rise to pressure fluctuations within the draft tube cone. Depending on the nature of the vortex rope, the resulting fluctuations can be stochastic or cyclic. Periodic motion of the vortex rope gives rise to forced pressure oscillations within the draft tube cone. These conditions of surge can lead to the development of noise, vibration, power swings, vertical displacement of the runner and shaft, as well as disturbances that propagate back through the penstock. The well-defined motion of the vortex rope can result in a frequency that matches the natural frequency of the hydraulic system, thereby leading to a resonance condition that amplifies the existing pressure fluctuations.

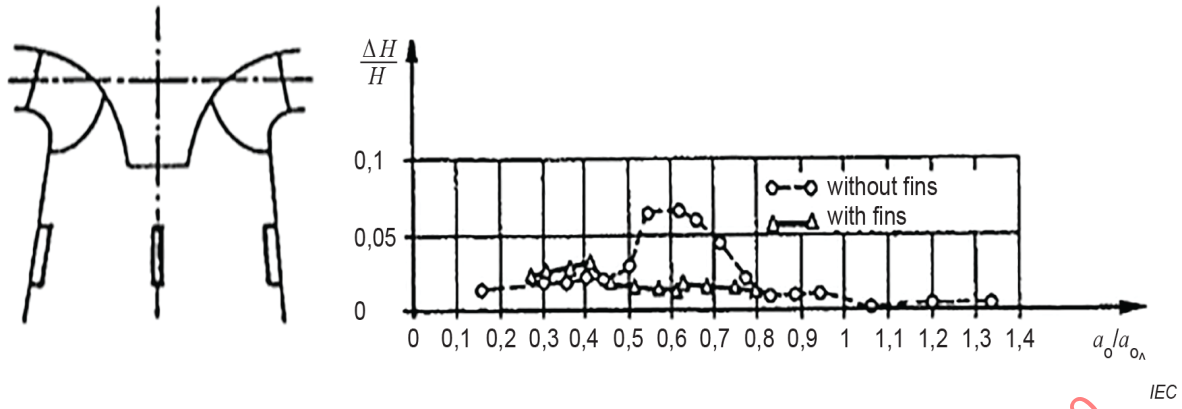
Several mitigation techniques can be used to reduce draft tube pressure fluctuations by influencing the vortex rope size and/or frequency. A brief description of the most common mitigations for draft tube pressure fluctuations are provided in 8.1.2 to 8.1.5.

NOTE There is no single mitigation that addresses all types of draft tube pressure fluctuations.

8.1.2 Draft tube fins

Draft tube fins can be used to reduce pressure fluctuations by reducing the swirl in the upper portion of draft tube during off-design operation. The main effect of draft tube fins on the part-load fluctuation is to reduce the amplitude of the pressure source Δp_{EX}, and therefore also the synchronous fluctuation. Fins of this nature are typically comprised of narrow extensions that are oriented vertically on the inside wall of the draft tube cone. Figure 23 provides an example of typical fin placement in the draft tube cone and the influence on draft tube pressure fluctuations.

IECNORM.COM : Click to view the full PDF of IEC TS 62882:2020



Source: Henry 1983 [63], Grein 1980 [61]

Figure 23 – Example of fins in the draft tube and influence on the pressure fluctuations

The addition of draft tube fins influences turbine efficiency by impacting the flow characteristics and friction losses within the draft tube. In general, the use of draft tube fins decreases turbine efficiency across the operating range. At best efficiency, the flow exiting the runner is nearly axial and the impact of efficiency is smallest. At off-design conditions with increased swirl, the efficiency decreases are larger than those observed at best efficiency operation. It should be noted that there are some cases where special fin designs have resulted in a small efficiency increase to a narrow band of the operating range.

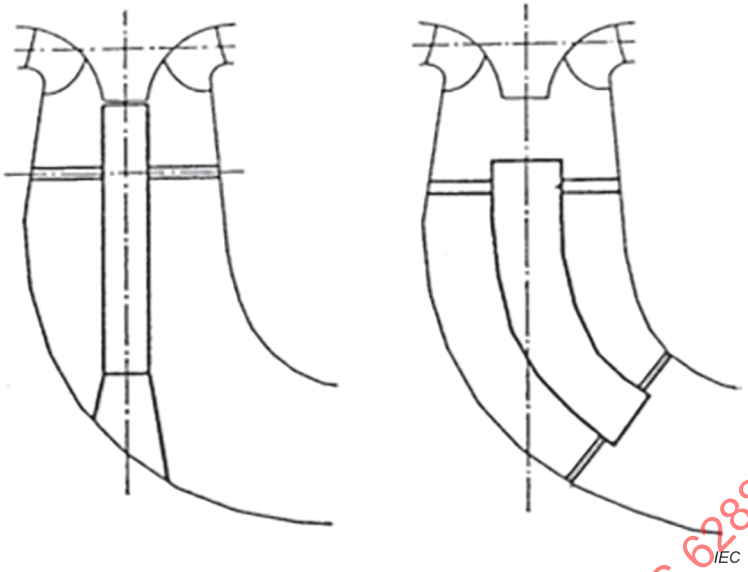
During operation, changes in flow incidence at the fin leading edge can give rise to cavitation. Aerating fins can be used to admit atmospheric air locally at the low pressure zone and mitigate cavitation damage.

Care should be also taken to ensure that the fins are designed to ensure robustness. Improper fin designs have resulted in structural failure that resulted in the fin detaching from the draft tube cone wall. In the case of sediment in the water, the fin should be designed according to particle erosion criteria.

8.1.3 Draft tube with a central column

Draft tube surges can also be reduced by means of other types of draft tube inserts. Placing a central tube in the draft tube axis, between the runner hub and elbow, can provide smoother operation. Figure 24 illustrates the central column concept.

IECNORM.COM : Click to view the full PDF of IEC TS 62882:2020



Source: Grein 1980 [61], Jacob 1988 [20]

Figure 24 – Example of the draft tube with central column extension

This design was probably inspired by the much older Moody cone. The central column also has some effect on the pressure source. There is a considerable lateral force of the vortex rope acting on the central tube; therefore, sufficient radial support is essential. Stress concentrations at locations where radial struts join the draft tube wall and central tube are possible problem areas to be considered.

A variation of the central column concept involves extending the runner cone into the upper portion of the draft tube. Examples of runner cone modifications are shown in Figure 25.

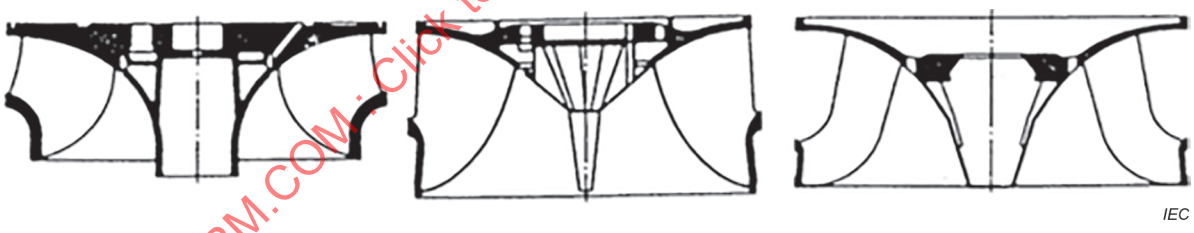


Figure 25 – Typical runner cone extensions used for reducing draft tube pressure fluctuations

IECNORM.COM : Click to view the full PDF of IEC TS 62882:2020

8.1.4 Air admission

Air admission or air injection downstream of a Francis or pump-turbine operating as a turbine can be an effective way to mitigate a variety of draft tube pressure fluctuations. The presence of the air can help to damp the asynchronous component of the pressure fluctuation. Air can also influence the acoustic characteristics of the component, thereby altering the draft tube natural frequency. For this reason, air can be used to reduce pressure fluctuations related to resonance.

In practice, there are two primary methods of air admission used for draft tube pressure fluctuations. These methods are often referred to as central aeration and peripheral aeration and correspond to where the air is being introduced into the water passage. Each method has a unique piping system that transports air from outside the turbine to the air injection location located within the water passage. Illustrations of common central and peripheral aeration configurations are provided below in Figure 26.

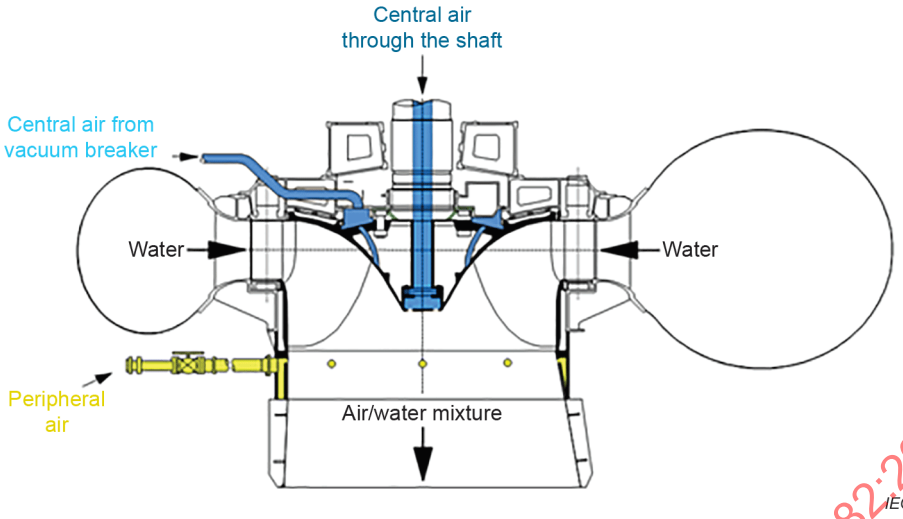
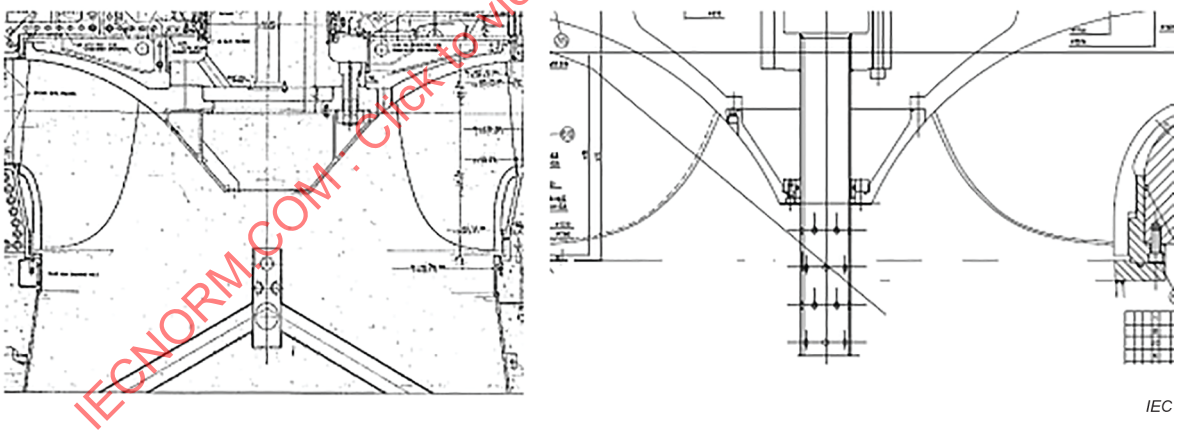


Figure 26 – Central and peripheral air admission locations for draft tube pressure fluctuations on a radial flow turbine

Natural air admission sometimes removes flow instability by manipulating the hydraulic transmission behaviour – in particular by lowering the draft tube natural frequency. This effect can also be counterproductive in certain cases because a resonance of the synchronous draft tube fluctuation may be produced by air injection in a pump turbine or Francis turbine with rather high submergence.

Depending on turbine characteristics, it is often necessary to add inserts into the draft tube, like tripods or pipes protruding from the draft tube wall. Illustrations of a tripod or central aerating pipe are provided in Figure 27.



a) With a tripod b) With a perforated pipe

Figure 27 – Central air admission

8.1.5 AVR or PSS parameter tuning

An average voltage regulator (AVR) and possible power system stabilizers (PSS) acting on the excitation system of the generator rotor have a significant influence on the generator local mode of oscillation also known as the "generator natural frequency". Therefore, if significant active power fluctuations arise in case of hydroelectric resonance between a draft tube induced pressure fluctuations and the electrical system, it is possible to adjust specifically the parameters of the AVR and PSS devices in order to modify the generator local mode of oscillation to reduce the amplitudes of active power fluctuations. Such parameter tuning will however have no impact on the hydraulic system pressure fluctuations.

IECNORM.COM : Click to view the full PDF of IEC TS 62882:2020

8.2 Runner inter-blade vortex

To some extent, the limits of occurrence can be pushed back by adequate layout of the runner blade profile. If the range of operating heads in a Francis turbine is extreme, the occurrence of inter-blade vortex at partial load and high head may become unavoidable.

As an example, in a large plant, the maximum head is 2,6 times higher than the minimum head. At very high head – about 125 % of best efficiency head –, the operation becomes very rough and extremely noisy. In such a case, air injection upstream of the runner is often highly effective in vibration and noise abatement.

8.3 Blade interaction

The combination of blade numbers Z_B and guide vane numbers Z_G shall be selected carefully. Depending on this combination, different mode shapes of vibration will occur. Inadequate blade number selection can lead to unwelcome fluctuation, vibration, and noise. In some cases, the consequences may go as far as to necessitate replacement of the runner by another one with different blade numbers Z_B.

If excitation levels are high, it is advisable to avoid resonance between the possible modes of pressure excitation due to blade row interaction and the corresponding vibration modes of the runner. The consequences of resonance are most severe if the interaction occurs at a low order of the runner harmonic k. However, the ultimate criteria for acceptability are vibration and dynamic stress levels rather than the presence or absence of resonance. The radial clearance between the guide vane and runner blade exterior edge has an important influence on the disturbances created by RSI. This explains the particular importance of RSI in pump turbines and high-head Francis turbines. In nonregulated machines – storage pumps and multistage pump turbines –, it may be possible to increase the radial gap between the runner and diffuser.

Some reduction of the intensity of interaction may be obtained by increasing the runner blade lean angle. The impact of the runner pressure pulse with the stator is then distributed over a longer time interval as the rotor-stator blades are not exactly aligned. At the same time, the magnitude of the disturbance averaged across the height of the flow channel is reduced.

8.4 Operation restriction

In the worst case, the operating range shall be restricted. Pressure fluctuation measurements are then coupled with other parameters which have fluctuation limits beyond which the mechanical integrity of the machine and the electrical stability of the grid are impacted.

IECNORM.COM : Click to view the full PDF of IEC TS 62882:2020

Annex A
(informative)

Example of pressure fluctuation records

Annex A shows some typical records of pressure fluctuations. Figure A.1 to Figure A.9 include three diagrams as follows.

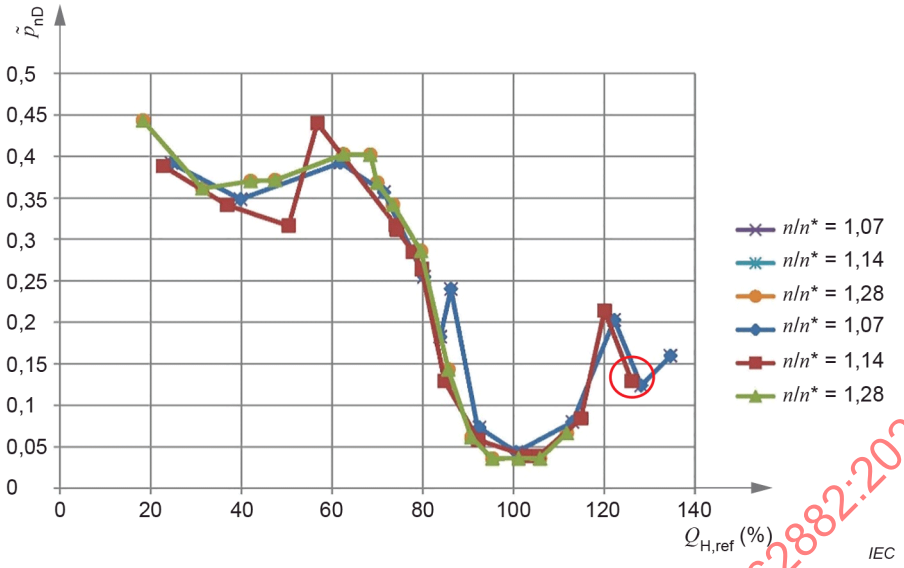
a) A diagram showing the pressure fluctuation coefficient, $\tilde{p}_{\mathrm{nD}}$, as a function of relative flow, $Q_{\mathrm{H,ref}}$. In this diagram, the point in question is circled. This diagram gives a quick overview of where in the operating zone we are and what type of fluctuation mode can be expected.

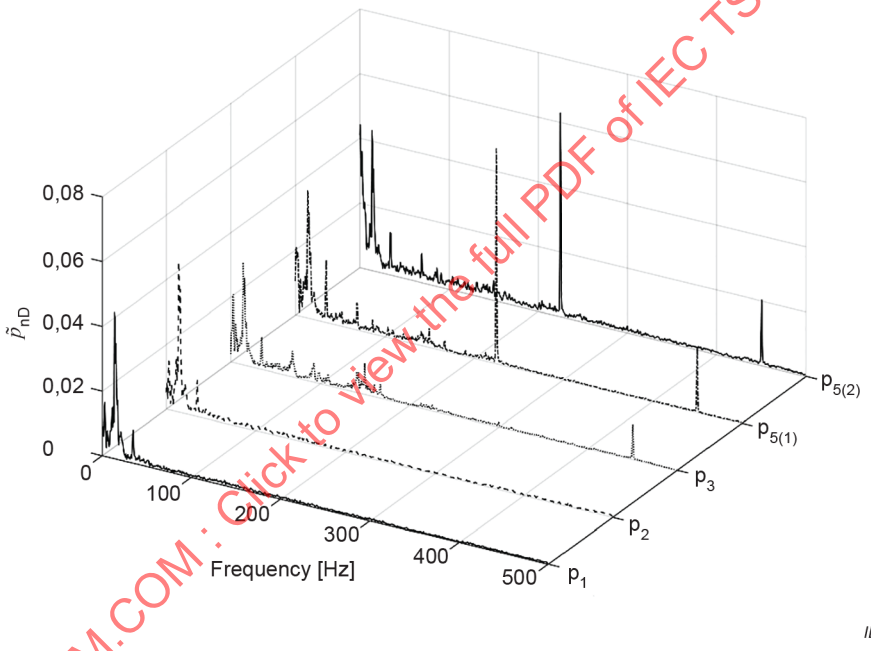
b) A diagram in the frequency domain showing the $\tilde{p}_{\mathrm{nD}}$ as a function of fluctuation frequency. This diagram is obtained by performing a fast Fourier transform (FFT) on the time signals. This diagram contains data for the relevant pressure transducer locations in a waterfall format. The fln relationship for the dominant frequency is also noted.

NOTE For measuring points $p_{5(1)}$ and $p_{5(2)}$, the pressure fluctuation coefficient is based on the runner inlet diameter (D_1) instead if the runner nominal diameter (D). This pressure fluctuation coefficient is called $\tilde{p}_{\mathrm{nD1}}$.

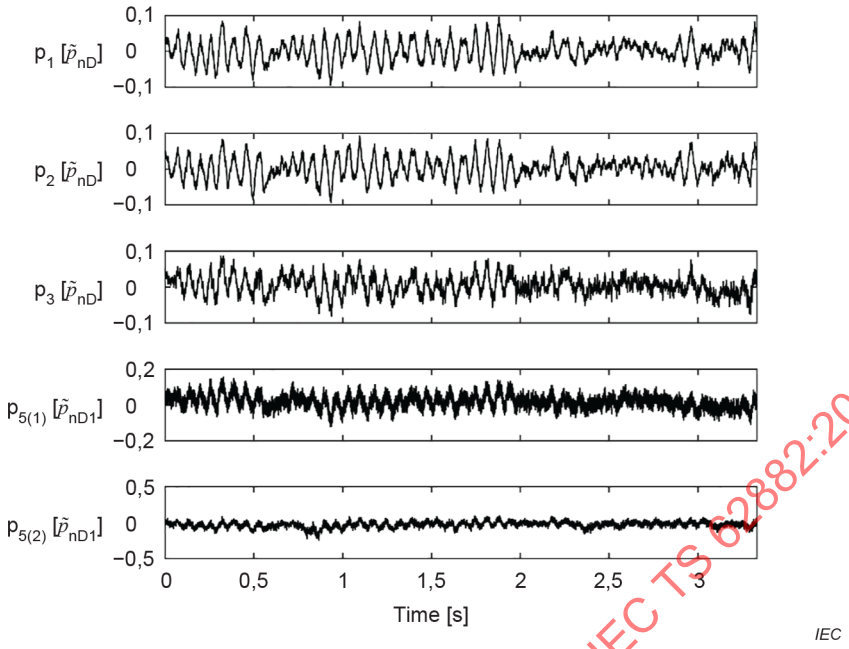
c) A diagram in the time domain of the same signals as those under the frequency domain.

IECNORM.COM : Click to view the full PDF of IEC TS 62882:2020





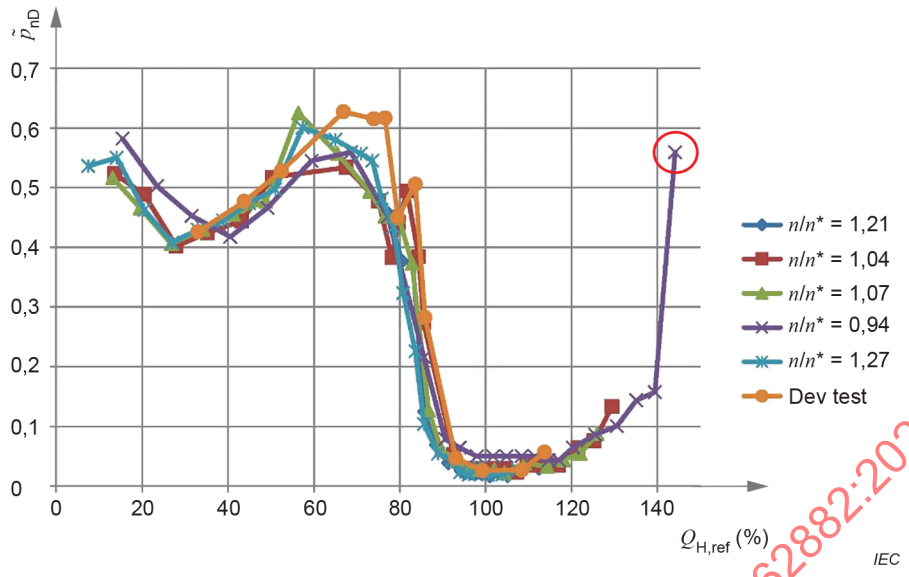
IECNORM.COM : Click to view the full PDF of IEC TS 62882:2020

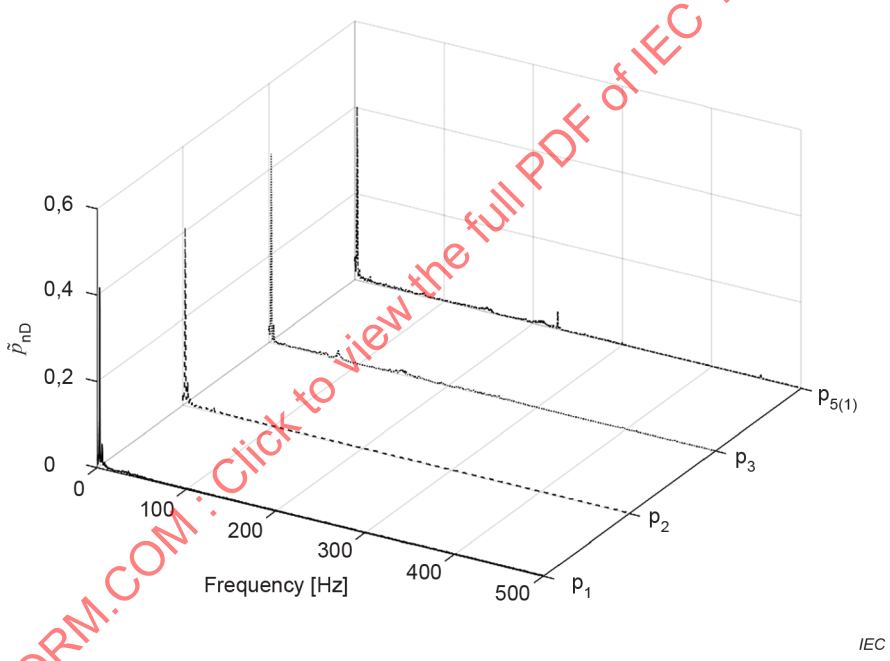


NOTE fln = 0,85

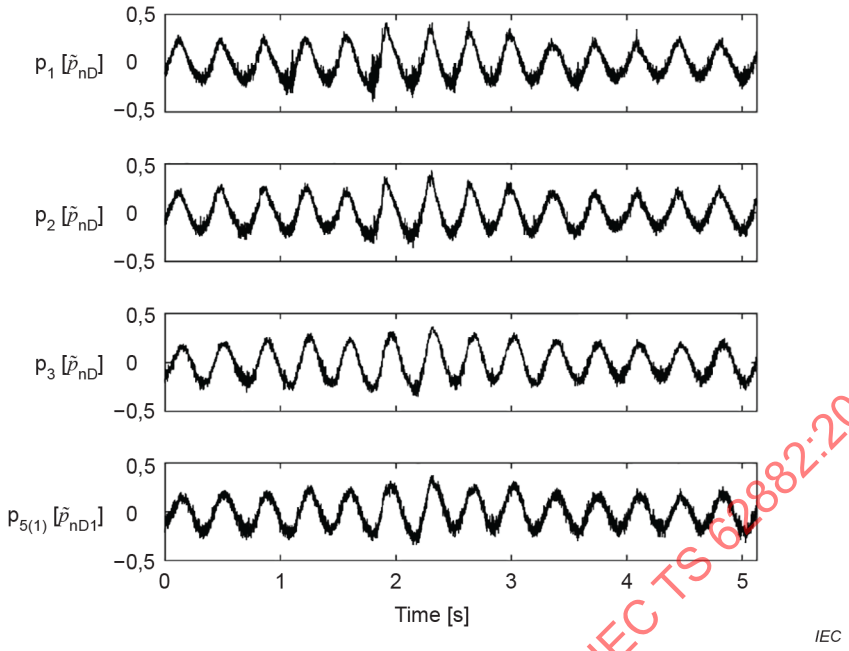
Figure A.1 – Example 1: a case corresponding to mode 1 (a limited high load)

IECNORM.COM : Click to view the full PDF of IEC TS 62882:2020





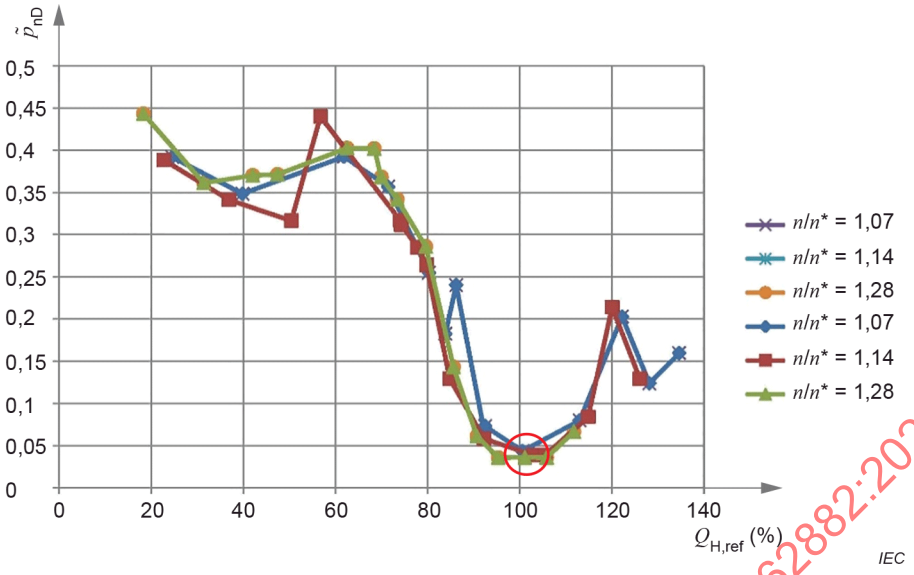
IECNORM.COM : Click to view the full PDF of IEC TS 62882:2020

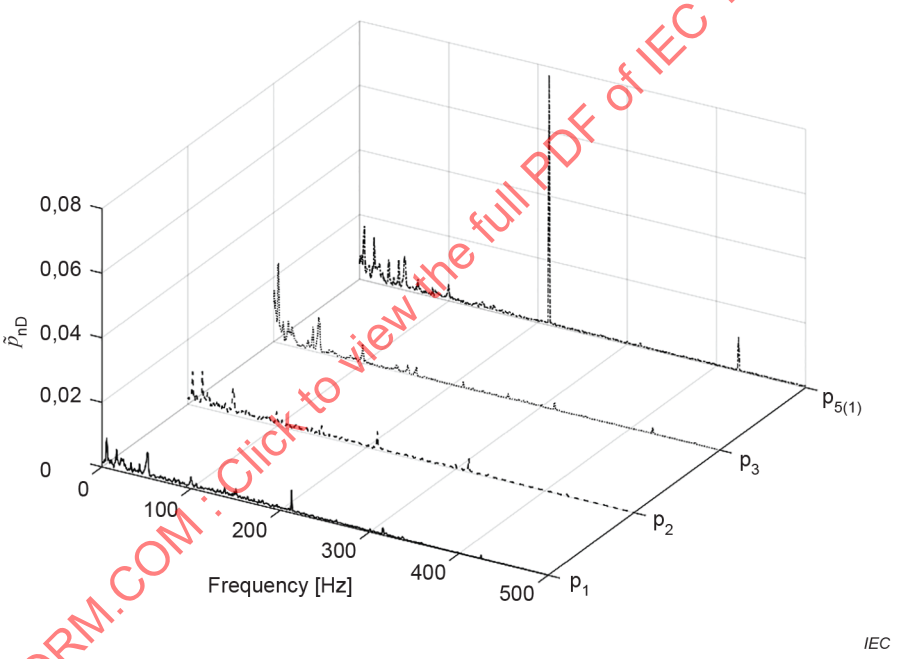


NOTE f/n = 0,15

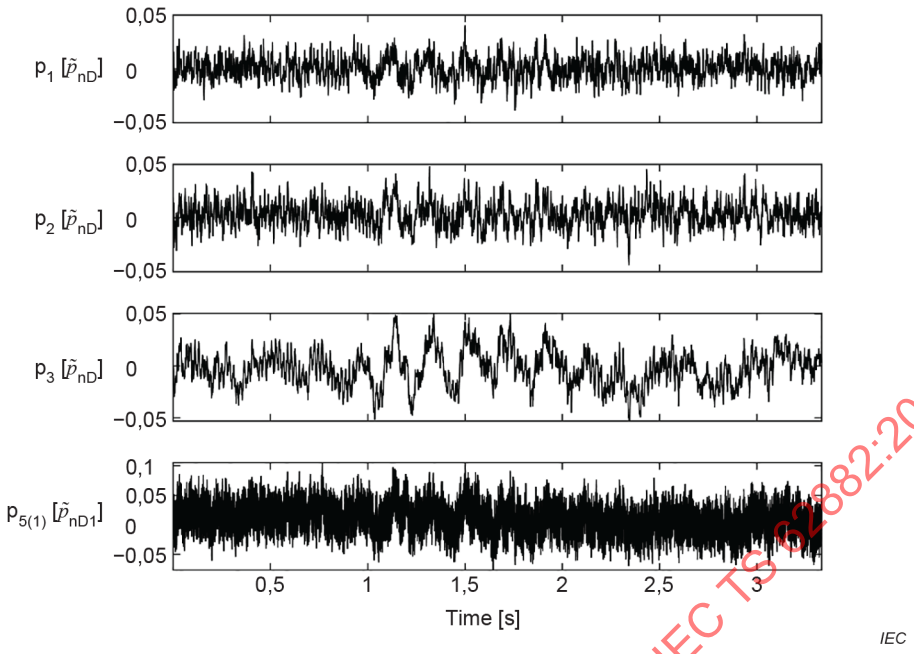
Figure A.2 – Example 2: a case corresponding to mode 1 (a large overload)

IECNORM.COM : Click to view the full PDF of IEC TS 62882:2020





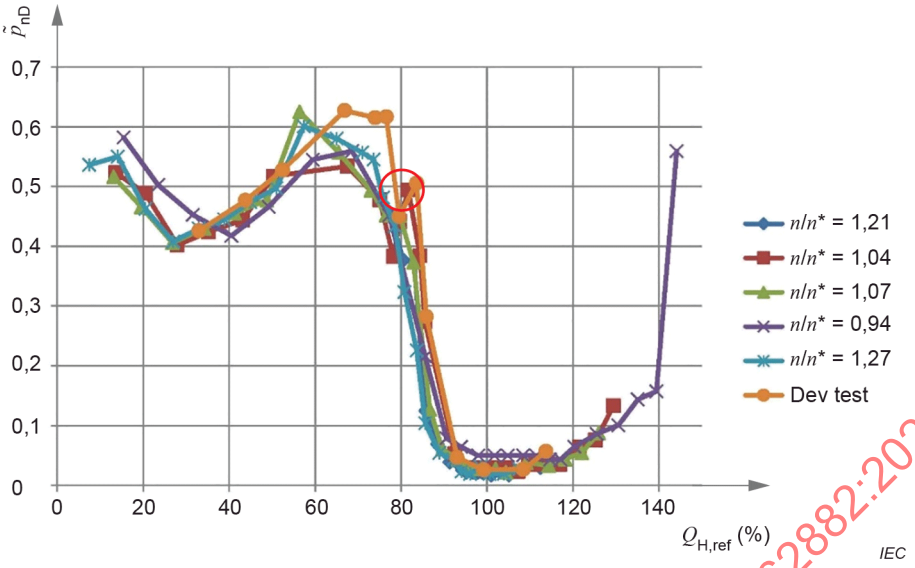
IECNORM.COM : Click to view the full PDF of IEC TS 62882:2020

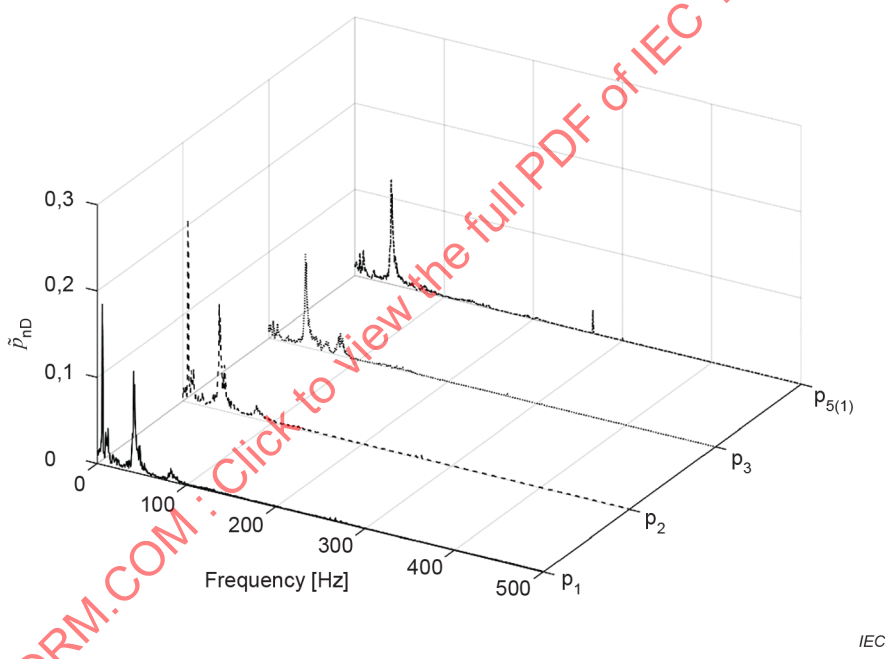


NOTE fln = undefined.

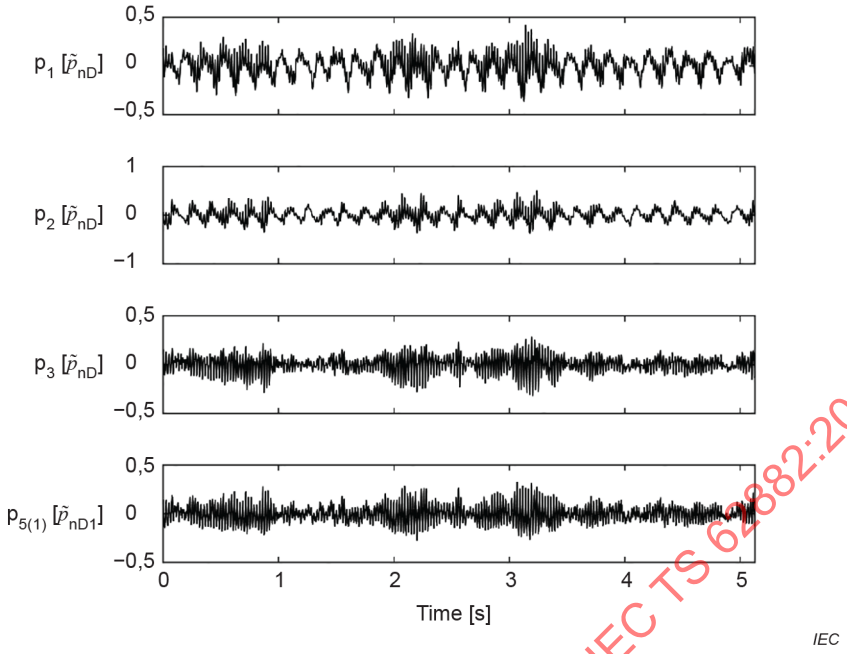
Figure A.3 – Example 3: a case corresponding to mode 2

IECNORM.COM : Click to view the full PDF of IEC TS 62882:2020





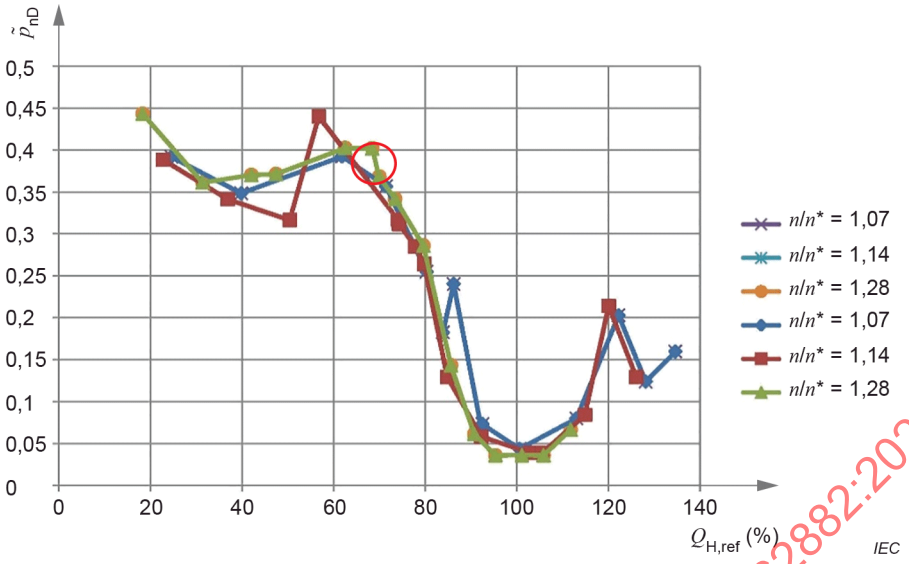
IECNORM.COM : Click to view the full PDF of IEC TS 62882:2020

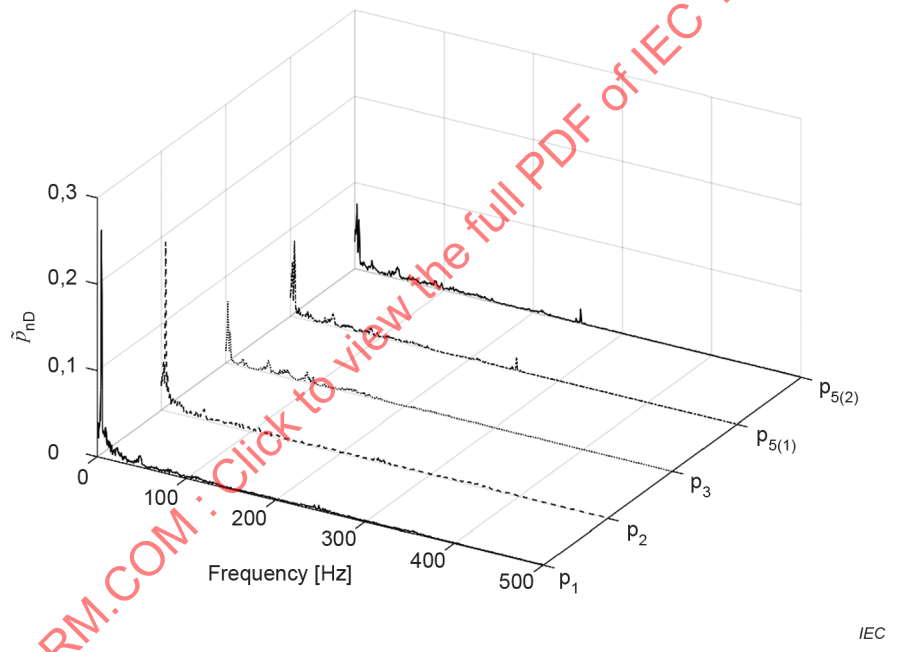


NOTE fln = 0,3; fln = 2,0.

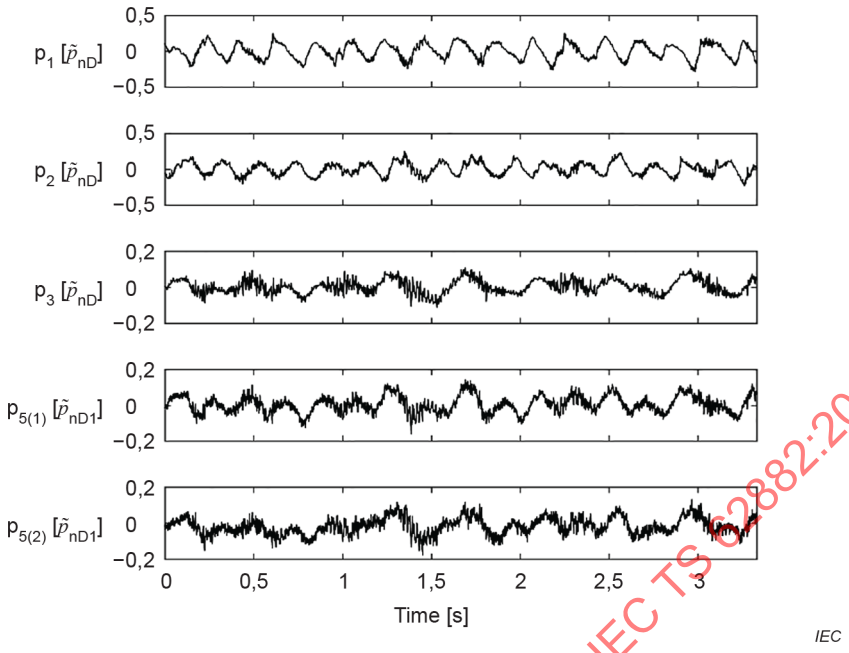
Figure A.4 – Example 4 : a case corresponding to mode 3

IECNORM.COM : Click to view the full PDF of IEC TS 62882:2020





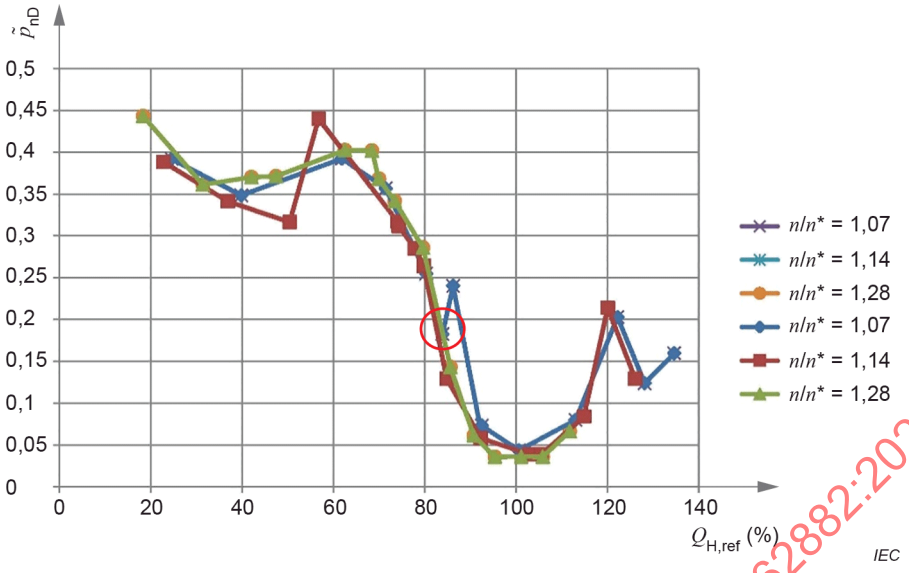
IECNORM.COM : Click to view the full PDF of IEC TS 62882:2020

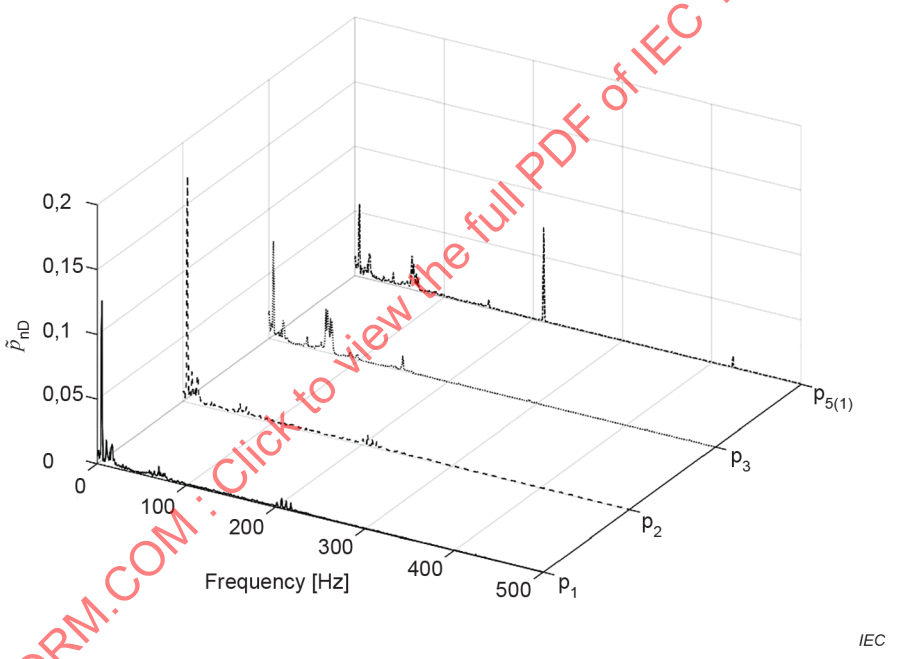


NOTE fln = 0,25.

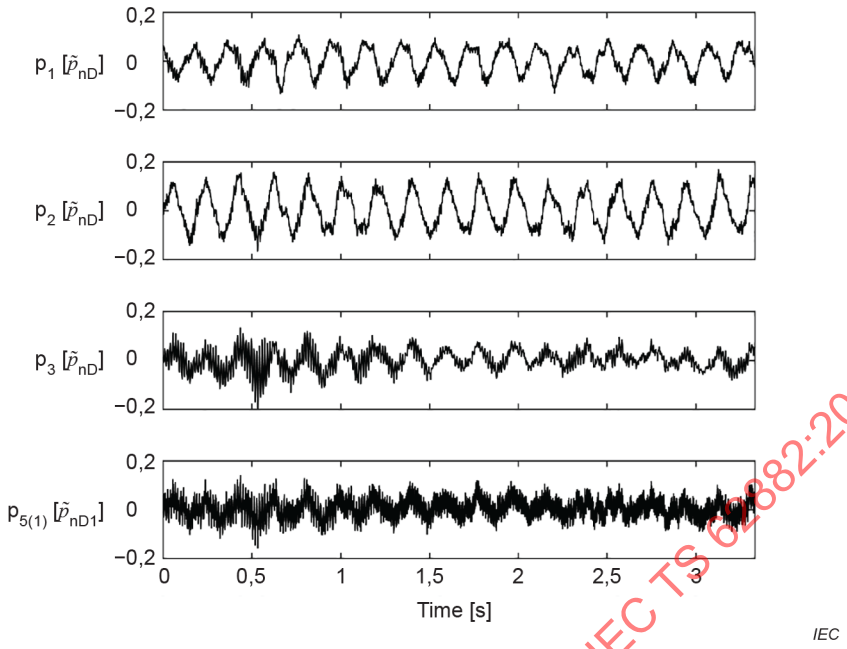
Figure A.5 – Example 5 : a case corresponding to mode 4.a and 4.b

IECNORM.COM : Click to view the full PDF of IEC TS 62882:2020





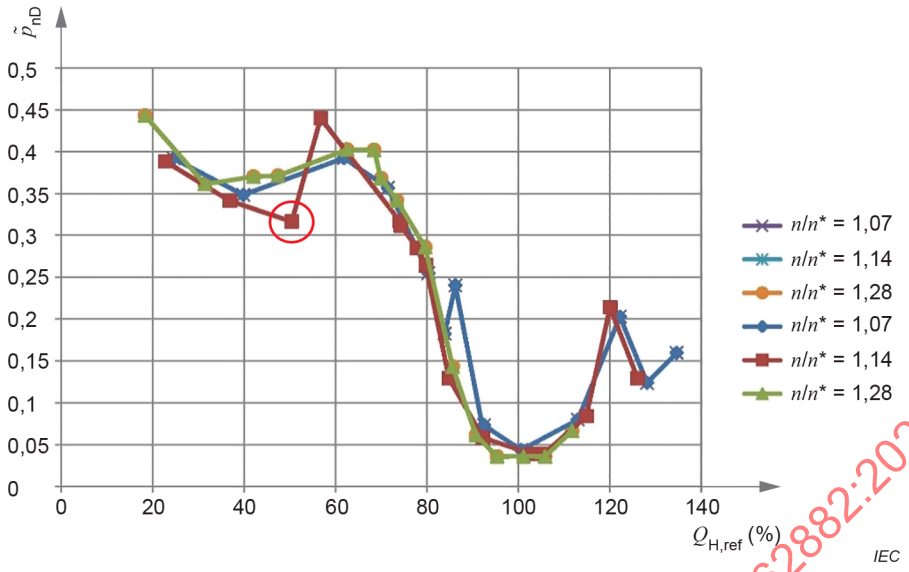
IECNORM.COM : Click to view the full PDF of IEC TS 62882:2020

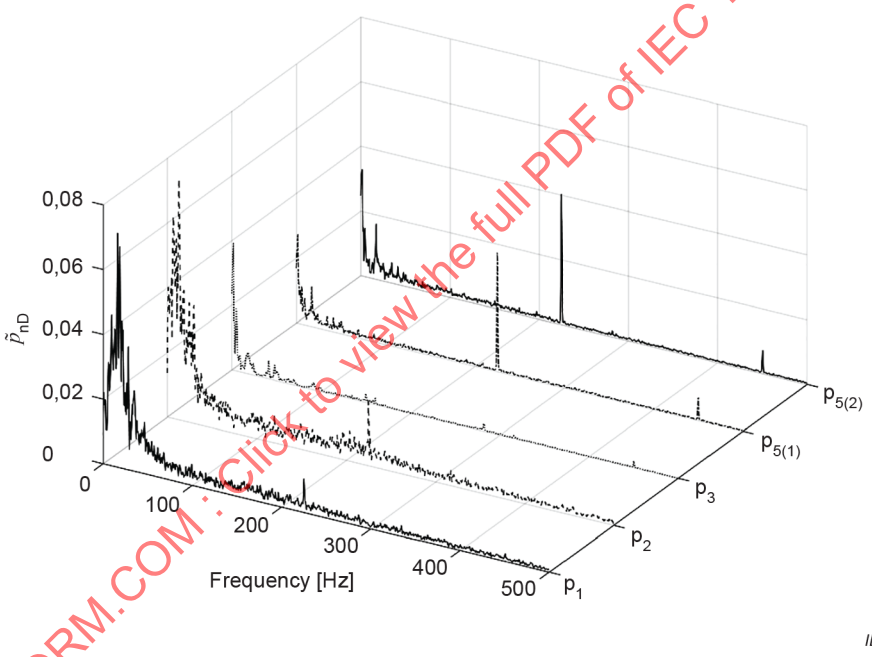


NOTE fln = 0,31.

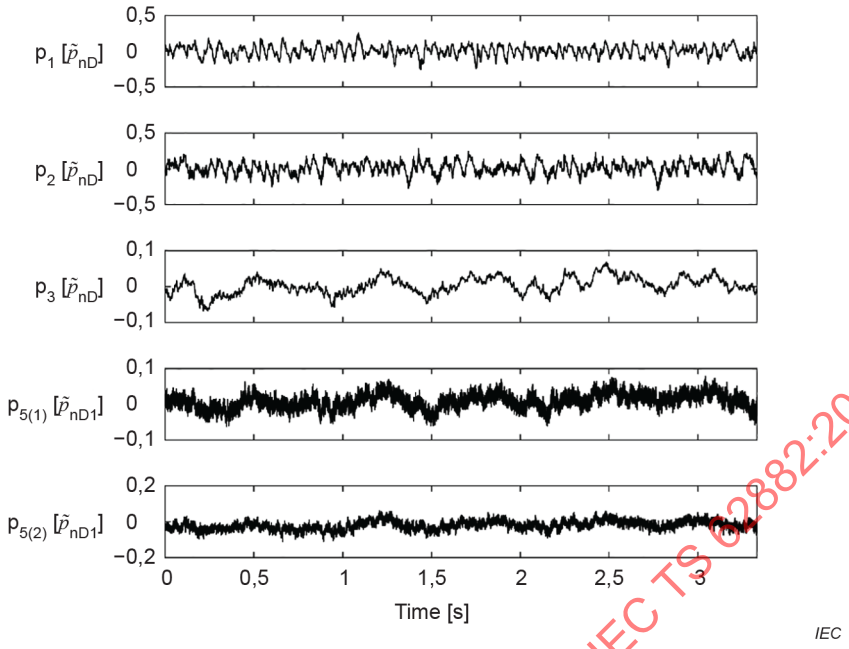
Figure A.6 – Example 6: a case corresponding to mode 4.a and 4.b

IECNORM.COM : Click to view the full PDF of IEC TS 62882:2020





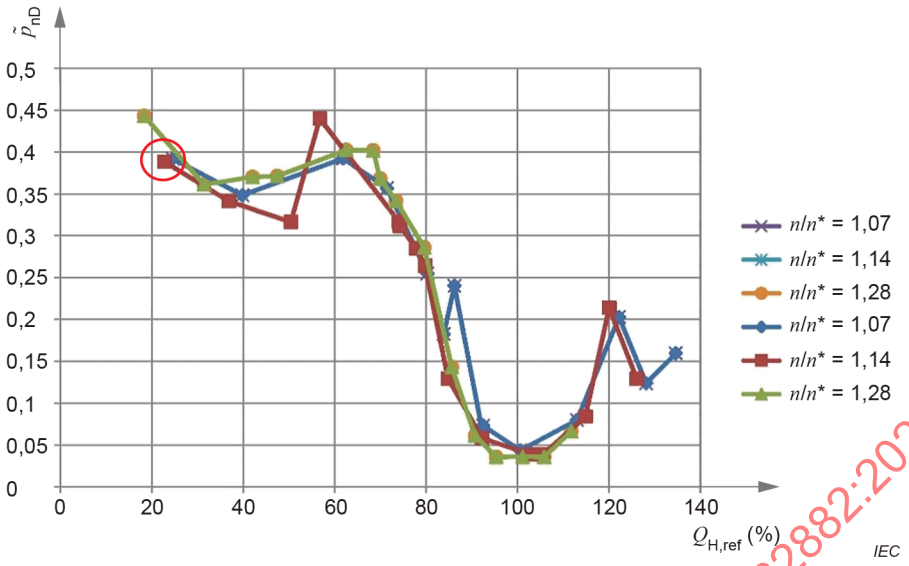
IECNORM.COM : Click to view the full PDF of IEC TS 62882:2020

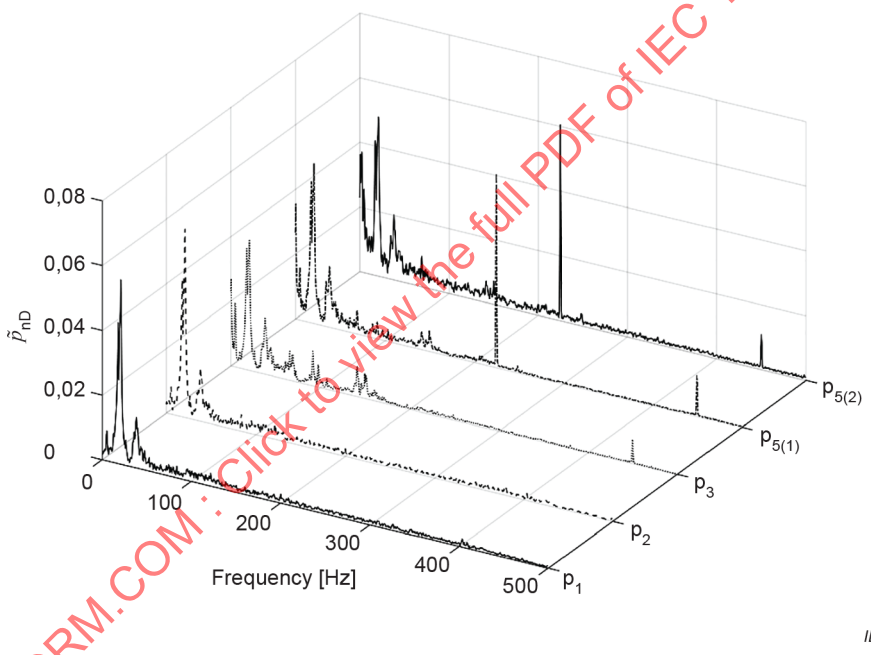


NOTE fln = 1,00; fln = 0,77.

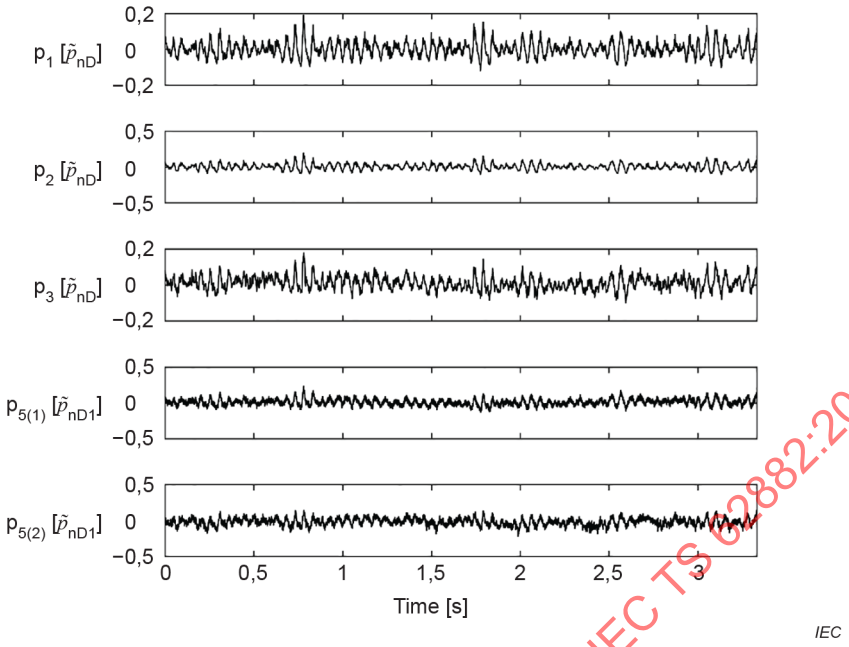
Figure A.7 – Example 7: a case corresponding to mode 4.c

IECNORM.COM : Click to view the full PDF of IEC TS 62882:2020





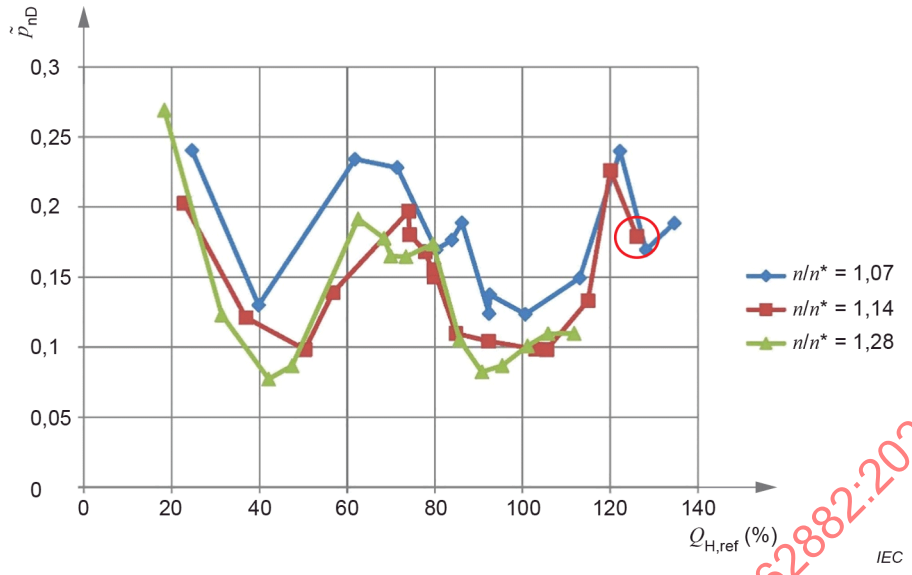
IECNORM.COM : Click to view the full PDF of IEC TS 62882:2020

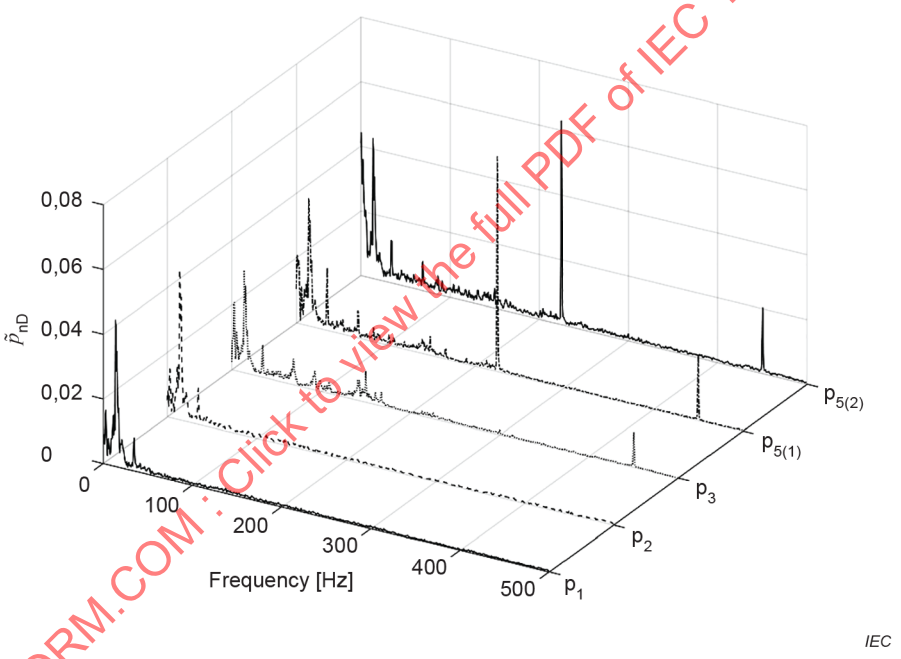


NOTE fln = undefined.

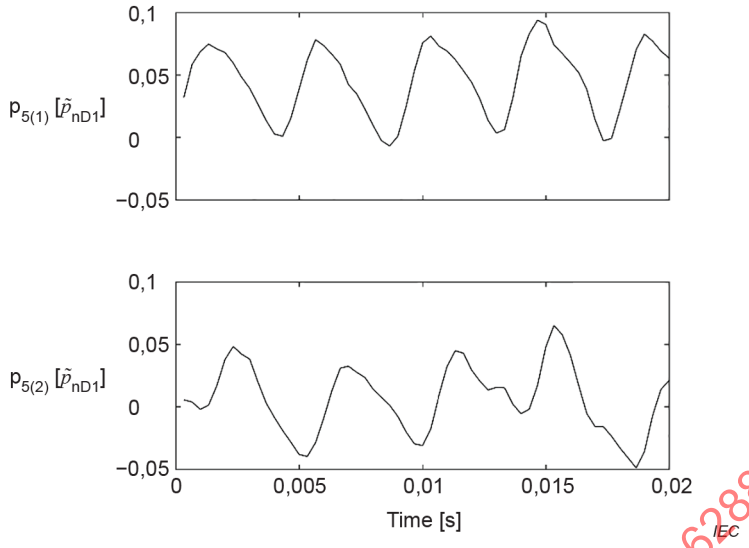
Figure A.8 – Example 8: a case corresponding to mode 5.b

IECNORM.COM : Click to view the full PDF of IEC TS 62882:2020





IECNORM.COM : Click to view the full PDF of IEC TS 62882:2020



NOTE $fln = 13 = Z_r$.

Figure A.9 – Example 9: a case corresponding to mode 6.a

IECNORM.COM : Click to view the full PDF of IEC TS 62882:2020

Annex B
(informative)

Typical pressure fluctuation transducers parameters for model test

It is recommended to adopt high resolution dynamic pressure transducers for measurement of the model turbine pressure fluctuation .

The typical parameters listed below correspond to a transducer typically used for different model locations:

high resolution:	±1 % ρE
pressure measuring range:	> 70 kPa
rising time:	< 5 µs
resonant frequency:	> 200 kHz
low frequency response:	< 1 Hz
non-linearity:	2 % FS

The frequency range of the transducers should be such that the complete frequency band of interest can be measured.

When designing the signal path of transducers and amplifiers, it should reduce the impact of circumstance on the signals, such as being far away from the power line, to avoid big temperature variation. Take care of shielding and grounding properly. Join and connecting terminal should have reliable mechanical and electrical stability.

The parameters listed below correspond to a transducer typically used for a prototype (range changes with head and expected maximum pressure):

pressure measuring range:	70 mbar to 100 bar
resonance frequency:	> 2 kHz
non-linearity, hysteresis and repeatability:	< 2 % FS

IECNORM.COM : Click to view the full PDF of IEC TS 62882:2020

Annex C
(informative)

Pressure transducer dynamic calibration

C.1 Fast valve opening method

Figure C.1 is the schematic diagram of jump pressure standards with a quick open valve method. Because of its large pressure range and long holding time of pressure platform, this method is suitable for the sensitivity and low frequency characteristics of pressure transducers.

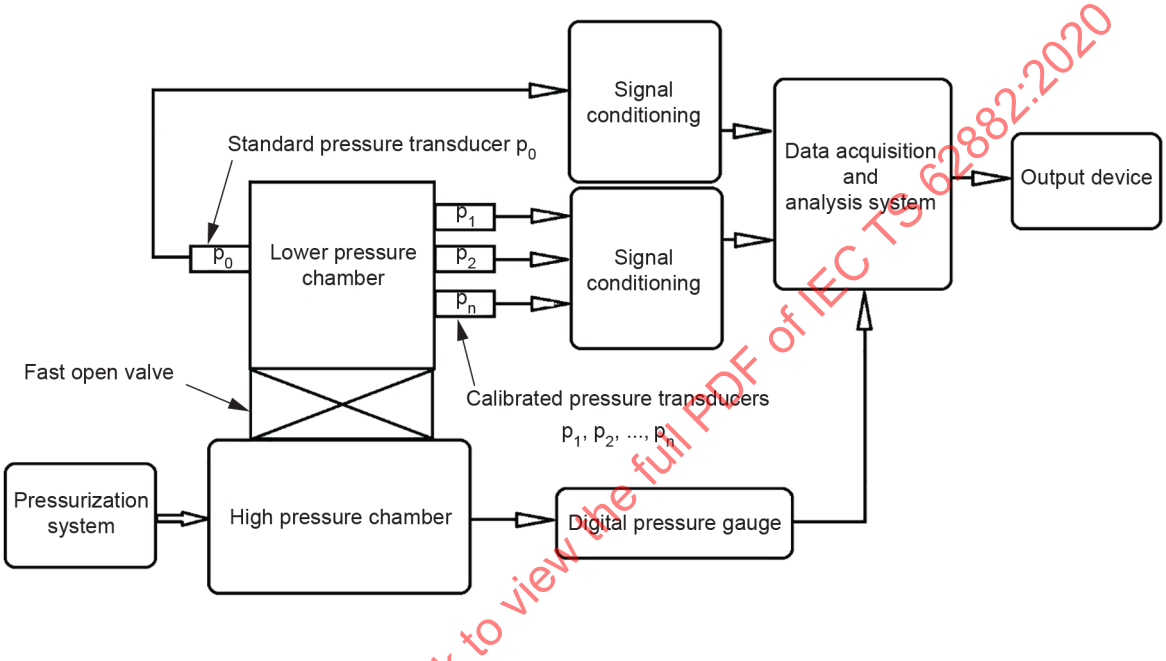


Figure C.1 – Pressure transducer dynamic calibration schematic diagram with fast open valve method

C.2 Rotating valve method

Figure C.2 presents an example of a facility to perform a dynamic calibration of a pressure transducer with the rotating valve method. The facility is a closed loop system which includes a feeding pump, a linking pipe to a test section instrumented with several pressure transducers flush mounted at the same elevation then connected to a rotating valve, a flow control valve and an air vessel that supply the feeding pump. The rotational speed of the rotating valve is controlled in order to generate pressure fluctuations in the test section over a wide frequency range, while a flow control valve enables to adjust the discharge of the test loop and thus the amplitudes of the pressure fluctuations in the test section. The test section should include a reference pressure transducer provided with supplier dynamic calibration. Simultaneous acquisition of pressure time history from the test pressure transducers and reference pressure transducer enables to compute the transfer function between the test and reference pressure transducers for frequency response evaluation.

IECNORM.COM : Click to view the full PDF of IEC TS 62882:2020

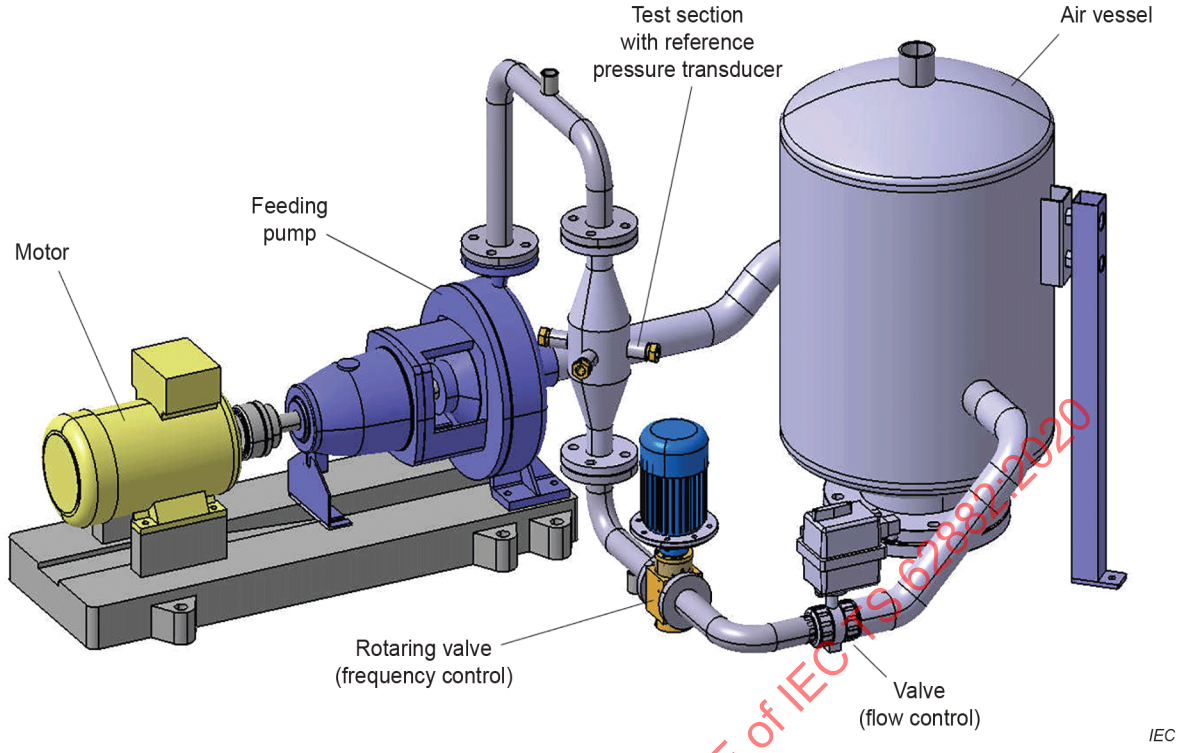


Figure C.2 – Pressure transducer dynamic calibration with rotating valve method

C.3 Electrical spark method

To create an impulse excitation in water, an electrical spark plug can be used (see Figure C.3). Pressure transducers and a spark plugs shall be flush mounted on the wall on the flange of a test vessel fully filled with water. Tests performed with the discharge of a 1,55 µF capacitor under a 4,3 kV voltage supply in a very short time (Δt < 25 µs) generate a discharge energy of 14,3 J producing a rapid increase of the water temperature. The explosive growth of a vapour bubble produces a pressure wave traveling towards the pressure transducers at the speed of sound. The impulsive excitation of test and reference pressure transducers over a wide frequency range enables to compute the transfer function for frequency response evaluation. The reference pressure transducer should be provided with supplier dynamic calibration.

IECNORM.COM : Click to view the full PDF of IEC TS 62882:2020



Figure C.3 – Spark plug used as to generate an impulse excitation in water for pressure transducer dynamic calibration

Annex D
(informative)

Proposed remote pressure measurement fluctuation correction

D.1 General

Pressure transducers are, ideally, mounted flush with the wetted internal surface (local sensor). It is not always possible to do this. If a sensor is mounted at the end of a connecting pipe (remote sensor), its peak-to-peak value is influenced by the first tubing natural frequency. Tubes are generally in steel of ½ inch or ¾ inch (which is about 1,27 cm or 1,905 cm) diameter, embedded in concrete, and their length can be from 1 m to 30 m. The natural frequency can either be evaluated knowing the tubing mechanical characteristics or measured by recording the rapid closure of the drainage valve. From there, one can remove the distorted part in the frequency domain and compute the peak-to-peak value in the time domain. Annex D is a case study for the spiral case inlet pressure that is often measured remotely. In Annex D, p_{local} is the local pressure fluctuation in the spiral case, p_1 to p_4 is the remote pressure fluctuation in the spiral case.

D.2 Correction method theory

The goal is to characterise the wave propagation in the tube to remove the distorted part measured at the tubing end (pressure sensor), to obtain the pressure at the other end (pressure tap, flush with the wetted internal surface in the penstock). The analysis is made in the frequency domain.

For a homogenous tube, wave propagation is essentially characterised by the speed and damping ratio. Pressure (P_{tap}) and speed (V_{tap}) at the pressure tap are linked to the pressure (P_{sensor}) and speed (V_{sensor}) at the sensor by the following transfer function:

$$\begin{pmatrix} p_{tap} \\ V_{tap} \end{pmatrix} = \begin{bmatrix} \cos\left(k_f L\right) & jZ_f \sin\left(k_f L\right) \\ j\sin\left(k_f L\right)/Z_f & \cos\left(k_f L\right) \end{bmatrix} \begin{pmatrix} P_{sensor} \\ V_{sensor} \end{pmatrix} \quad (D.1)$$

where

L is the tubing length between pressure the tap and sensor;

k_f is the complex number characterizing wave propagation in the tube;

Z_f is the fluid impedance.

Since the tube is closed at the sensor end, V_{sensor} is zero. Pressure at the tap is therefore related to the pressure at the sensor by Formula (D.2).

$$p_{tap} = \cos\left(k_f L\right) p_{sensor} \quad (D.2)$$

The wave number k_f is related to the speed propagation c_f by Formula (D.3).

$$k_f = \frac{2\pi f}{c_f}\left(1 + jn_f\right) \quad (D.3)$$

where

IECNORM.COM : Click to view the full PDF of IEC TS 62882:2020

f is the frequency;

c_f is the wave speed propagation in the tube ($4Lf_{1/4}$);

$f_{1/4}$ is the tube resonance frequency (open-closed tube).

and

$$n_f = \frac{dec}{2\pi f_{1/4}} \quad (D.4)$$

where

dec is the decay constant;

n_f is the damping ratio;

k_f is determined by generating a water hammer with the drainage valve.

The tube frequency response is therefore measured. The water hammer signal may be clipped, because the sensor can saturate, or it can simply characterize the tube. The water hammer generates a damped sinusoidal wave form as given in Formula (D.5).

$$p(t) = A\cos(2\pi f_{1/4} t + \varphi) e^{-dec\ t} \quad (D.5)$$

where

$p(t)$ is the pressure as a function of time;

A is the initial amplitude of the envelope;

φ is the phase shift at t = 0.

The identification of $f_{1/4}$ and dec in the resulting signal makes it possible to compute k_f. No error is made on the correction because $k_f L$ does not depend on L.

D.3 Measuring and estimating tube frequency response

Measuring the tube frequency response can be made by recording the rapid closure of the tubing drainage valve. Figure D.1 presents typical results of such records when the unit is in standstill. Each drainage valve was opened and closed one after the other.

IECNORM.COM : Click to view the full PDF of IEC TS 62882:2020

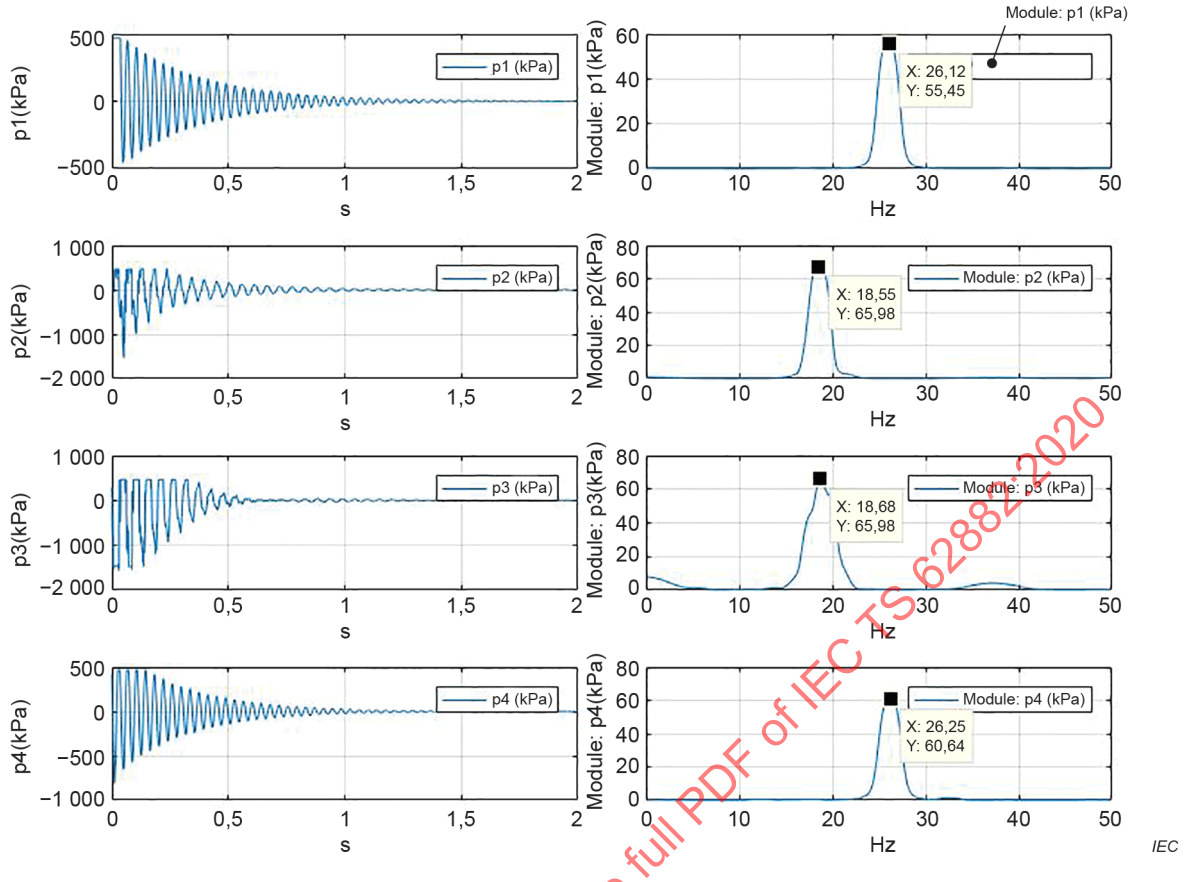


Figure D.1 – Typical results obtained by shutting off drainage valve

Variables $f_{1/4}$ and dec can be calculated using a curve fitting tool. In this particular example, Table D.1 presents the results.

Table D.1 – $f_{1/4}$ and dec calculated for p_1 to p_4

Locations	$f_{1/4}$ (Hz)	dec (1/s)
p_1	26,12	2,869
p_2	18,43	3,714
p_3	18,68	4,051
p_4	26,25	3,195

These frequencies are near the ones estimated knowing the tube mechanical characteristics. The following verification ensures the obtained frequencies are not way off.

In Formula (D.3), c_f depends on water temperature, pressure, air content, tube stiffness, etc. For cylindrical tubing, which is almost always the case, c_f is derived from Formula (D.6).

$$\frac{1}{c_f} = \frac{1}{c} + \frac{\rho D_i}{Ee} \qquad (D.6)$$

IECNORM.COM : Click to view the full PDF of IEC TS 62882:2020

where

c is the thermodynamic speed of sound in water;

ρ is the water density;

E is the modulus of elasticity of the wall (Young's modulus);

e is the wall thickness;

D_i is the connecting pipe internal diameter.

Formula (D.6) is a simplified one based on the following assumptions: axial strain (Poisson effect) and wall mass inertia are neglected, and wall deformation does not involve hydro-elastic interactions.

For this case study, Table D.2 shows tubing mechanical properties and computed first natural frequencies using Formulae (D.3) and (D.6).

Table D.2 – Estimated frequencies based on tubing mechanical characteristics

Variable	Unit	Definition	p_1, p_4	p_2, p_3	Source
c	$m \cdot s^{-1}$	Thermodynamic sound in water.	1 428	1 428	Belogol'skii at 5 °C and 1 450 kPa
ρ	$kg \cdot m^{-3}$	Water density.	1 000	1 000	
E	GPa	Young's modulus of wall.	200	200	
D_i	m	Internal diameter of pipe.	0,0118 11	0,0118 11	5/8'' outer diameter
e	m	Wall thickness.	0,002 032	0,002 032	Cedule 80
L	m	Length of tubing connecting the sensor to the penstock.	15,25	20,94	Estimated based on drawings
c_f	$m \cdot s^{-1}$	Velocity of wave propagation in the connecting piping.	1387,5	1387,5	
$c_f / 4L$	Hz	1st tubing natural frequency (calculation).	22,8	16,6	
$c_f / 4L$	Hz	1st tubing natural frequency (test).	23,4	17,1	

Natural frequency is estimated to be 22,8 Hz for short length tubes (p_1, p_4 = 15,25 m) and 16,6 Hz for longer ones (p_2, p_3 = 20,94 m).

NOTE Since D_i is small, these estimated frequencies are only 3 % smaller than those calculated with the thermodynamic speed of sound in water.

D.4 Pressure fluctuation correction

Figure D.2 shows the time signal and the frequency content of pressure signals p_1 to p_4 measured remotely along with p_{local} measured flush with the penstock. We notice clearly the pressure amplification at around 26 Hz for p_1 and p_4 and around 18 Hz for p_2 and p_3. This behaviour is not seen with local pressure tap p_{local}. Table D.3 presents the peak-to-peak in the 97 % confidence interval of all signals along with the error with respect to p_{local}.

IECNORM.COM : Click to view the full PDF of IEC TS 62882:2020

Table D.3 – Peak-to-peak value on the raw signals

Locations	Δp (kPa)	Error (%)
p_{local}	292	
p_1	334,9	14,7
p_2	342,2	15,0
p_3	339,2	13,8
p_4	326,3	10,1

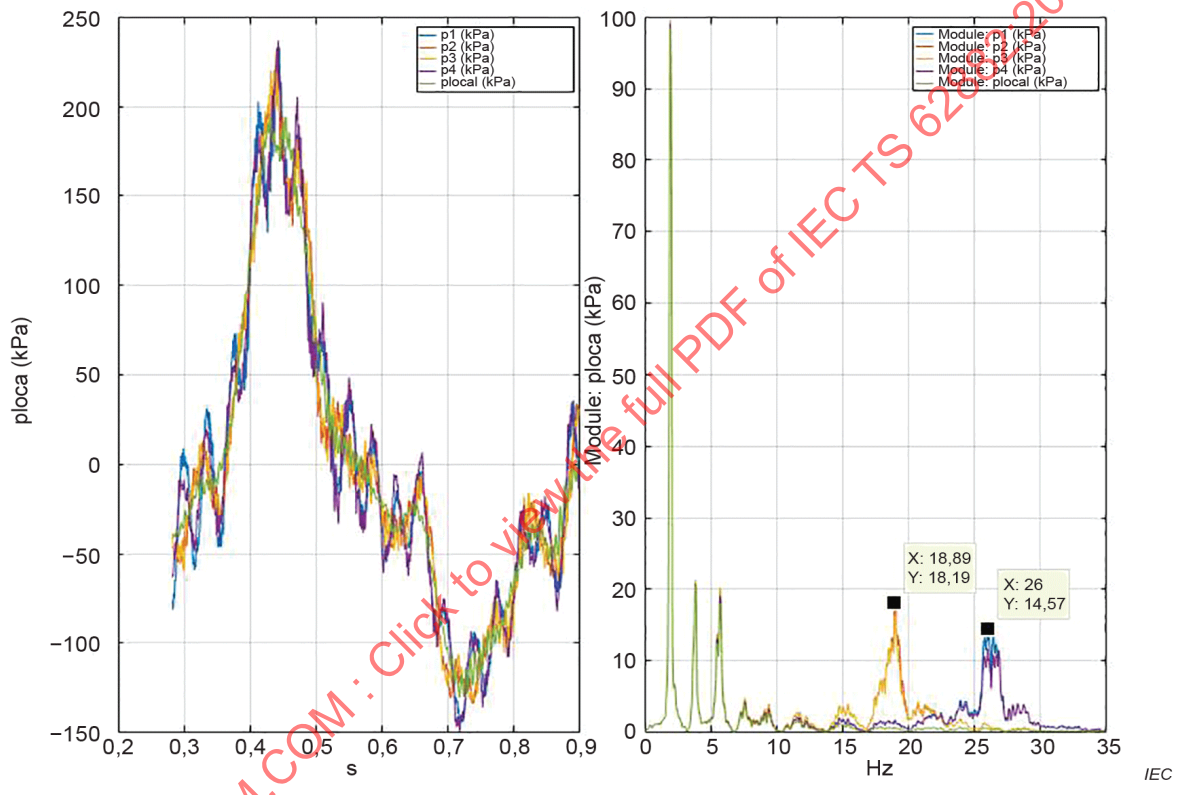


Figure D.2 – Signal and spectrum of four remote sensors and one local sensor

Using the estimated tubing length L, c_f and n_f were calculated using Formulae (D.3) and (D.4) (L can be anything since it cancels out in the process) and are shown in Table D.4.

Table D.4 – Wave speed and damping ratio

Locations	L (m)	c_f (1/s)	n_f
p_1	15,25	1 593,3	0,017 5
p_2	20,94	1 543,7	0,032 1
p_3	20,94	1 564,6	0,034 5
p_4	15,25	1 601,3	0,019 4

IECNORM.COM : Click to view the full PDF of IEC TS 62882:2020

The correction is done in the frequency domain as explained in Clause D.2. A sample of MATLAB®[3] is included here for information.

```
Yfft=fftshift(fft(Y)); % Y is the pressure signal
n=numel(Y); % n is the number of array elements
T=dt*n; % dt is the sampling period
df=1/T;
if ~mod(n,2);
    f = df*(-n/2:n/2-1); % n is even
else
    f = df*(-(n-1)/2:(n-1)/2); % n is odd
end
kf=2*pi*f/cf*(1+i*nf); % equation 3
fP=cos(kf'*L).*Yfft; % equation 2
Ycorr=ifft(ifftshift(fP),'symmetric'); % corrected pressure signal
```

Figure D.3 shows the exact same time signal as Figure D.2, but with corrected signals. Pressure amplification was removed successfully. Table D.5 present the peak-to-peak 97 % values obtained on the corrected signals.

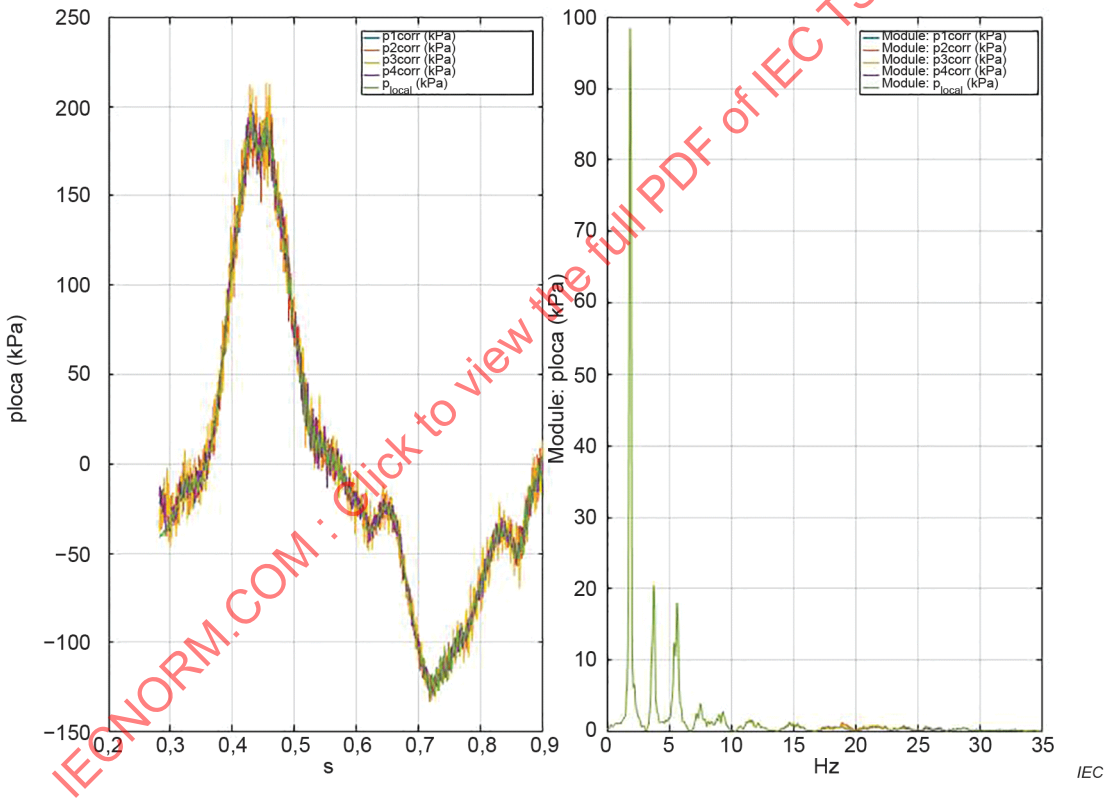


Figure D.3 – Signal and spectrum of four remote sensors (corrected) and one local sensor

IECNORM.COM : Click to view the full PDF of IEC TS 62882:2020

3 MATLAB is the trademark of a product supplied by MathWorks. This information is given for the convenience of users of this document and does not constitute an endorsement by IEC of the product named. Equivalent products may be used if they can be shown to lead to the same results.

Table D.5 – Peak-to-peak value on the corrected signals

Locations	Δp (kPa)	error (%)
p_{local}	292,0	
p_1	291,8	-0,1
p_2	292,0	0,0
p_3	294,2	0,7
p_4	292,1	0,0

D.5 Limitations

This correction works on measuring tubes having the same material over its length. For heterogeneous material (half steel, half plastic), more errors were noted after correction.

The tubing shall be outside the penstock; otherwise, the remote pressure sensor senses the pressure in the penstock (at the tap) and the pressure fluctuations along all the tubing length.

IECNORM.COM : Click to view the full PDF of IEC TS 62882:2020

Annex E
(informative)

Forced response analysis for Francis turbines operating in part load conditions

E.1 General

Francis turbines operating in part load conditions experience cavitating vortex rope in the draft tube resulting from the swirling flow of the runner outlet. This precessing vortex rope induces convective and synchronous pressure fluctuation at the precession frequency. The synchronous component propagates through the entire hydraulic circuit and corresponds to the response of the hydraulic system to a momentum excitation source located in the draft tube elbow. The frequency of the vortex rope precession comprises between 0,2 times and 0,4 times the turbine rotational speed. There is a risk of resonance between the hydraulic circuit, the synchronous machine and the turbine itself acting as excitation source.

Two methodologies to assess the Francis turbine part load resonance risk are presented in Annex E. One is a systematic methodology based on detailed modelling of the hydroelectric power plant and the other is a simplified approach based on the hydroacoustic properties of the hydraulic system.

E.2 Systematic methodology based on detailed modelling of hydroelectric power plant

E.2.1 Description of the test case

The test case features a Francis turbine, a penstock and a draft tube (see Figure E.1).

The hydraulic power plant is equipped with a Francis turbine of 5 MW under a maximum head of 100 mWC. The main characteristics of the unit are given in Table E.1 and the performance hill chart is described in Figure E.2. In this study case, the Francis turbine is operated at 60 % of the rated operating condition.

The penstock is characterized by a length of 300 m, a wave speed of 1 250 m/s and a diameter of 1,2 m. The friction factor λ is equal to 0,012 for an equivalent roughness of 0,1 mm.

For resonance risk assessment purposes, the Francis turbine draft tube can be properly modelled by a pressure source excitation in series with two pipes [176]. The draft tube length is equal to 10 m and the diameter is equal to 1,2 m. For this test case, the diameter of the pipes in the draft tube is assumed to be constant. However, to obtain a more accurate model, the numerical model can be used to take also into account the divergent geometry of the draft tube and the convective terms of the momentum equation [171]. For a given operating point, the wave speed a and the bulk viscosity μ'' depend on the cavitation volume of the vortex rope. These parameters can be estimated with the methodology presented in Annex G. Usually, the wave speed of the liquid-gas mixture drops to very low values with respect to the cavitation rope volume [175]. In this study case, the response of the hydraulic system to a momentum excitation source is analysed for wave speed values between 50 m/s and 100 m/s. The bulk viscosity is assumed to be constant and equal to 20 000 Pa·s.

IECNORM.COM : Click to view the full PDF of IEC TS 62882:2020

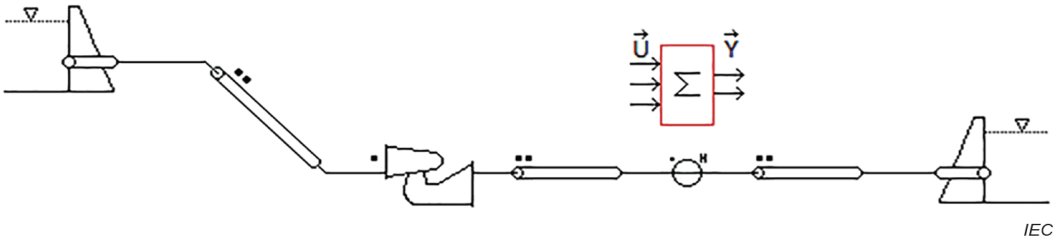


Figure E.1 – SIMSEN [4] model of the test case

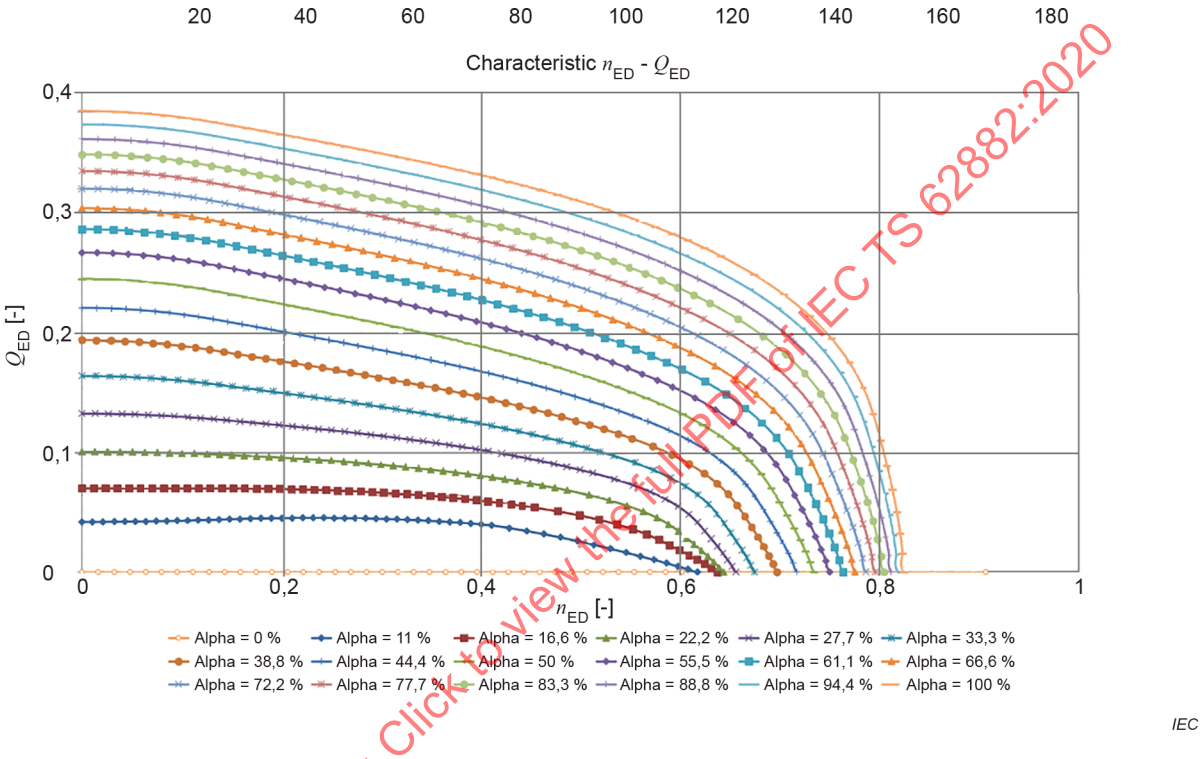


Figure E.2 – Performance hill chart of the Francis turbine for different guide vane openings

Table E.1 – Francis turbine parameters

Rated power P_n [MW]	5
Rated discharge Q_n [m^3/s]	5
Rated net head H_n [mWC]	100
Rated rotational speed N_n [rpm]	750
Reference diameter D_{ref} [m]	0,846
Specific speed N_q [-]	53

IECNORM.COM : Click to view the full PDF of IEC TS 62882:2020

E.2.2 Modelling of the hydraulic power plant

By assuming uniform pressure and velocity distributions in the cross section and neglecting the convective terms, the one-dimensional momentum and continuity balances for an elementary

4 SIMSEN is the trademark of a product supplied by Power Vision Engineering. This information is given for the convenience of users of this document and does not constitute an endorsement by IEC of the product named. Equivalent products may be used if they can be shown to lead to the same results.

pipe filled with water of length dx, cross section A and wave speed a (see Figure E.3) yield to the following set of hyperbolic partial differential equations [181]:

$$\begin{cases} \dfrac{\partial h}{\partial t} + \dfrac{a^2}{gA} \cdot \dfrac{\partial Q}{\partial x} = 0 \\ \dfrac{\partial h}{\partial x} + \dfrac{1}{gA} \cdot \dfrac{\partial Q}{\partial t} + \dfrac{\lambda |Q|}{2gDA^2} \cdot Q = 0 \end{cases} \tag{E.1}$$

This system is solved using the finite difference method with a first order centre scheme discretization in space and a scheme of Lax for the discharge variable. This approach leads to a system of ordinary differential equations that can be represented as a T-shaped equivalent scheme [174,179]. The RLC parameters of this equivalent scheme are given by Formula (E.2):

$$R = \frac{\lambda \cdot |\overline{Q}| \cdot dx}{2 \cdot g \cdot D \cdot A^2} \quad L = \frac{dx}{g \cdot A} \quad C = \frac{g \cdot A \cdot dx}{a^2} \tag{E.2}$$

where

λ is the local loss coefficient;

D is the diameter of the elementary pipe.

The hydraulic resistance R, the hydraulic inductance L and the hydraulic capacitance C correspond respectively to energy losses, inertia and storage. An additional dissipation is introduced and represented in the electrical T-shaped circuit by a hydraulic resistance R_μ to consider the internal processes breaking the thermodynamic equilibrium between the cavitation volume and the surrounding liquid:

$$R_\mu = \frac{\mu''}{\rho_w g A dx} \tag{E.3}$$

where

μ" is the bulk viscosity;

ρ_w is the water density;

A and dx are the section and the length of the pipe element, respectively;

g is the gravity acceleration.

The model of a pipe of length L is made of a series of n_b elements based on the equivalent scheme of Figure E.3. The system of equations relative to this model is set-up using Kirchoff laws [176],[180].

IECNORM.COM : Click to view the full PDF of IEC TS 62882:2020

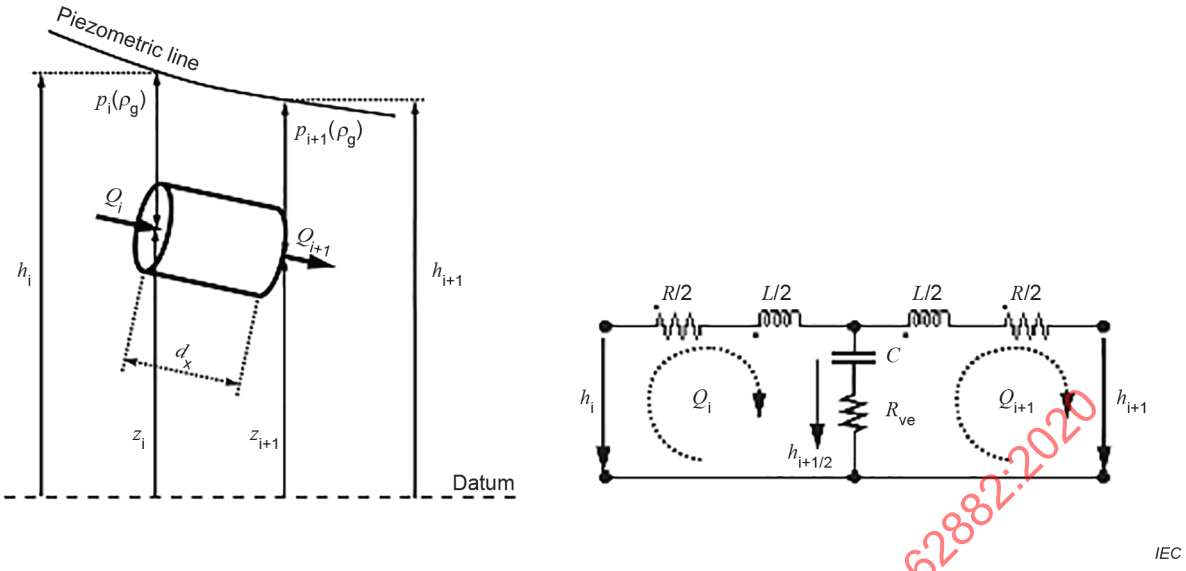


Figure E.3 – Elementary hydraulic pipe of length dx and its equivalent circuit

This electrical analogy of the hydraulic model describes the dynamic behaviour as a first order differential equation system in the matrix form:

$$[A]\frac{d\vec{x}}{dt}+\left[B\left(\vec{x}\right)\right]\cdot\vec{x}=\vec{V}\left(\vec{x}\right) \tag{E.4}$$

where

$[A]$ and $\left[B(\vec{x})\right]$ are the state global matrices of dimension $[n \times n]$;

$\vec{x}$ and $\vec{V}(\vec{x})$ are respectively the state vector and the boundary conditions vector with n components.

The linearization of the system of equations is described by Formula (E.5), where linearized $[B]$ becomes $[B_l]$:

$$[A]\frac{d\cdot\delta\vec{x}}{dt}+\left[B_l\right]\cdot\delta\vec{x}=\vec{0} \tag{E.5}$$

The eigenvalues $s_k=\alpha_k+j\omega_k$ of the system can be calculated from Formula (E.6):

$$det\left(\left[\mathrm{I}\right]s+\left[A\right]^{-1}\left[B_l\right]\right)=0 \tag{E.6}$$

By solving Formula (E.6), the eigenmodes shapes with related eigenfrequencies can be predicted. The real part of the eigenfrequency corresponds to the damping α while the imaginary part corresponds to the fluctuation of oscillation ω. Finally, the damping ratio is defined by Formula (E.7):

$$\eta=\frac{\alpha}{\sqrt{\omega^2+2\alpha^2}} \tag{E.7}$$

IECNORM.COM : Click to view the full PDF of IEC TS 62882:2020

Besides this modal analysis, the risk resonance assessment can be completed by a forced response analysis. This method allows the identification of the contribution of each eigenmode into the system response which depends on the system boundary conditions and the excitation source location [172]. With the forced response method, Formula (E.4) becomes:

$$[A]\frac{d\vec{x}}{dt} = \left[B\left(\vec{x}\right)\right]\cdot\vec{x} + [C]\cdot\vec{U} + \vec{V}\left(\vec{x},\vec{U}\right) \tag{E.8}$$

where

$\vec{U}$ is the input vector with p components; $[C]$ is the input matrix of dimension $[n \times p]$.

Combining forced response analysis with eigenmodes computation, the system response to hydraulic excitation induced by the cavitation vortex rope in the turbine draft tube can be investigated.

E.2.3 Forced response analysis of the test case

The forced response of the hydraulic system to a momentum excitation source located in the draft tube is illustrated for wave speeds between 50 m/s and 100 m/s (Figure E.4 to Figure E.6), while typical values can be derived from reduced cavitation compliance [173]. The response to the excitation is analysed at three different locations:

– inlet of the penstock;
– middle of the penstock;
– outlet of the penstock.

For all wave speeds, the third eigenmode of the hydraulic power plant is present in the vortex rope excitation range around 4,1 Hz (see Figure E.7 to Figure E.9). This eigenmode has a small interaction with the draft tube (see Figure E.10). For a wave speed between 50 m/s and 60 m/s, a second, third eigenmode is present in the vortex rope excitation range with a higher interaction with the draft tube (see Figure E.11). For a wave speed equal to 100 m/s, the second eigenmode is identified in the vortex rope excitation range and has a strong interaction with the draft tube (see Figure E.12).

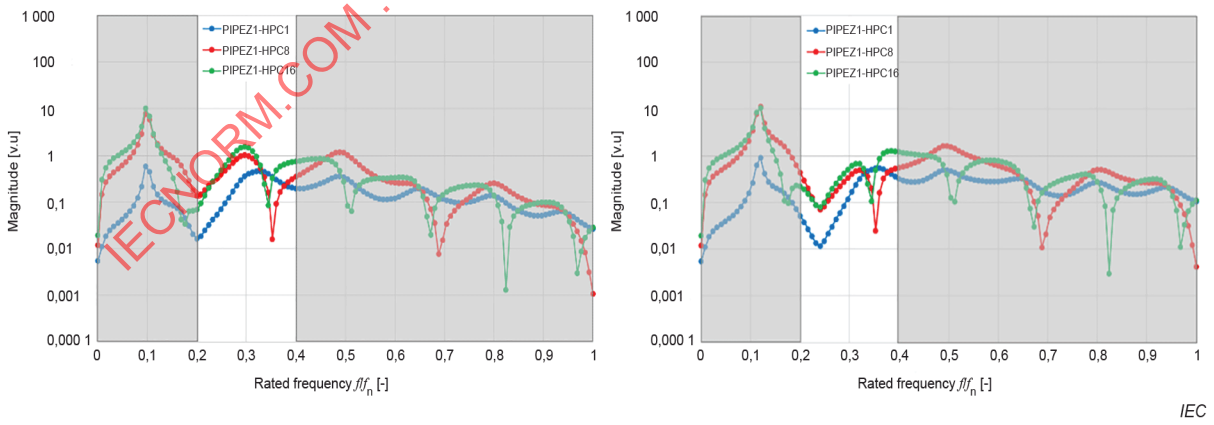


Figure E.4 – Forced response for a = 50 m/s (left) and a = 60 m/s (right)

IECNORM.COM : Click to view the full PDF of IEC TS 62882:2020

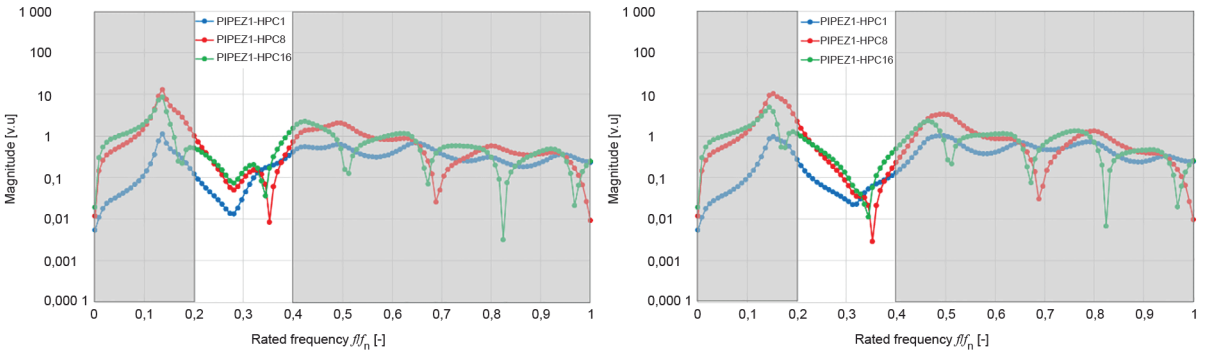


Figure E.5 – Forced response for a = 70 m/s (left) and a = 80 m/s (right)

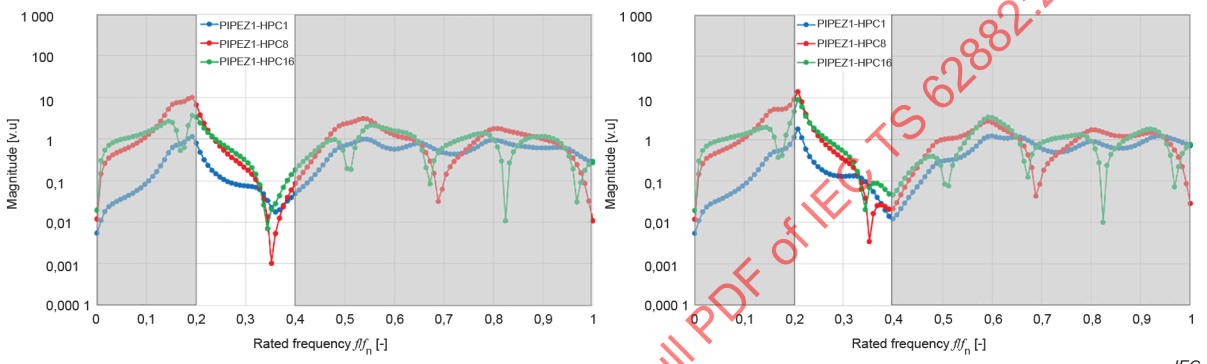


Figure E.6 – Forced response for a = 90 m/s (left) and a = 100 m/s (right)

a = 50 m/s

Damping α	Eigenpulsation ω	Damping ratio η	Eigenfrequency f
[rad/s]	[rad/s]	[-]	[Hz]
-0,250 9	7,772 0	-0,032 2	1,236 9
-2,030 3	13,162 3	-0,150 7	2,094 8
-2,023 8	23,038 5	-0,087 2	3,666 7
-2,195 9	26,281 0	-0,083 0	4,182 7
-5,392 7	37,647 9	-0,140 4	5,991 8
-2,413 0	38,640 4	-0,062 2	6,149 8
-2,295 4	50,941 8	-0,045 0	8,107 6
-10,678 5	51,198 5	-0,200 0	8,148 5
-15,994 2	61,486 9	-0,244 1	9,785 9
-2,303 5	62,755 4	-0,036 7	9,987 8
-21,717 8	70,568 6	-0,282 2	11,231 3
-2,313 2	73,933 9	-0,031 3	11,766 9

a = 60 m/s

Damping α	Eigenpulsation ω	Damping ratio η	Eigenfrequency f
[rad/s]	[rad/s]	[-]	[Hz]
-0,287 264	9,194 072 4	-0,031 2	1,463 3
-1,957 107 2	13,331 370 4	-0,143 7	2,121 8
-1,986 942 7	25,479 291 1	-0,077 5	4,055 2
-2,148 704 7	28,498 010 7	-0,075 0	4,535 6
-2,186 407 8	38,629 479 1	-0,056 4	6,148 1
-5,422 247 2	45,317 834 2	-0,118 0	7,212 6
-2,343 784 6	51,048 880 8	-0,045 8	8,124 7
-10,534 723 1	61,897 998 9	-0,165 5	9,851 4
-2,371 762 8	62,749 551 8	-0,037 7	9,986 9
-2,375 737	73,966 071 6	-0,032 1	11,772 1
-15,912 077 5	74,603 543 3	-0,204 2	11,873 5

IEC

Figure E.7 – Damping and eigenfrequency for a = 50 m/s (left) and a = 60 m/s (right)

a = 70 m/s

Damping α	Eigenpulsation ω	Damping ratio η	Eigenfrequency f
[rad/s]	[rad/s]	[-]	[Hz]
-0,434 0	10,495 0	-0,041 3	1,670 3
-1,765 6	13,597 1	-0,127 7	2,164 0
-2,043 6	25,822 0	-0,078 7	4,109 7
-1,981 3	32,666 6	-0,060 4	5,199 1
-2,183 9	38,906 7	-0,056 0	6,192 2
-2,436 4	50,664 8	-0,048 0	8,063 5
-5,170 0	53,267 9	-0,096 2	8,477 8
-2,343 6	62,826 3	-0,037 3	9,999 1
-10,335 2	72,578 7	-0,139 6	11,551 3
-2,473 5	73,951 0	-0,033 4	11,769 7

a = 80 m/s

Damping α	Eigenpulsation ω	Damping ratio η	Eigenfrequency f
[rad/s]	[rad/s]	[-]	[Hz]
-0,828 4	11,539 1	-0,071 4	1,836 5
-1,321 6	14,091 2	-0,093 0	2,242 7
-2,053 6	25,964 6	-0,078 6	4,132 4
-1,855 8	36,402 5	-0,050 8	5,793 6
-2,187 6	39,731 6	-0,054 9	6,323 5
-2,199 5	50,942 1	-0,043 1	8,107 7
-4,763 8	60,464 9	-0,078 3	9,623 3
-2,787 5	63,068 2	-0,044 1	10,037 6
-2,391 9	73,988 0	-0,032 3	11,775 5

IEC

Figure E.8 – Damping and eigenfrequency for a = 70 m/s (left) and a = 80 m/s (right)

IECNORM.COM : Click to view the full PDF of IEC TS 62882:2020

a = 90 m/s

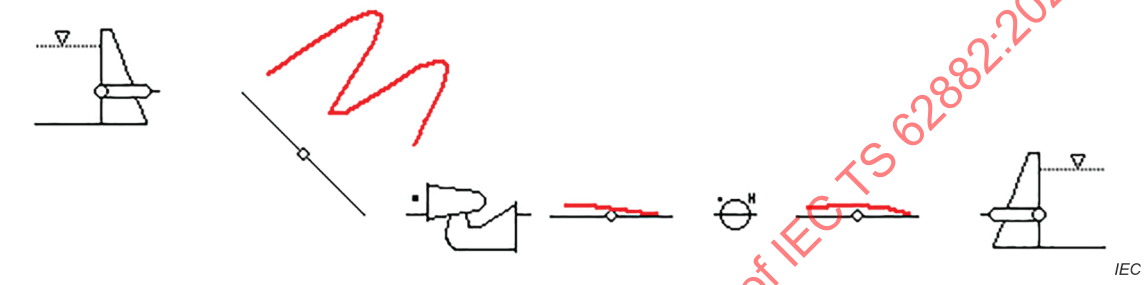
Damping α	Eigenpulsation ω	Damping ratio η	Eigenfrequency f
[rad/s]	[rad/s]	[-]	[Hz]
-1,323 3	12,016 0	-0,108 8	1,912 4
-0,775 9	15,116 7	-0,051 2	2,405 9
-2,047 4	26,089 9	-0,078 0	4,152 3
-1,968 2	37,969 6	-0,051 7	6,043 1
-1,943 2	42,621 1	-0,045 5	6,783 4
-2,194 5	51,218 7	-0,042 8	8,151 7
-2,309 4	62,467 7	-0,036 9	9,942 0
-4,840 9	68,403 6	-0,070 4	10,886 8
-2,558 5	74,299 6	-0,034 4	11,825 1

a = 100 m/s

Damping α	Eigenpulsation ω	Damping ratio η	Eigenfrequency f
[rad/s]	[rad/s]	[-]	[Hz]
-1,582 3	12,182 9	-0,127 7	1,939 0
-0,469 7	16,406 9	-0,028 6	2,611 2
-2,027 0	26,229 7	-0,076 8	4,174 6
-2,034 2	38,337 9	-0,052 9	6,101 7
-1,743 8	46,363 3	-0,037 6	7,379 0
-2,189 3	51,747 1	-0,042 2	8,235 8
-2,219 4	62,784 2	-0,035 3	9,992 4
-2,696 9	73,157 4	-0,036 8	11,643 4
-4,397 5	76,746 8	-0,057 1	12,214 6

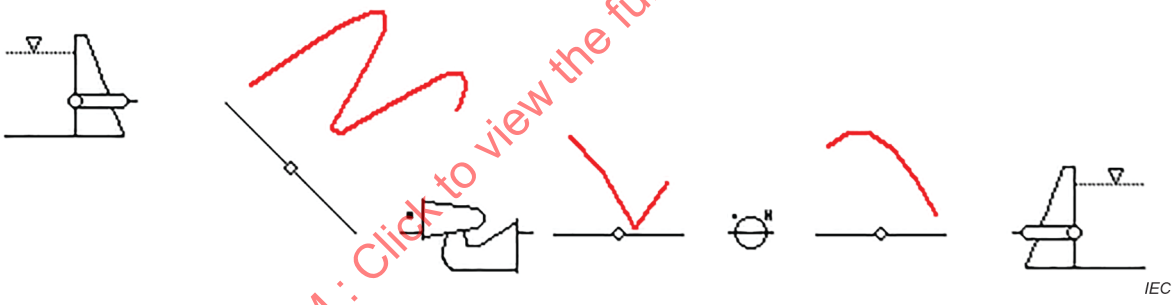
IEC

Figure E.9 – Damping and eigenfrequency for a = 90 m/s (left) and a = 100 m/s (right)



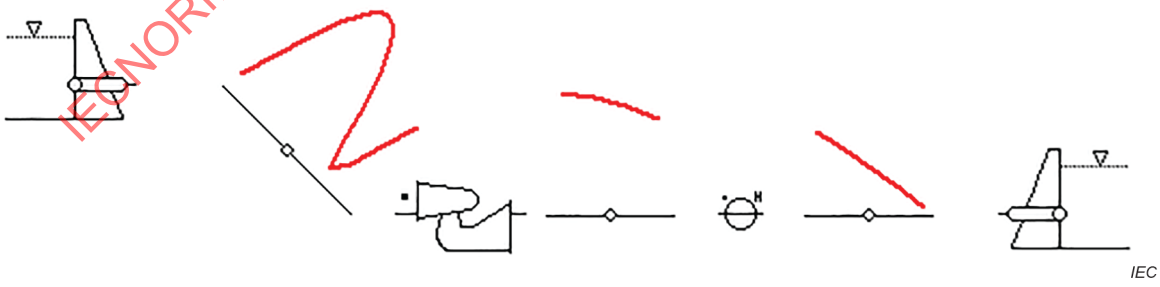
IEC

Figure E.10 – Eigenmode for a = 50 m/s and eigenfrequency f = 4,18 Hz



IEC

Figure E.11 – Eigenmode for a = 50 m/s and eigenfrequency f = 3,67 Hz



IEC

Figure E.12 – Eigenmode for a = 100 m/s and eigenfrequency f = 2,61 Hz

IECNORM.COM : Click to view the full PDF of IEC TS 62882:2020

E.3 Simplified approach based on the hydroacoustic properties of the hydraulic system

E.3.1 General

The methodology to assess Francis turbine part load resonance risk presented in Clause E.2 is based on detailed modelling of hydroelectric power plant and requires specific simulation tools to be addressed. At any stage of the project, it is useful to dispose of a simplified methodology to evaluate potential resonance risk. At part load operation, the frequency of the cavitating vortex rope precession is equivalent to between 0,2 times and 0,4 times the turbine rotational speed and corresponds to a forced excitation of the entire hydraulic system including the turbine itself. Resonance occurs if the part load excitation frequency matches one of the hydraulic system natural frequencies. A first estimation of the hydraulic system natural frequencies can be achieved based on the hydroacoustic properties of the hydraulic system such as pipe length, cross section area and wave speed.

E.3.2 Cavitating draft tube first natural frequency

Figure E.13 presents the simplified hydroacoustic model of the frictionless cavitating draft tube composed of the cavitation compliance C_{DT} and of the draft tube inductance L_{DT} given by:

$$C_{DT} = \frac{l_{DT} \cdot g \cdot \overline{A}_{DT}}{a_{DT}^2} \qquad L_{DT} = \frac{l_{DT}}{g \cdot \overline{A}_{DT}}$$

where

l_{DT} is the equivalent draft tube length [m];

$\overline{A}_{DT}$ is the mean draft tube cross section area [m^2];

a_{DT} is the mean cavitating draft tube wave speed [$m \cdot s^{-1}$];

g is the acceleration due to gravity [$m \cdot s^{-2}$];

and where the mean cross section area of the draft tube can be calculated based on equivalent inductance approach enabling to calculate the equivalent cross section area as follows:

$$A_{equ} = \frac{l_{tot}}{\sum \frac{l_i}{A_i}}$$

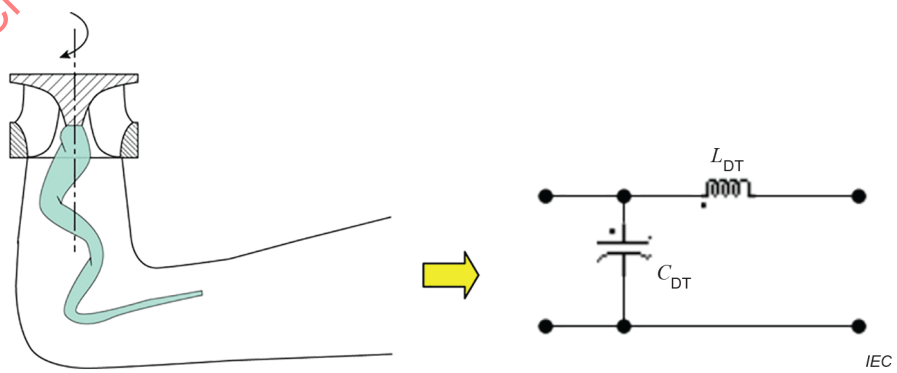


Figure E.13 – Draft tube modelled with cavitation compliance and draft tube inductance

IECNORM.COM : Click to view the full PDF of IEC TS 62882:2020

Assuming that the draft tube is connected downstream to an infinite reservoir and that the turbine runner represents an infinite hydraulic resistance upstream the draft tube, the first natural frequency of this system is given by [63]:

$$f_o = \frac{1}{2\cdot\pi}\frac{1}{\sqrt{L_{DT}\cdot C_{DT}}} = \frac{1}{2\cdot\pi}\frac{a_{DT}}{l_{DT}} \tag{E.9}$$

When the draft tube is connected to a downstream tailrace pipe (see Figure E.14), the inertia of this pipe is dominant and the corresponding simplified model includes the draft tube cavitation compliance C_{DT} and the tailrace pipe inductance L_{TR} given by:

$$L_{TR} = \frac{l_{TR}}{g\cdot A_{TR}}$$

where

l_{TR} is the tailrace pipe length [m];

A_{TR} is the tailrace pipe cross section area [m^2].

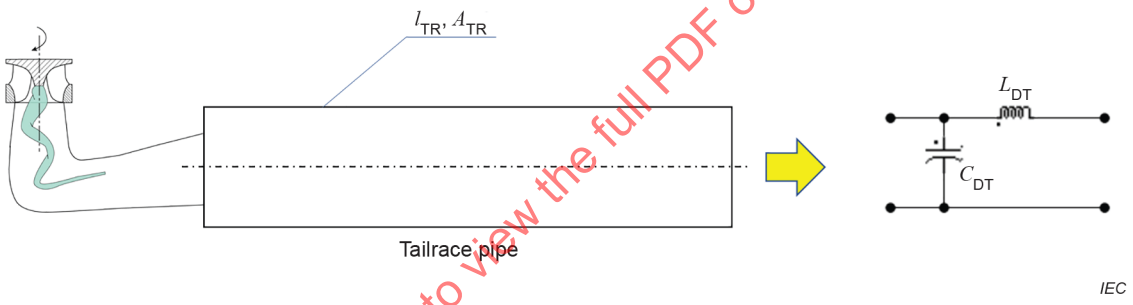


Figure E.14 – Simplified model of a cavitation draft tube connected to a tailrace pipe composed by cavitation compliance of the draft tube and downstream inductance of the tailrace pipe

Assuming again that the tailrace pipe is connected downstream to an infinite reservoir and that the turbine runner represents an infinite hydraulic resistance upstream the draft tube, the first natural frequency of this system is given by [1]:

$$f_o = \frac{1}{2\cdot\pi}\frac{1}{\sqrt{L_{TR}\cdot C_{DT}}} = \frac{1}{2\cdot\pi}\frac{a_{DT}}{\sqrt{l_{DT}\cdot l_{TR}\dfrac{\bar{A}_{DT}}{A_{TR}}}} \tag{E.10}$$

The tailrace pipe may also include the inertia characteristics of the draft tube.

E.3.3 Hydraulic circuit natural frequencies

To estimate the higher order natural frequencies of the hydraulic circuit including the cavitation draft tube, it is possible to model the piping system comprised between the upstream reservoir and downstream reservoir, or surge tanks, by an equivalent pipe (see Figure E.15), characterized by a total length l_{tot} and an equivalent wave speed a_{equ} given by:

IECNORM.COM : Click to view the full PDF of IEC TS 62882:2020

$$l_{tot} = \sum_{i=1}^{n} l_i \quad a_{equ} = \frac{l_{tot}}{\sum_{i=1}^{n} \frac{l_i}{a_i}}$$

The total length l_{tot} and an equivalent wave speed a_{equ} shall include the draft tube length l_{DT} and the draft tube wave speed a_{DT}.

Neglecting inlet or outlet singular losses, the upper and lower reservoirs or surge tanks correspond to constant pressure boundary conditions. Therefore, the wave length of equivalent pipe k natural modes shapes is given by [178]:

$$\lambda_k = \frac{2}{k} \cdot l_{tot} \text{ with: } k = 1, \ldots, n$$

The corresponding natural frequencies are then given by:

$$f_k = \frac{a_{equ}}{\lambda_k} = \frac{a_{equ}}{2 \cdot l_{tot}} \cdot k \tag{E.11}$$

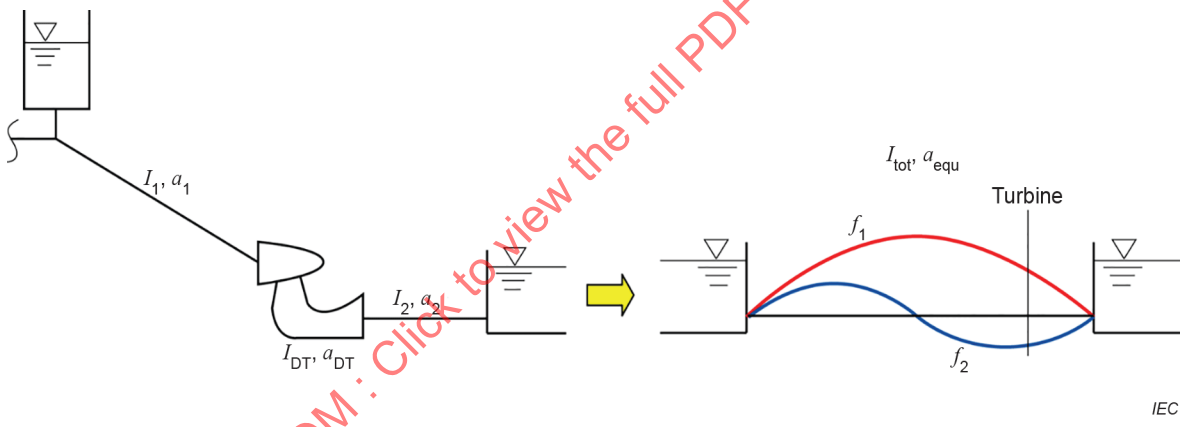


Figure E.15 – Hydraulic system modelled by an equivalent pipe and corresponding modes shapes for the first and second natural frequencies

E.3.4 Example of applications

The calculation of the system natural frequencies based on Formulae (E.9), (E.10) and (E.11) is applied to three different hydraulic systems to evaluate part load resonance risk. These hydraulic systems presented in Figure E.16 include:

– hydraulic system 1: an upper reservoir, a penstock, a Francis turbine, a draft tube, a downstream reservoir;

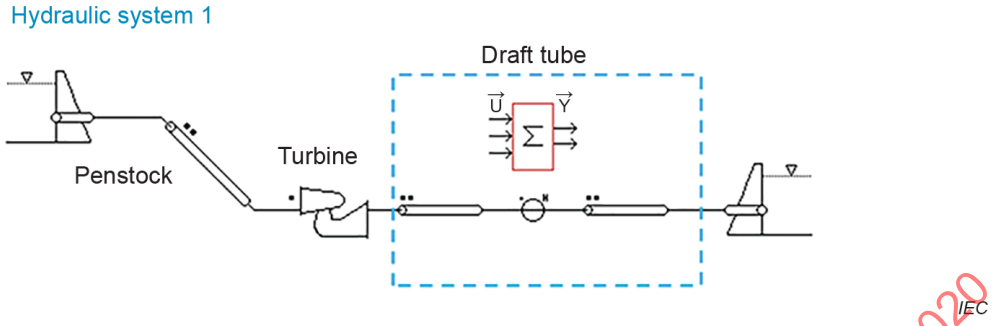
– hydraulic system 2: same as hydraulic system 1 with adjunction of a tailrace pipe with the same diameter as the draft tube;

– hydraulic system 3: same as hydraulic system 1 with adjunction of a tailrace pipe with a different diameter than the draft tube.

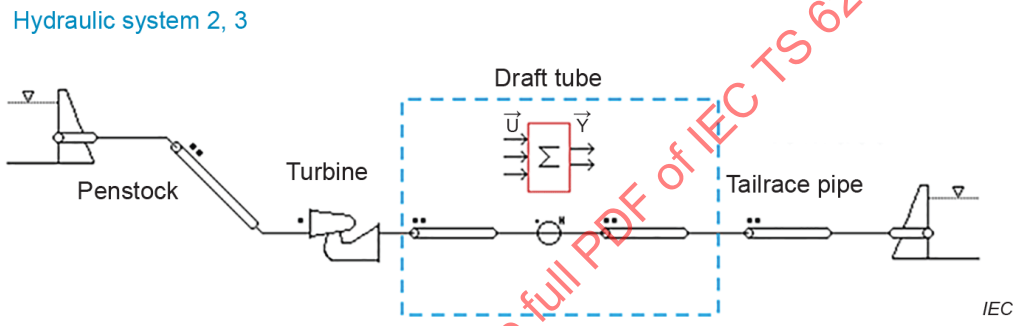
The hydraulic system 1 is identical to the system presented in Clause E.2 and is also modelled in SIMSEN to compute reference eigenvalues to compare with simplified analytical methods. The parameters of the hydraulic systems 1 to 3 are summarized in Table E.2. According to the Francis turbine rotational speed, the vortex rope pressure fluctuation frequency is expected to

IECNORM.COM : Click to view the full PDF of IEC TS 62882:2020

be comprised between 2,5 Hz and 5 Hz. If one of the hydraulic system natural frequencies falls into this interval, resonance could take place.



a) Hydraulic system 1: with penstock, Francis turbine



b) Hydraulic systems 2 and 3: with additional tailrace pipe

Figure E.16 – Hydraulic systems 1, 2 and 3

Table E.2 – Parameters of the hydraulic systems 1, 2 and 3

Penstock		Turbine		Draft tube		Tailrace pipe	
L	300 m	P_n	5 MW	L	10 m	L	100 m
D	1,2 m	Q_n	5 m^3/s	D	1,2 m	D	1,2 m and 2 m
a	1 250 m/s	H_n	100 m	a	50 100 m/s	a	1 250 m/s
λ	0,012	N_n	750 r/min	λ	0,012	λ	0,012
		D_{ref}	0,864 m				
		N_q	53				
		f_{exct}	2,5 Hz to 5 Hz				

IECNORM.COM : Click to view the full PDF of IEC TS 62882:2020

The parameters of the equivalent pipes of the hydraulic systems 1, 2 and 3 computed with draft tube wave speed of 50 m/s and 100 m/s are provided respectively in Table E.3, Table E.5, and Table E.7. The related natural frequencies computed based on Formulae (E.9), (E.10) and (E.11) which are compared with the results of eigenvalue calculation as described in Clause E.2 are provided respectively in Table E.4, Table E.6, and Table E.8 with the corresponding errors. The range of prototype draft tube wave speed selected for this analysis has shown to provide rather good results with site measurements for couple of test cases. The wave speed can also be deduced from the reduced cavitation compliance [3]. The first natural frequency f_0 is computed with Formula (E.9) for hydraulic system 1 and with Formula (E.10) for hydraulic systems 2 and 3. The natural frequencies f_1 to f_6 are then calculated according to Formula (E.11). Resonance has already been found up to the 5th hydraulic system natural frequencies; this is why the first

six natural frequencies have been computed. In principle, the higher the order, the higher the relative damping, reducing the amplitude of the hydraulic circuit to a forced excitation.

The analysis of the errors obtained for the natural frequencies f_2 to f_6 shows for each hydraulic system a rather good agreement between the analytical approach and the eigenvalue calculation with a maximum error of 14 %. Regarding the natural frequencies f_0 and f_1, which are both compared with the first natural frequency obtained by the eigenvalue calculation, it could be noticed that for the hydraulic system 1 without tailrace pipe, better agreement is found with the natural frequency f_1 computed with Formula (E.11) even if the frequency f_0 computed with Formula (E.9) gives the right order of magnitude. However, for the hydraulic systems 2 and 3, very good agreement is found for f_0 with Formula (E.10), while Formula (E.11) leads to very large differences for f_1. Therefore, in practice, it is recommended to compute both natural frequencies f_0 and f_1, and also the natural frequencies up to f_6, and to check possible resonance risk. If such a risk is identified, it is recommended to perform additional investigations with the more detailed approach of Clause E.1, in order for example to anticipate possible mitigation measures during the design phase, which can be also analysed during reduced scale model tests.

In Table E.4, Table E.6 and Table E.8, the natural frequencies which can potentially lead to resonance with draft tube vortex rope excitation in the range of 2,5 Hz to 5 Hz are highlighted in bold. The hydraulic system 1 is the simplified model of a prototype unit which suffers from part load resonance between the cavitating vortex rope and the 3rd natural frequency. Site measurements showed a resonance frequency value of 3,8 Hz, which is in good agreement with the results from Table E.4.

Table E.9 presents the pressure mode shape obtained by eigenvalue and eigenvector calculation for the three first natural frequencies f_1, f_2 and f_3 of the hydraulic systems 1 and 2 featuring respectively 1, 2 or 3 pressure antinodes. It could be noticed that the modes f_2 and f_3 correspond to elastic pressure mode shapes. For the first natural frequency, for the hydraulic system 1, the pressure mode shape features also an elastic mode shape, while the hydraulic system 2 is characterized by a rigid column mode shape, similar to surge tank mass oscillation between the tailrace pipe and the draft tube compliance. It explains why the value of natural frequency is better captured with Formula (E.10) than with Formula (E.11).

Table E.3 – Parameters of the equivalent pipe of the hydraulic system 1

System 1	*L* [m]	*a* [m/s]	*D* [m]
Penstock	300	1 250	1,2
Draft tube	10	50	1,2
		100	
Equivalent pipe	310	704,5	1,2
		911,8	

IECNORM.COM : Click to view the full PDF of IEC TS 62882:2020

Table E.4 – Estimation of the natural frequencies f_0 to f_6 of the hydraulic system 1 based on Formulae (E.9) and (E.11) and comparison with results obtained with eigenvalue calculation and corresponding errors

System1	Analytical calculation		Eigen calculation		Error	
	a_DT_min	a_DT_max	a_DT_min	a_DT_max	a_DT_min	a_DT_max
f_0[Hz]	0,80	1,59	1,24	1,94	-36 %	-18 %
f_1[Hz]	1,14	1,47	1,24	1,94	-8 %	-24 %
f_2[Hz]	2,27	**2,94**	2,09	2,61	9 %	13 %
f_3[Hz]	**3,41**	**4,41**	3,67	4,17	-7 %	6 %
f_4[Hz]	**4,55**	5,88	4,18	6,10	9 %	-4 %
f_5[Hz]	5,68	7,35	5,99	7,38	-5 %	0 %
f_6[Hz]	6,82	8,82	6,15	8,24	11 %	7 %

NOTE The natural frequencies which can potentially lead to resonance with draft tube vortex rope excitation in the range of 2,5 Hz to 5 Hz are highlighted in bold.

Table E.5 – Parameters of the equivalent pipe of the hydraulic system 2

System2	L [m]	a [m/s]	D [m]	A [m^2]
Penstock	300	1 250	1,2	1,13
Draft tube	10	50	1,2	1,13
		100		
Tailrace	100	1 250	1,2	1,13
Equivalent pipe	410	788,5		
		976,2		

Table E.6 – Estimation of the natural frequencies f_0 to f_6 of the hydraulic system 2 based on Formulae (E.10) and (E.11) and comparison with results obtained with eigenvalue calculation and corresponding errors

System1	Analytical calculation		Eigen calculation		Error	
	a_DT_min	a_DT_max	a_DT_min	a_DT_max	a_DT_min	a_DT_max
f_0[Hz]	0,25	0,50	0,27	0,55	-7 %	-8 %
f_1[Hz]	0,96	1,19	0,27	0,55	256 %	116 %
f_2[Hz]	1,92	2,38	2,04	2,10	-6 %	13 %
f_3[Hz]	**2,88**	**3,57**	2,53	4,05	14 %	-12 %
f_4[Hz]	**3,85**	**4,76**	4,12	4,88	-7 %	-2 %
f_5[Hz]	**4,81**	5,95	4,87	6,18	-1 %	-4 %
f_6[Hz]	5,77	7,14	5,16	6,36	12 %	12%

NOTE The natural frequencies which can potentially lead to resonance with draft tube vortex rope excitation in the range of 2,5 Hz to 5 Hz are highlighted in bold.

IECNORM.COM : Click to view the full PDF of IEC TS 62882:2020

Table E.7 – Parameters of the equivalent pipe of the hydraulic system 3

System3	L [m]	a [m/s]	D [m]	A [m^2]
Penstock	300	1 250	1,2	1,13
Draft tube	10	50	1,2	1,13
		100		
Tailrace	100	1 250	2,0	3,14
Equivalent pipe	410	788,5		
		976,2		

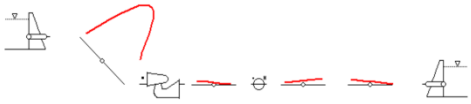
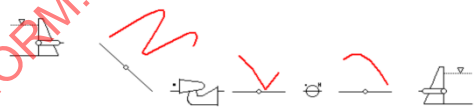
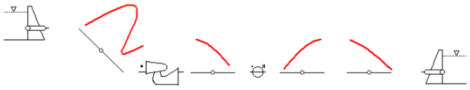
IECNORM.COM : Click to view the full PDF of IEC TS 62882:2020

Table E.8 – Estimation of the natural frequencies f_0 to f_6 of the hydraulic system 3 based on Formulae (E.10) and (E.11) and comparison with results obtained with eigenvalue calculation and corresponding errors

System1	Analytical calculation		Eigen calculation		Error	
	a_DT_min	a_DT_max	a_DT_min	a_DT_max	a_DT_min	a_DT_max
f_0[Hz]	0,42	0,84	0,42	0,81	0 %	4 %
f_1[Hz]	0,96	1,19	0,42	0,81	129 %	47 %
f_2[Hz]	1,92	2,38	2,04	2,10	-6 %	13 %
f_3[Hz]	**2,88**	**3,57**	2,55	4,03	13 %	-11 %
f_4[Hz]	**3,85**	**4,76**	4,12	4,72	-7 %	-1 %
f_5[Hz]	**4,81**	5,95	4,84	6,14	-1 %	-3 %
f_6[Hz]	5,77	7,14	6,16	6,55	-6 %	9 %

NOTE The natural frequencies which can potentially lead to resonance with draft tube vortex rope excitation in the range of 2,5 Hz to 5 Hz are highlighted in bold.

Table E.9 – Pressure mode shape obtained by eigenvalue and eigenvector calculation for the three first natural frequencies f_1, f_2 and f_3 of the hydraulic systems 1 and 2

	Hydraulic system 1	Hydraulic system 2
f_1		
f_2		
f_3		

IECNORM.COM : Click to view the full PDF of IEC TS 62882:2020

E.3.5 Limitations of the methodology

The proposed methodology has given good results for a simple hydraulic system with a single branch hydraulic layout. For systems with parallel branches, as a first approach, the parallel branches can be modelled by a single branch with equivalent parameters to obtain a first order of magnitude of the system natural frequencies. However, the real system will feature much more complex and numerous eigenvalues, due to the hydraulic system asymmetry, change of diameters and all bifurcations which are neglected in a single branch approach.

Annex F
(informative)

Influence of Thoma number on pressure fluctuation

The model pressure fluctuation test is always carried out at plant Thoma number. However, at prototype operating conditions, the tail water level varies at a wide range as a function of discharge and environmental conditions. This will cause the model test Thoma number to deviate from the prototype. Figure F.1 represents the influence of Thoma number on Francis turbine pressure fluctuation at the part load condition and rated condition. Figure F.1a) and Figure F.1b) are the influence of the Thoma number on Francis turbine draft tube pressure fluctuation amplitude at the two typical conditions. Figure F.1c) and Figure F.1d) are the corresponding influence analysis in the time domain, in which the X-axis is the relative frequency dimensionless by the rotation frequency n and the Y-axis is the pressure fluctuation amplitude of the component frequency through FFT (fast Fourier transformation) analysis; different colours represent different Thoma numbers. The direction of the decreasing Thoma number is from bottom to top.

IECNORM.COM : Click to view the full PDF of IEC TS 62882:2020

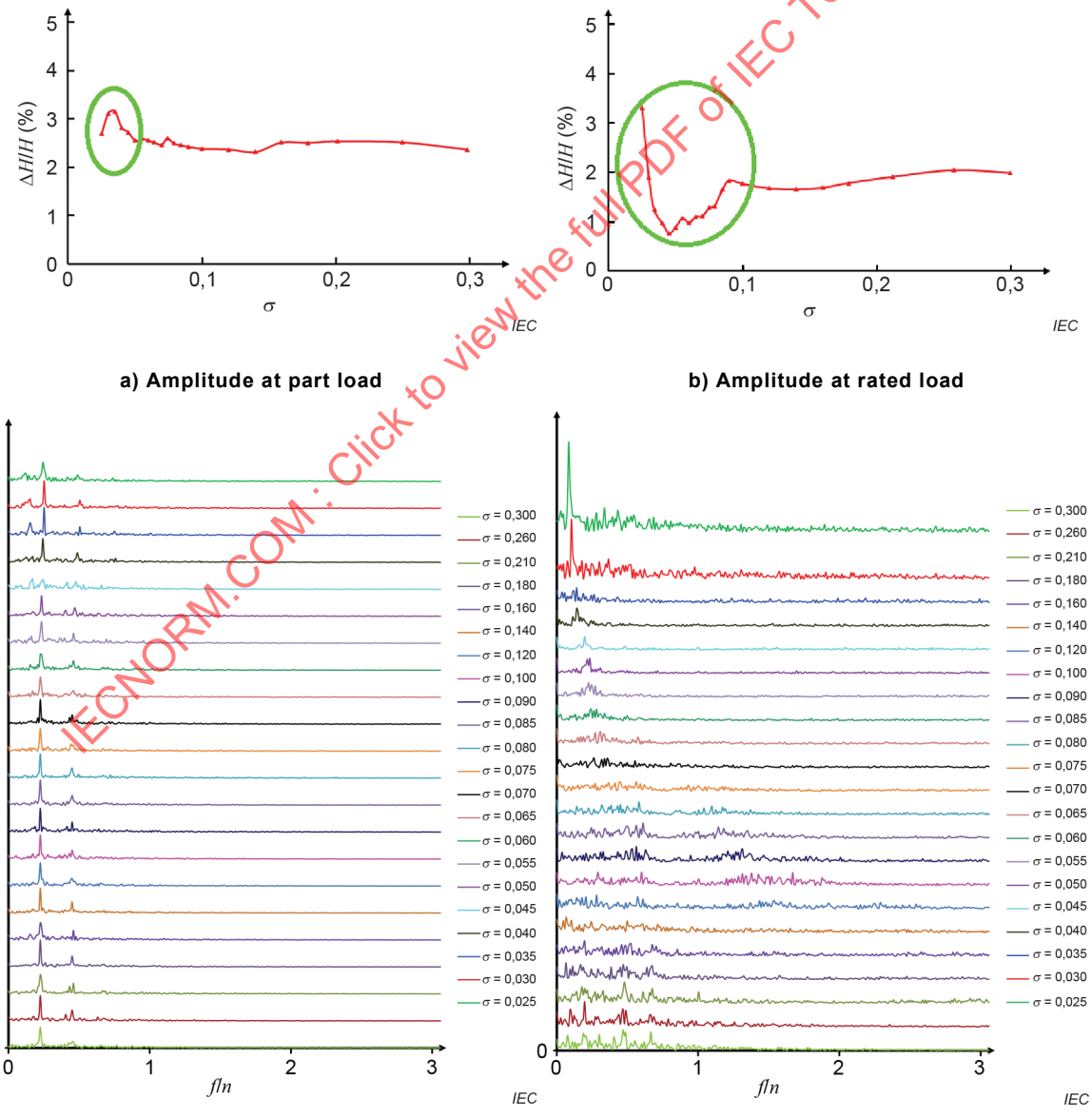
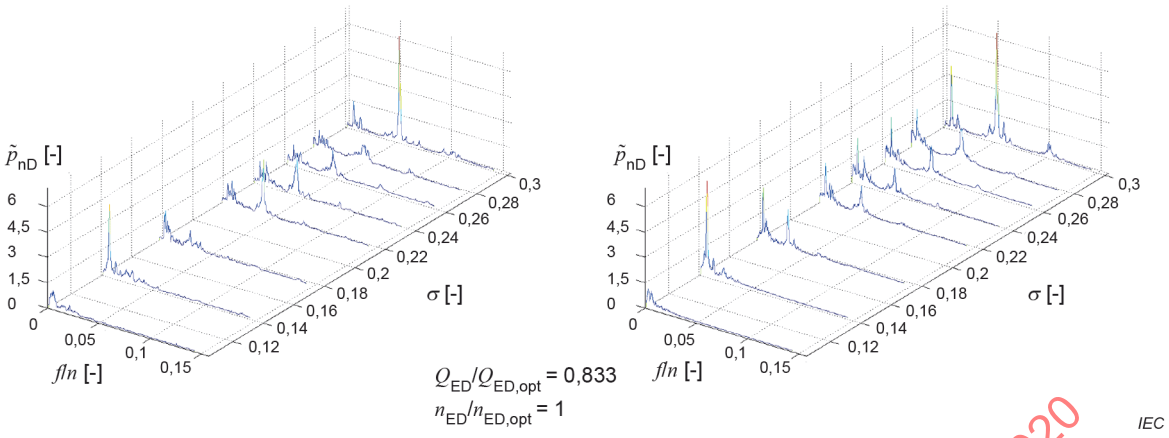


Figure F.1 – Influence of Thoma number on pressure fluctuation



a) At the spiral case inlet **b) At the upstream cone**

Figure F.2 – Example of waterfall diagram of the pressure fluctuations as function of the frequency and Thoma number

From Figure F.1 and Figure F.2, it can be found that Thoma number does not just have a substantial influence on Francis turbine draft tube pressure fluctuation but also on the frequency component distribution. So, when studying the pressure fluctuation similarity between model and prototype, the influence of the Thoma number should be considered.

IECNORM.COM : Click to view the full PDF of IEC TS 62882:2020

Annex G
(informative)

Transposition of synchronous pressure fluctuations from model to prototype for Francis turbines operating at off-design conditions

G.1 General

G.1.1 Overview

The pressure fluctuations taking place in a Francis turbine operating at part load can be decomposed into an asynchronous and synchronous part. If the asynchronous part of these pressure fluctuations can fairly be transposed according to Clause 7 methods, the transposition of the synchronous part propagating into the entire system is more challenging. Annex G proposes ways to achieve such a transposition and assesses the possible risk of resonance at the prototype scale.

Contrary to the asynchronous part, which only depends on the flow conditions in the draft tube, the synchronous part depends on the interaction between the excitation source induced by the cavitation vortex and the hydraulic circuit. Therefore, it cannot be directly transposed from the model to the prototype due to differences between both hydraulic circuits. It is for instance illustrated in Figure G.1. The hydroacoustic resonance observed at part load does not occur at the same value of discharge factor on the model and the prototype.

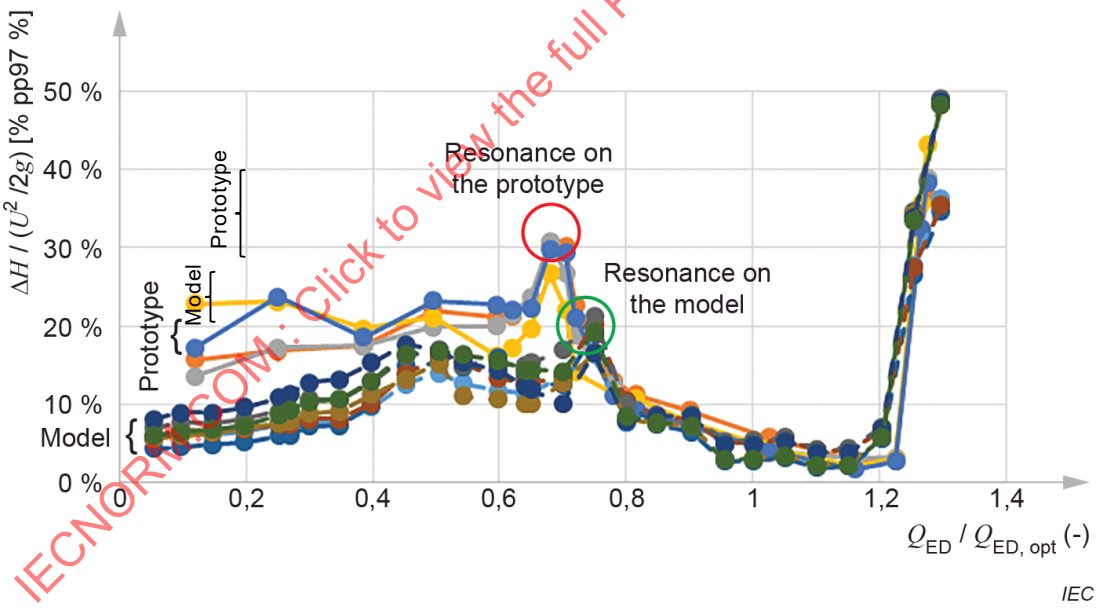


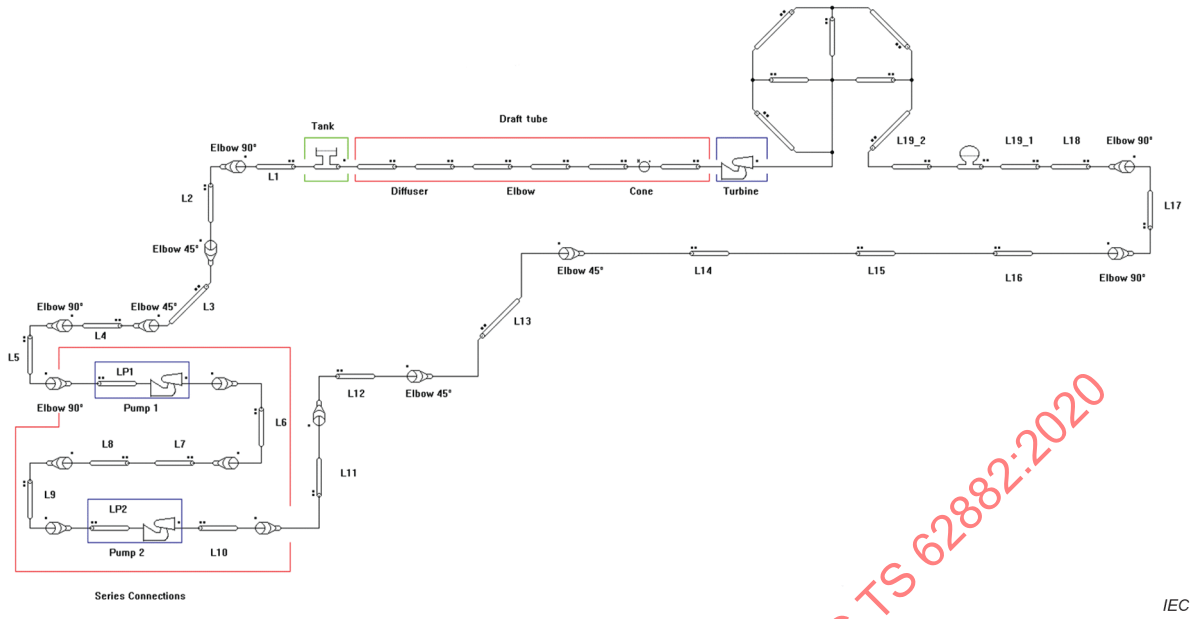
Figure G.1 – Peak-to-peak value of pressure fluctuations as a function of the discharge factor measured on the model and the corresponding prototype

In G.1.2 to G.1.6, a methodology for predicting the synchronous pressure fluctuations at the prototype scale is described. It is based on 1-D numerical models of hydraulic circuits and reduced scale model tests.

G.1.2 Step 1: 1-D numerical modelling of both the test rig at the model scale and the corresponding hydropower unit operating in off-design conditions

Unsteady numerical simulations of hydroelectric systems require a proper one-dimensional (1-D) modelling of each hydraulic component. 1-D hydroacoustic numerical models of both the test rig at the model scale and the hydropower plant generating unit shall be established [188]. An example of a layout of a test rig 1-D hydroacoustic model is given in Figure G.2 [186],[187].

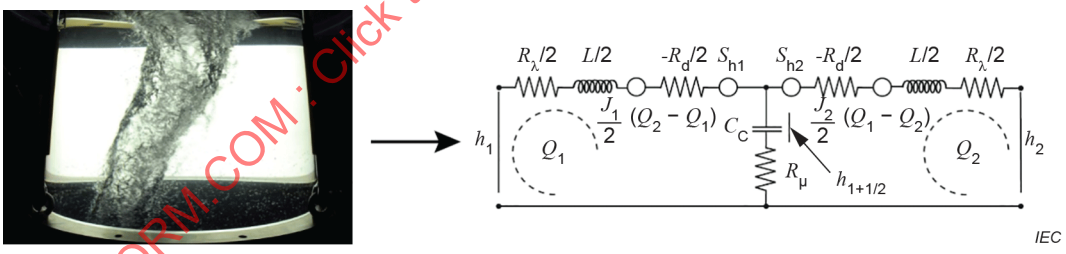
IECNORM.COM : Click to view the full PDF of IEC TS 62882:2020



Source: Landry 2015 [187]

Figure G.2 – Layout of EPFL test rig PF3 1-D hydroacoustic model

The cavitation vortex rope developing in a Francis turbine draft tube operating in part load and full load conditions shall be properly modelled to take into account the additional compressibility and dissipation induced by the presence of a gaseous volume in the draft tube, as well the excitation pressure source induced by the precession of the vortex at part load. More advanced models [183] can be used to take also into account the divergent geometry of the draft tube and the convective terms of the momentum equation. The corresponding equivalent electrical T-shaped circuit is given in Figure G.3.



Source: Landry et al. 2016 [186]

Figure G.3 – Electrical T-shaped representation of the cavitation vortex rope developing in Francis turbine draft tube in part load conditions

Also, there are some researches about the additional terms modelling the presence of the cavitation vortex rope [183], [186]:

- An additional dissipation, which is introduced and represented in the electrical T-shaped circuit by a hydraulic resistance R_μ to take into account the internal processes breaking the thermodynamic equilibrium between the cavitation volume and the surrounding liquid:

$$R_\mu = \frac{\mu''}{\rho_w g A dx} \tag{G.1}$$

IECNORM.COM : Click to view the full PDF of IEC TS 62882:2020

where

μ'' is the bulk viscosity;

ρ_w is the water density;

A and dx are the section and the length of the pipe element, respectively;

g is the gravity acceleration.

- An additional compressibility introduced by the presence of a cavitation volume in the draft tube, modelled by the cavitation compliance C_c:

$$C_c = -\frac{\partial V}{\partial h} \tag{G.2}$$

where

h is the piezometrical head.

It implicitly defines the local wave speed α in the draft tube if the compliance of the draft tube, including the wall and the water volume, is assumed negligible compared to the cavitation compliance:

$$C_c \approx \frac{gAdx}{a^2} \tag{G.3}$$

- A momentum excitation source S_h, modelling the periodical momentum excitation source induced by the processing vortex rope at part load conditions.
- A mass flow gain factor, modelling the variation of the cavitation volume with respect to the discharge, which is however often neglected at part load conditions.

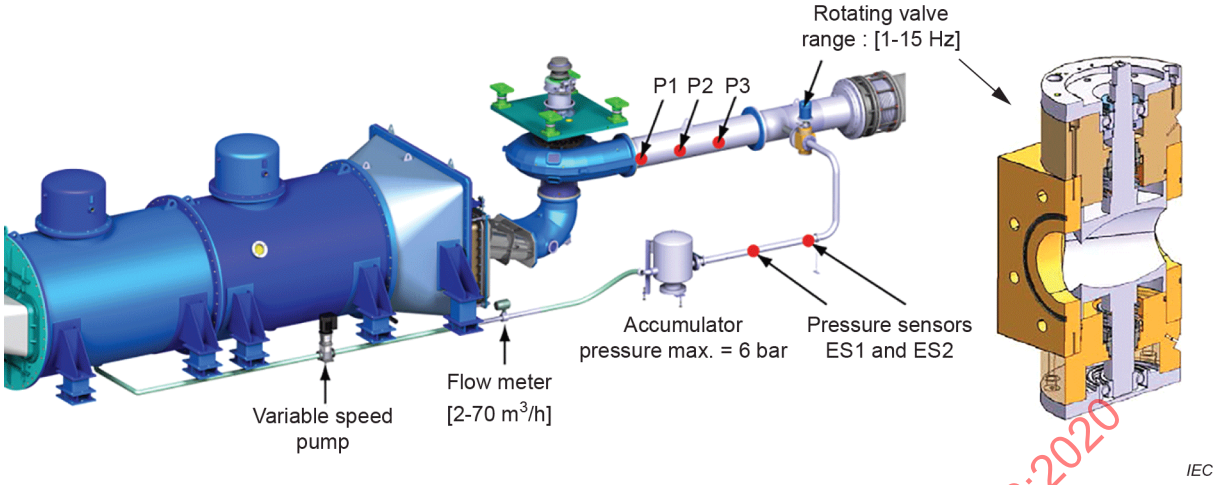
All these parameters shall be first identified on the reduced scale model and, then, transposed to the prototype scale.

G.1.3 Step 2: Experimental identification of the parameters of interest on the reduced scale model

G.1.3.1 Identification of hydroacoustic parameters modelling the cavitation vortex rope

For a given operating point, the wave speed α and the bulk viscosity μ'' can be experimentally identified on the reduced scale model by modal analysis. An external excitation system injecting periodical discharge fluctuations at a given frequency and with a given amplitude can be used (see Figure G.4 [186]). Pressure sensors are installed throughout the test rig to capture accurately the forced harmonic response of the hydraulic circuit to the external excitation. By changing systematically the excitation frequency, imposed by the frequency of the rotating valve, it is possible to identify the first eigenfrequency and the corresponding forced harmonic response of the hydraulic circuit to the external excitation.

IECNORM.COM : Click to view the full PDF of IEC TS 62882:2020



Source: Landry et al. 2016 [186].

Figure G.4 – Excitation system and 3D cut-view of the rotating valve

The identification of the wave speed α is based on the link between its value and the value of the frictionless eigenfrequency of the test rig. Simultaneously, the bulk viscosity μ'' is identified by quantifying the amount of energy injected in the test rig by the excitation system and measuring the forced harmonic response of the test rig by pressure sensors located throughout the pipes.

The wave speed and bulk viscosity are simultaneously adjusted in the 1-D numerical model of the test rig to obtain numerical results equivalent to the experimental ones in terms of eigenfrequencies and forced harmonic response of the test rig [186], [187].

Both hydroacoustic parameters are identified for a large number of Froude and Thoma numbers at two distinct part load operating points and defined two dimensionless numbers [186]: the dimensionless wave speed Π and the dimensionless bulk viscosity M'', as follows:

$$\Pi = \frac{\rho_{\mathrm{w}} a^2}{p_{\mathrm{cone}} - p_{\mathrm{v}}} \tag{1}$$

$$M'' = \frac{\mu'' f_0}{p_{\mathrm{cone}} - p_{\mathrm{v}}} \tag{2}$$

where

p_{cone} is the mean pressure in a reference section of the draft tube cone;

f_0 is the first eigenfrequency of the hydraulic circuit.

It was demonstrated that the relation between these dimensionless parameters and the void fraction β in the draft tube can be approximated by single power functions that are valid whatever the value of the speed factor, discharge factor, Thoma number and Froude number for a given machine.

G.1.3.2 Identification of the excitation source frequency and amplitude at part load

For a given part load operating point, the excitation frequency induced by the vortex, i.e. its precession frequency, can be identified directly by spectral analysis of the pressure signals measured during the modal analysis of the test rig.

IECNORM.COM : Click to view the full PDF of IEC TS 62882:2020

To identify the amplitude of the momentum excitation source, a methodology based on the comparison between experimental and 1-D numerical results is proposed [187]. For a given operating point, the amplitude of the excitation source is adjusted in the 1-D numerical model to obtain a numerical forced harmonic response of the test rig excited by the precession of the vortex equivalent to the experimental one. More details are given for the identification and the modelling of this excitation source in the 1-D numerical model [187].

G.1.3.3 Expression of the precession frequency and hydroacoustic parameters as a function of the swirl number

Predicting the synchronous pressure fluctuations on the complete operating range of the prototype requires the identification of the hydroacoustic parameters and the precession frequency of the vortex at the model scale for a wide number of operating points to take into account the influence of both the speed and discharge factors.

However, it is shown for a given test case that the influence of both parameters can be represented by a single parameter, the swirl number [184]. An analytical expression of the swirl number as a function of the speed and discharge factors has been defined as follows:

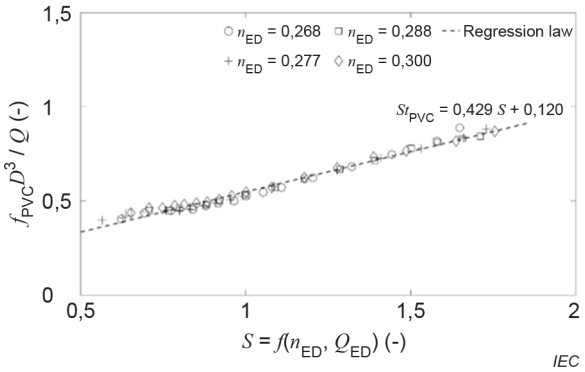
$$S = n_{ED}\frac{\pi^2}{8}\left(\frac{1}{Q_{ED}} - \frac{1}{Q_{ED}^0}\right) \quad \text{(G.6)}$$

where

Q_{ED}^0 is the discharge factor in swirl-free conditions for a given speed factor.

By plotting the Strouhal number of the precession frequency as a function of the swirl number, the data collapse in one single linear curve with a certain level of dispersion, as illustrated in Figure G.5, whatever the value of the speed factor.

For the precession frequency, the law linking the Strouhal number and the swirl number can be in theory directly transposed from the model to the prototype scale, since the precession frequency only depends on the operating conditions of the machine. Since the law linking the Strouhal number with the swirl number is simple, few measurements at the model scale would enable the prediction of the precession frequency on the complete part load operating range of the machine.

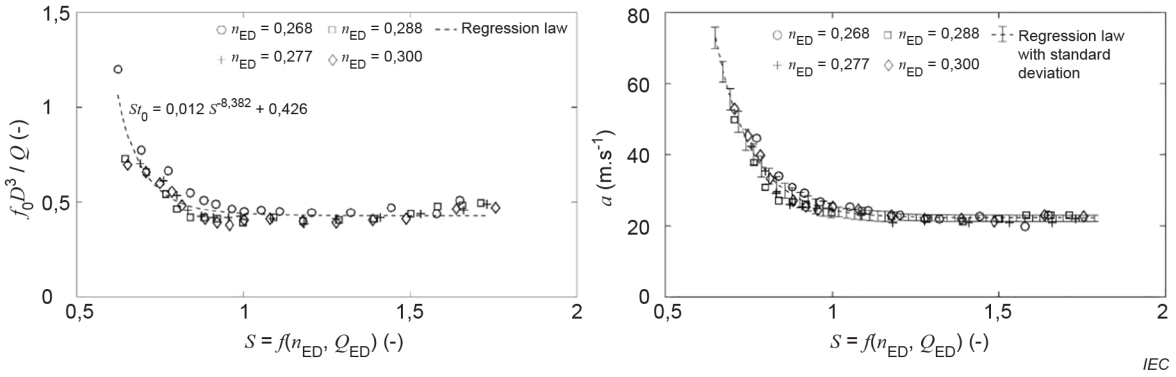


Source: Favrel et al. 2018 [184].

Figure G.5 – Strouhal number of the precession frequency as a function of the swirl number computed with Formula (G.6)

As illustrated in Figure G.6 a), if the Strouhal number of the first eigenfrequency is expressed as a function of the swirl number, all the data collapse in one single power curve. Similar results are obtained for the hydroacoustic parameters, as illustrated in Figure G.6 b).

IECNORM.COM : Click to view the full PDF of IEC TS 62882:2020



(a) Strouhal number of the first eigenfrequency of the test rig

(b) Wave speed in the draft tube determined in the 1-D model

Source: Favrel et al. 2019 [185].

Figure G.6 – Strouhal number of the first eigenfrequency of the test rig as a function of swirl number (a), the wave speed in the draft tube determined in the 1-D model (b)

It is important to notice that all the data shall be obtain for a given NPSH-level and Froude number on the prototype. To take into account the influence of both the Froude number and the NPSH-level, the dimensionless wave speed and bulk viscosity can be used and expressed as a function of the swirl number [186].

G.1.4 Step 3: Transposition of the hydroacoustic parameters from model to prototype

If the operating conditions on the prototype and the model are in similitude, i.e. the same value of speed factor, discharge factor, Froude and Thoma numbers, it can be assumed that the void fraction in the draft tube β is conserved between both scales. If these conditions are fulfilled, it can be demonstrated by a dimensionless analysis [187] that the wave speed and the bulk viscosity can be transposed from the model scale to the prototype scale by using the following relations:

$$a_P = a_M \frac{D_P}{D_M} \frac{n_P}{n_M} \tag{G.7}$$

$$\mu_P = \mu_M \left(\frac{D_P}{D_M}\right)^2 \left(\frac{n_P}{n_M}\right)^2 \frac{f_{0,M}}{f_{0,P}} \tag{G.8}$$

where

the subscripts M and P refer to the model and the prototype scales, respectively.

For the dimensionless wave speed and bulk viscosity, these are assumed to be conserved on the prototype for similar operating points. The corresponding wave speed and bulk viscosity can be determined at the prototype scale if the pressure in the cone on the prototype is known, which can be achieved by 1-D numerical simulation of the generating unit.

The amplitude A of the momentum excitation source S_h can be transposed by using the following relation:

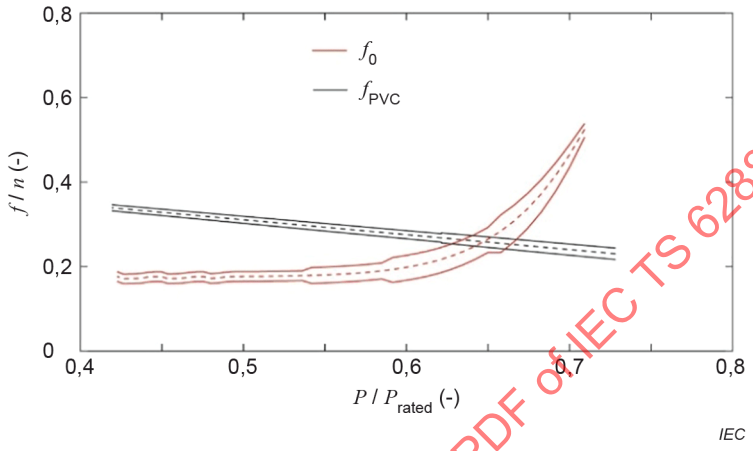
$$A_P = A_M \frac{D_P}{D_M} \tag{G.9}$$

IECNORM.COM : Click to view the full PDF of IEC TS 62882:2020

G.1.5 Step 4: Prediction of the precession frequency and eigenfrequencies at the prototype scale

For a given NPSH-level and Froude number, the precession frequency can be predicted by transposing directly the law linking the Strouhal number and the swirl number.

For the computation of the eigenfrequencies of the prototype at a given operating point, the transposed hydroacoustic parameters shall be first injected into a 1-D numerical model of the generating unit. The eigenfrequencies can then be computed by conducting an eigenvalue analysis of the non-linear hydraulic system [182].



Source: Favrel et al. 2019 [185].

Figure G.7 – Predicted values of precession frequency and first eigenfrequency at the prototype scale as a function of the output power of the generating unit

To illustrate the methodology, the predicted values of the precession frequency and the first eigenfrequency at the prototype scale are given in Figure G.7 as a function of the output power for a given test case [185]. These results are valid only for given values of n_{ED} and NPSH. For these conditions, the occurrence of resonance conditions was predicted for an output power equal to 65 % ± 2 % of the rated value.

G.1.6 Step 5: Prediction of pressure fluctuations at the prototype scale

Finally, to predict the synchronous pressure fluctuations of the machine at a given operating point, all the hydroacoustic parameters shall be injected into the 1-D numerical model of the hydropower generating unit, including the excitation source that shall be placed at the appropriate location in the 1-D model.

A 1-D time simulation of the dynamic behaviour of the generating unit enables finally the prediction of the pressure fluctuations through the complete hydraulic circuit.

G.2 Concluding remark: use of the local cavitation coefficient for transposition from model to prototype

The methodology presented in Annex G was applied to a 444 MW Francis turbine hydropower unit in the framework of the HYPERBOLE European research project (ERC/FP7-ENERGY-2013-1-Grant 608532). The vortex precession frequency (excitation frequency) was correctly predicted on a wide range of part load operating conditions (from 0,47 to 0,7 × P_{rated}). However, the predicted values of the first eigenfrequency of the hydropower unit, calculated assuming Thoma number similitude between model and prototype, were slightly different from the values measured on-site [185]. As a result, the difference between the predicted and the observed resonance conditions was equal to 7,3 % ± 2 % of the rated power.

IECNORM.COM : Click to view the full PDF of IEC TS 62882:2020

This difference is then explained by the non-equivalent energy losses in the draft tube between model and prototype, which makes the use of Thoma number as a similitude parameter less appropriate. A local cavitation coefficient based on the pressure value measured directly at the draft tube cone wall, i.e., next to the vortex rope, is then proposed as a better similitude parameter. It is defined as:

$$\chi_{nD} = \frac{p_{cone} - p_v}{\rho_w n^2 D^2}$$

where

p_{cone} is the mean pressure in a reference section of the draft tube cone;

p_v is the vapour pressure.

For the HYPERBOLE project test case, the hydropower unit's first eigenfrequency values are predicted from 0,47 P_{rated} to 0,7 P_{rated} making use of the local cavitation coefficient as pressure similitude parameter instead of the Thoma number. The pressure wave speed α_p in the cavitating draft tube cone of the prototype is calculated using two approaches:

1) making use of the identified pressure wave speed α_M at the reduced scale model and transposing directly assuming swirl number X_{nD} and Froude number similitude;
2) making using of the non-dimensional pressure wave speed Π defined with the reduced scale model tests and assuming swirl number and X_{nD} similitude only, Froude similitude becoming unnecessary.

The eigenfrequencies of the hydropower unit are then computed by injecting the transposed value of the wave speed into a 1-D numerical model of the hydropower unit. As illustrated in Figure G.8, both approaches to calculate α_p, making use of the local cavitation coefficient, lead to very accurate predictions of the first eigenfrequency of the hydropower unit at part load conditions.

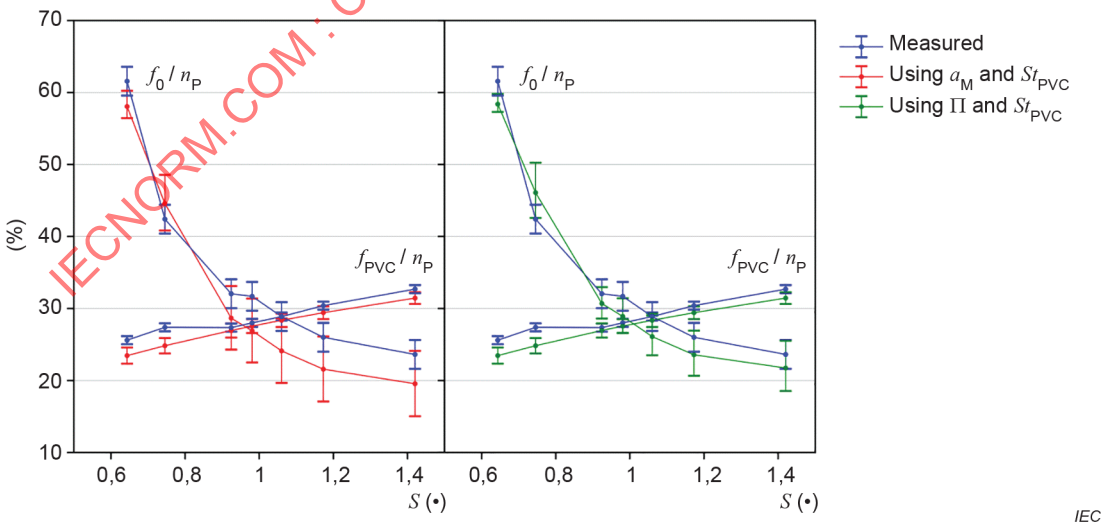


Figure G.8 – Comparison between observed and predicted values of the precession frequency f_{rope} and the first eigenfrequency f_0 of a 444 MW hydropower unit (HYPERBOLE project test case)

The similitude in terms of the local cavitation coefficient is used for the prediction of the eigenfrequencies [189].

IECNORM.COM : Click to view the full PDF of IEC TS 62882:2020

As illustrated by the hill chart of Figure G.9, assuming a constant pressure in the draft tube cone, p_{ref}, leading to a constant value of X_{nD} on the prototype, resonance conditions are expected to occur at a constant swirl number. Consequently, the active power output p_a where resonance is observed will vary according to the current conditions of head on the prototype.

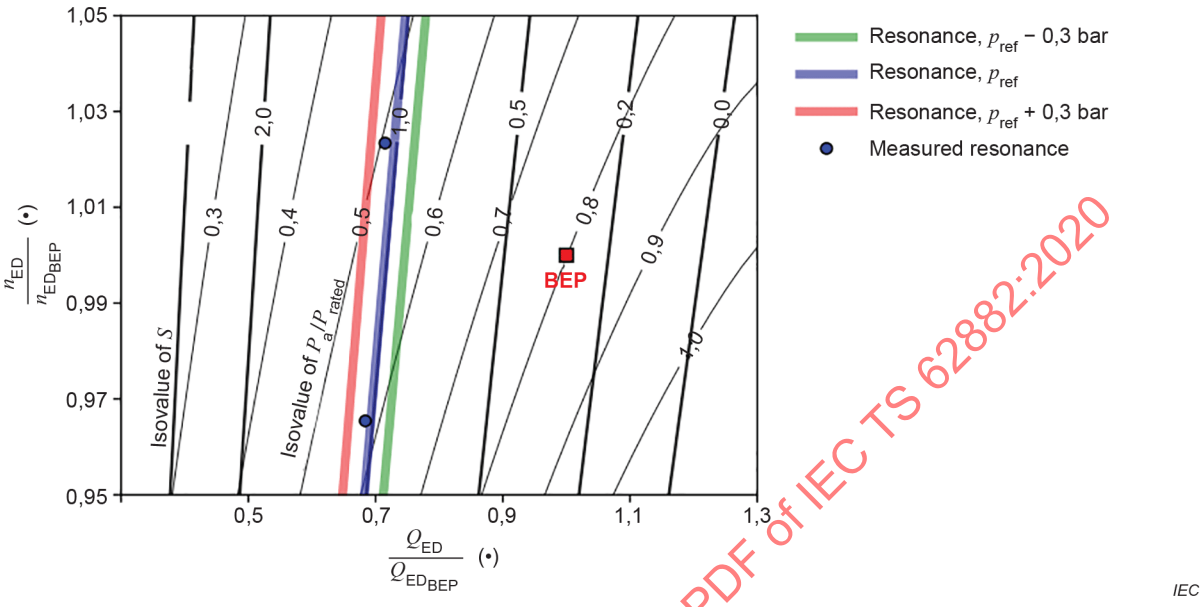


Figure G.9 – Hill chart comparing the measured and the predicted resonance conditions assuming a constant pressure value in the draft tube cone of the prototype

Resonance is expected to occur at a constant swirl number, but with a different power output on the prototype [189].

IECNORM.COM : Click to view the full PDF of IEC TS 62882:2020

Annex H
(informative)

Statistical analysis of pressure fluctuation data

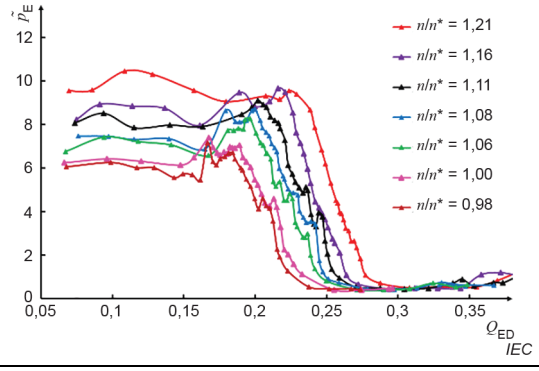
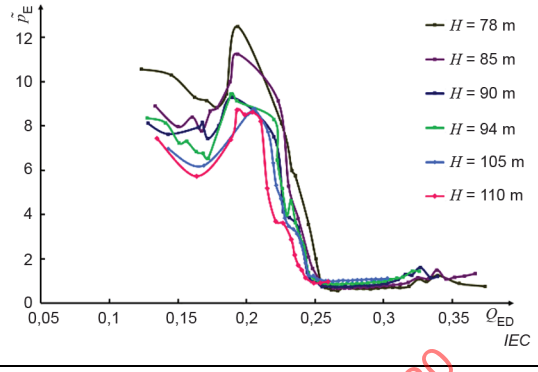
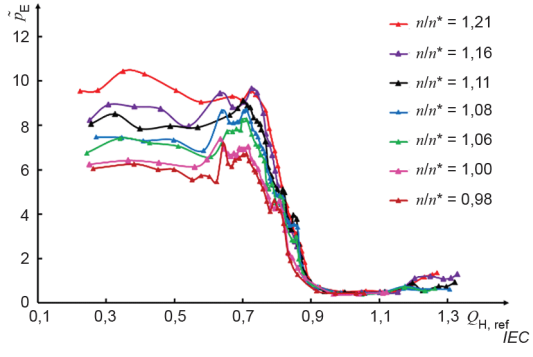
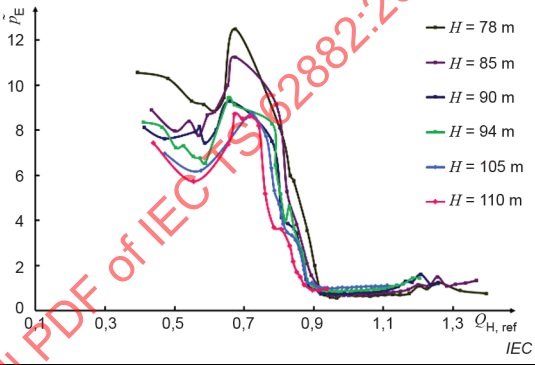
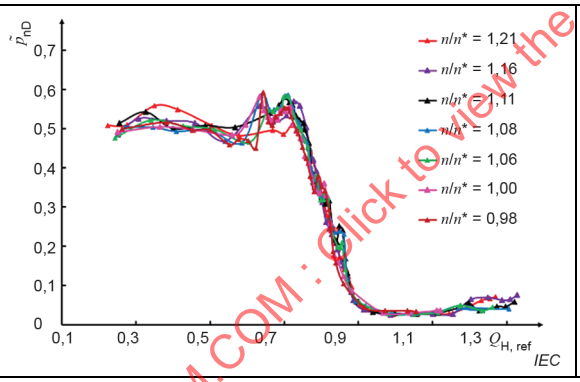
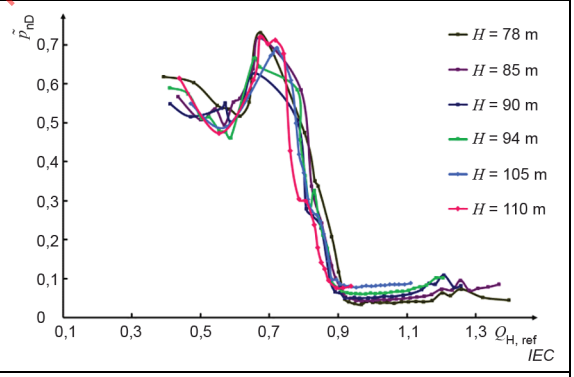
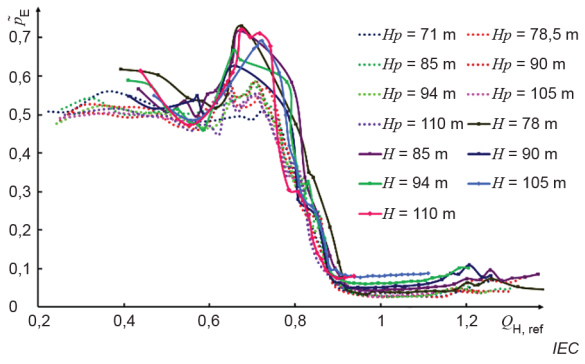
H.1 Normalizing step for the comparison of data

The measured pressure fluctuations in a reduced scale model and in the corresponding homologous prototype are represented as curves depending on the discharge factor Q_{H} and for a different net head H (Figure H.1). To compare the data, the discharge factor is normalized by the best efficiency discharge factor at a given head. This leads to a horizontal shift in all the curves (Figure H.2).

Finally, the pressure fluctuations are normalized by $\rho n^2 D^2$ and are represented by $\tilde{p}_{\mathrm{nD}}$ for the vaneless zone, the spiral case and the draft tube cone (Figure H.3).

Figure H.4 represents the way to compare in the same scalable pattern the pressure fluctuations of different models and the homologous prototype.

IECNORM.COM : Click to view the full PDF of IEC TS 62882:2020

	Model	Prototype
Measurement data		
	Figure H.1 – Pressure fluctuations versus discharge factor	
Discharge normalizing		
	Figure H.2 – Normalized discharge of pressure fluctuations	
Pressure amplitude normalizing		
	Figure H.3 – Normalized pressure amplitude of pressure fluctuations	
Comparison		
	Figure H.4 – Comparison of pressure fluctuations of model and prototype	

IECNORM.COM : Click to view the full PDF of IEC TS 62882:2020

H.2 Collected data

Eighteen test cases (models and prototypes) were collected from partners, and are summarized in Table H.1, The corresponding figures are presented in Clause H.3.

Table H.1 – World hydropower plant references

Nation	Number of power plant references	Specific speed N_{QE}
Canada	6	[0,15 to 0,16]
China	9	[0,12 to 0,23]
France	1	0,24
Norway	1	0,06
Sweden	1	0,18

H.3 Draft tube zone phenomena

Figure H.5 presents the comparison of draft tube pressure fluctuation amplitudes of eighteen hydropower plant references in the world. Figure H.6 to Figure H.9 show the difference, standard deviation, as well as transposition accuracy between model and prototype for the draft tube pressure fluctuation.

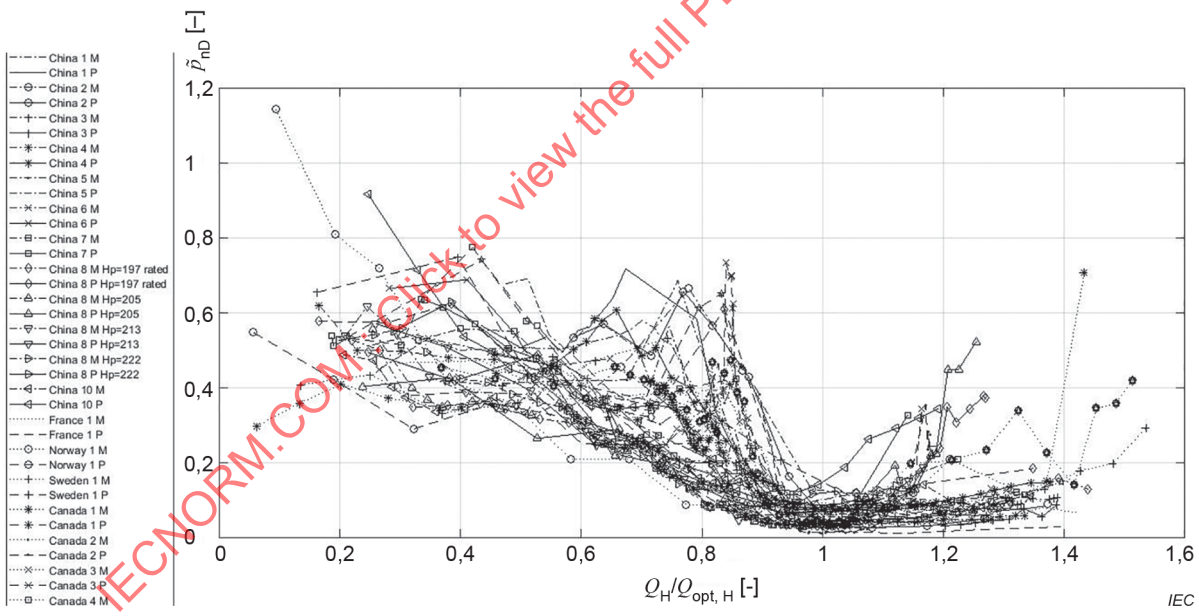


Figure H.5 – Set of pressure fluctuation of models and prototypes for draft tube analysis

IECNORM.COM : Click to view the full PDF of IEC TS 62882:2020

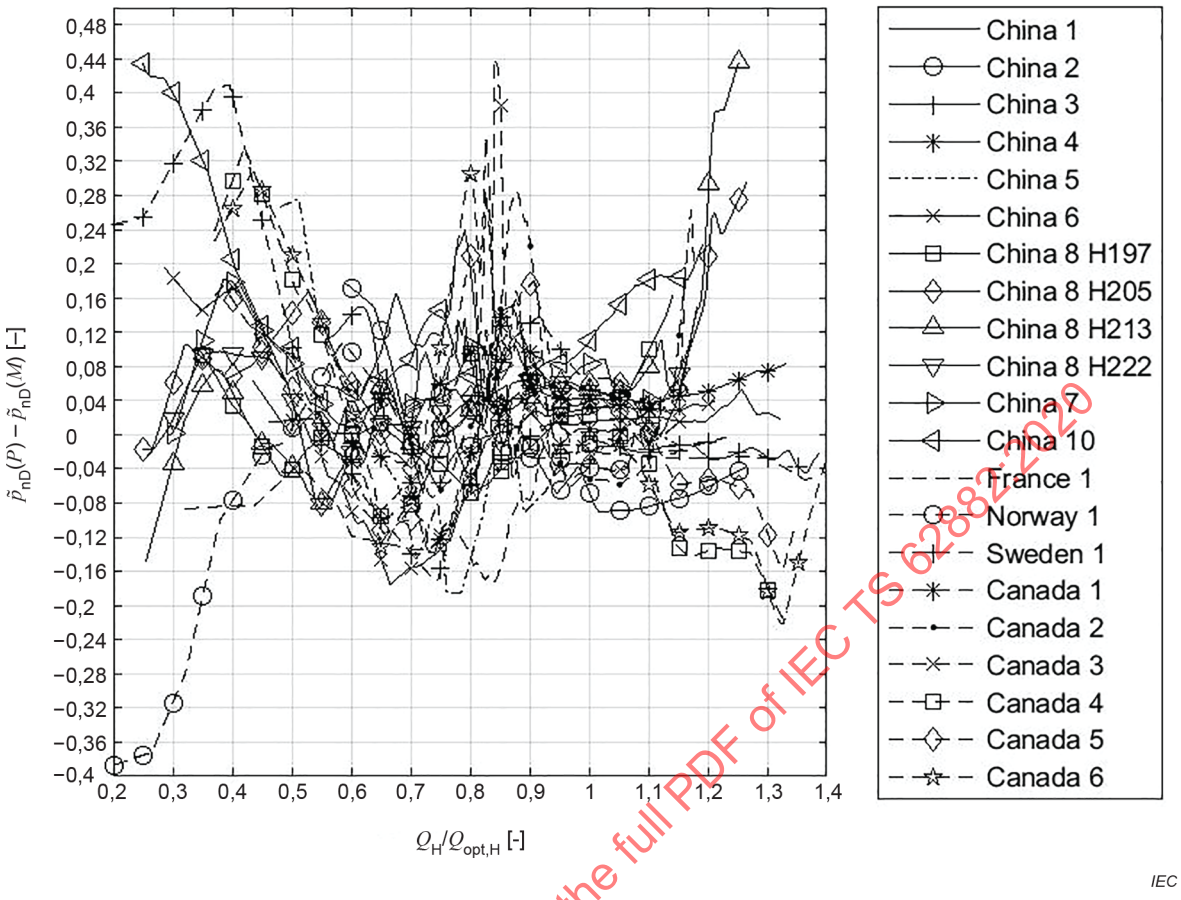


Figure H.6 – Difference between pressure fluctuations between the model and the prototype

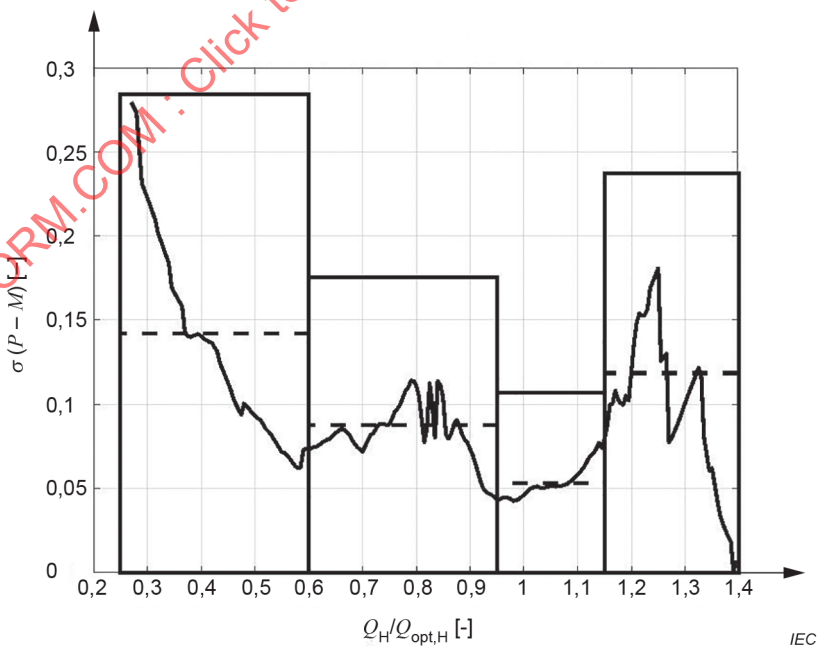


Figure H.7 – Standard deviation of difference of pressure fluctuation

IECNORM.COM : Click to view the full PDF of IEC TS 62882:2020